

國立交通大學

電子物理學系

博士論文

被動式 Q 開關光纖雷射之研究

The study of passively Q-switched fiber lasers

研究生：黃文政

指導教授：陳永富 教授

中華民國一百零三年五月

被動式 Q 開關光纖雷射之研究

學生：黃文政

指導老師：陳永富 教授

國立交通大學電子物理學系博士班

摘要

本文使用摻鏡的雙包層光纖作為主要的增益介質並使用被動式 Q 開關技術來研究高功率和高重複率的脈衝光源。首先我們使用孔徑 30 μm 的雙包層摻鏡光纖並分別利用半導體材料 AlGaInAs 和 $\text{Cr}^{4+}:\text{YAG}$ 晶體作為飽和吸收體，在 24W 幫浦功率下，使用 AlGaInAs 飽和吸收體可得到脈衝能量 0.45 mJ 且重複率為 30 kHz 的脈衝雷射，而使用 $\text{Cr}^{4+}:\text{YAG}$ 晶體則可得到脈衝能量 0.35 mJ 且重複率為 38 kHz 的脈衝雷射，同時並將兩者結果做一比較。

為進一步提升脈衝能量，我們改使用光纖孔徑達 70 μm 的光子晶體光纖作為增益介質，在使用 AlGaInAs 作為飽和吸收體時，脈衝能量大幅提升 2.4 倍至 1.1 mJ，且由於較短的腔長，使得脈衝寬度從 60 ns 減小至 10 ns，因此輸出尖峰功率從 7.5 kW 大幅提升至 110 kW，另外我們以此架構建立腔外光學參量振盪器，目前可得波長可調範圍為 1513 nm 至 1593 nm、脈衝能量 138 μJ 且重複率 6.5 kHz 的脈衝雷射輸出。而使用 $\text{Cr}^{4+}:\text{YAG}$ 飽和吸收體時，脈衝能量也有接近 2 倍的提升至 0.63mJ，而脈衝寬度也從 70 ns 降至 36 ns，也以此架構建構腔內光學參量振盪器，目前可得波長在 1515 nm 且輸出功率為 0.47 W 的脈衝雷射。

為了再減小脈衝寬以使脈衝功率能大幅提升，我們採用了 MOPA 放大器架構，利用被動式 Q 開關的 Nd:YVO₄/ $\text{Cr}^{4+}:\text{YAG}$ 雷射作為種子源和 30 μm 孔徑的雙包層摻鏡光纖作為放大器，我們得到脈衝寬度為 1.6 ns、能量為 0.192 mJ 且脈衝重覆率為 25 kHz 之輸出。我們另外完成將光子晶體光纖放大器作為基頻光光源的腔外非線性波長轉換，在輸入功率為 3.3 W 的條件下，可得波長為 532 nm 且輸出功率為 1.7 W 的二倍頻波長轉換，以及波長為 355 nm 且輸出功率為 1.1 W 的三倍頻波長轉換。

The study of passively Q-switched fiber lasers

Student: Wen-Cheng Huang

Advisor: Prof. Yung-Fu Chen

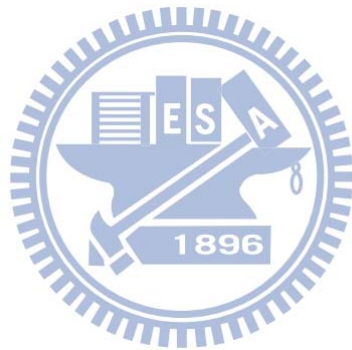
Institute and Department of Electrophysics
National Chiao-Tung University

Abstract

The double-cladding Yb-doped fiber as the gain medium and the passively Q-switching technique have been utilized in study of high power and high-repetition rate fiber lasers. First we use the double-cladding fiber with core diameter of 30 μm , and the AlGaInAs semiconductor material and the Cr⁴⁺:YAG crystal are used as the saturable absorbers (SA) respectively. By using the AlGaInAs as the SA, pulse energy up to 0.45 mJ with the repetition rate of 30 kHz in the pump power of 24 W can be attained. With the Cr⁴⁺:YAG crystal as the SA, we can have the laser output with a pulse energy of 0.35 mJ at the pulse repetition rate of 38 kHz in the same pump power. We also have comparative studies between these two SAs.

For scaling energy further, the photonic crystal fiber (PCF) with the core diameter of up to 70 μm is used as the gain medium. With the AlGaInAs as the SA, the pulse energy is significantly increased 2.4 times to 1.1 mJ, and the shorter cavity length results in the pulse width reducing from 60 ns to 10ns. As a sequence, the peak power is boosted up from 7.5 kW to 110 kW. This scheme is also used for pumping the extracavity optical parametric oscillator (OPO), and the output energy of 138 μJ with the repetition rate of 6.5 kHz at the wavelength which can be tunable from 1513 nm to 1593 nm is obtained. By employing the Cr⁴⁺:YAG SA, the pulse energy also has almost 2-times enhancement to 0.63 mJ and the pulse width decreases from 70 ns to 36 ns. An intracavity OPO was demonstrated based on this scheme, output power of 0.47 W at 1515 nm was obtained.

To achieve higher peak power, it is necessary to have smaller pulse width, so we adopt the configuration of master oscillator fiber amplifier (MOFA). By using a Nd:YVO₄/ Cr⁴⁺:YAG passively Q-switching laser as the seed laser and a 30- μ m-core double-cladding fiber as the amplifier, the amplifier can generate pulses with energy of 0.192 mJ at the repetition rate of 25 kHz and the pulse width is down to 1.6 ns. In addition, a PCF MOFA was used to pump the extracavity nonlinear wavelength conversions module, output powers of 1.7 W of the second harmonic generation at 532 nm and 1.1 W of the third harmonic generation at 355 nm were realized at the fundamental pump power of 3.3 W.



誌謝

Acknowledgement

當初碩士班只差一個名額無法如願進入電物系，心裡總是有那麼一點點的遺憾，沒想到工作多年之後竟然有機會進入電物系博士班繼續研習，這就是人生，事情總是出乎意料之外。

在這六年中不僅學到了許多研究方法，也認識了許多好友。首先感謝我的指導教授 陳永富老師這幾年來對我的指導提攜，陳老師指導學生的熱忱、學術研究的熱情和生活態度的樂觀都是我學習的標竿。同時也非常感謝黃凱風老師和蘇冠暉老師給予的寶貴建議讓論文更為完善。再來感謝實驗室的同仁，跟你們相處好像又回到那純真又充滿活力的學生時代，感謝哲彥初期的指導，感謝威哲大力的幫忙，另外很開心能認識彥廷、興弛、怡萍、郁仁、舜子、小江、毓捷、建至、段必、易純、小佑、政猷及容辰。

感謝籃球校隊陳忠強教練讓我有幸參與學校一年一度重要的梅竹賽事，讓我見識到年輕人的熱血，比賽的盛況將永遠烙印在我心中。

感謝公司的長官願意在人力窘困情況下仍讓我出來進修，感謝伯澤、寵棟、舜治和威霖在工作上的協助，讓我在繁忙的任務中得以抽空出來進修。

最後要感謝我的太太佩璇和我的家人，有妳們的鼓勵與協助，才能讓我克服許多低潮和挫折並全力以赴完成課業與論文。

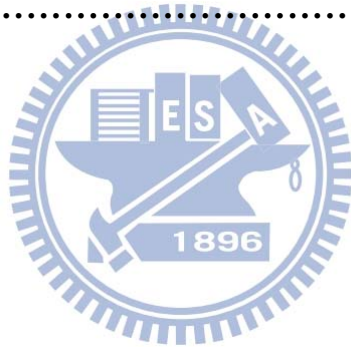
Contents

Abstract (Chinese)	I
Abstract	II
Acknowledgement	IV
Contents	V
List of tables	VIII
List of figures	IX

Chapter 1 Overview	1
1.1 Fiber lasers	2
1.1.1 History.....	2
1.1.2 Advantages.....	4
1.2 Fiber concept	6
1.2.1 Ytterbium doped fiber	6
1.2.2 Double-cladding fibers(DCFs)	8
1.2.3 Photonic crystal fibers(PCFs)	9
1.3 Q-switching	11
1.3.1 Types of Q-switching.....	12
1.3.2 Passively Q-switching laser	15
1.4 Motivation	19
Reference	21
Chapter 2 Passively Q-switched double-cladding fiber lasers	28
2.1 Passively Q-switched double-cladding fiber laser with AlGaInAs quantum wells	29
2.1.1 Introduction.....	29
2.1.2 Characteristics of semiconductor saturable absorber	30
2.1.3 Experimental setup	30
2.1.4 Results and discussions.....	32
2.1.5 Conclusion	34
2.2 Comparative studies for Cr⁴⁺:YAG crystal and AlGaInAs quantum wells in passively Q-switched double-cladding fiber lasers	35
2.2.1 Introduction.....	35

2.2.2	Characteristics of saturable absorbers	36
2.2.3	Experimental setup	37
2.2.4	Results and discussions.....	39
2.2.5	Conclusion	43
	Reference.....	44
Chapter 3	<i>Passively Q-switched photonic crystal fiber lasers.....</i>	47
3.1	Passively Q-switched photonic crystal fiber laser with AlGaInAs quantum wells.....	48
3.1.1	Introduction.....	48
3.1.2	AlGaInAs QWs absorber and experimental setup	49
3.1.3	Experimental results and discussions.....	52
3.1.4	Conclusion	58
3.2	A widely tunable eye-safe based on a passively Q-switched PCF laser	59
3.2.1	Introduction.....	59
3.2.2	Diode pumped PCF laser with AlGaInAs semiconductor absorber.....	60
3.2.3	Tunable eye-safe laser with an external-cavity OPO	64
3.2.4	Conclusion	67
3.3	Passively Q-switched photonic crystal fiber laser with Cr ⁴⁺ :YAG and its application	68
3.3.1	Introduction.....	68
3.3.2	Experiment setup	69
3.3.3	Experimental results and discussions.....	70
3.3.4	The application for OPO	72
3.3.5	Conclusion	75
	Reference.....	76
Chapter 4	<i>Passively Q-switched fiber laser based on a MOFA configuration.....</i>	85
4.1	Passively Q-switched double-cladding fiber amplifier	86
4.1.1	Introduction.....	86
4.1.2	Analysis and optimization of the PQS laser	87
4.1.3	Experimental results for the PQS laser.....	92
4.1.4	Experimental results for the mopa system	94
4.1.5	Conclusion	98
4.2	Passively Q-switched photonic crystal fiber amplifier and its applications.....	100

4.2.1	Introduction.....	100
4.2.2	Single-stage rod-like fiber amplifier.....	101
4.2.3	Second and third harmonic generation.....	104
4.2.4	Conclusions.....	107
	Reference.....	108
Chapter 5 Summary and Future works		113
5.1	Summary.....	114
5.1.1	Passively Q-switched double-cladding fiber lasers	114
5.1.2	Passively Q-switched photonic crystal fiber lasers	114
5.1.3	Passively Q-switched fiber laser based on a MOFA configuration	115
5.2	Future work.....	116
	Reference.....	116
Curriculum Vitae.....		117
Publication List.....		118



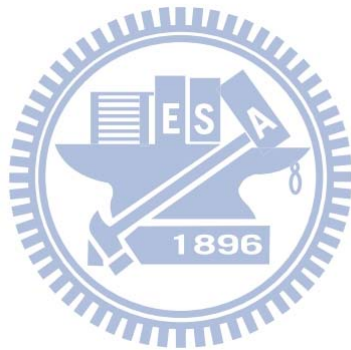
List of tables

Chapter 1

Table 1. 1 The reported values of σ_{gs} and σ_{es} of the Cr^{4+} :YAG crystal	18
--	----

Chapter 5

Table 5. 1 Performances of the passively Q-switched fiber laser	114
Table 5. 2 Performances of the passively Q-switched PCF laser.....	115
Table 5. 3 Performances of the OPO.....	115
Table 5. 4 The performances of MOFA-based fiber lasers seeded by Nd:YVO ₄ /Cr ⁴⁺ :YAG PQS lasers	115



List of figures

Chapter 1

Fig 1. 1 Growth in multimode and single-mode reliable continuous waves power for 9XX-nm [11].	3
Fig 1. 2 The structure of an optical fiber.	4
Fig 1. 3 The optical fiber can be designed to support multimode or single mode.	5
Fig 1. 4 An optical fiber has a good thermal dissipation due to (a) a large ratio of heat-dissipating surface to active volume and (b) a long length.	5
Fig 1. 5 Energy levels of Yb ³⁺ ions.	7
Fig 1. 6 Absorption and emission cross sections of Yb ³⁺ in silica glass [21].	7
Fig 1. 7 Double-cladding fiber structure.	8
Fig 1. 8 Various designs of double-clad fibers.	9
Fig 1. 9 Microscope picture of a 7-cell core Yb-doped air-clad fiber.	10
Fig 1. 10 Q-switching can be achieved by rotating one of the laser mirrors at a high speed.	12
Fig 1. 11 Electrooptic Q-switching is achieved by placing a Pockels cell and polarizer in the laser cavity. Vertical polarization is maintained when $V = 0$. When a voltage $V = V_{\pi/2}$ is applied, the polarization is rotated from vertical to horizontal after passing through the Pockels cell twice.	13
Fig 1. 12 In acousto-optic Q-switching, sound waves create a refractive-index grating that diffracts part of the beam, spoiling the Q of the cavity.	14
Fig 1. 13 Placing a saturable absorber inside the laser cavity causes the laser to self-Q-switch.	15
Fig 1. 14 Nonlinear transmission of a saturable absorber versus fluence normalized to the saturation fluence E_s of the absorber [47].	15
Fig 1. 15 Schematic energy-level diagram of Cr ⁴⁺ : YAG with ESA. The solid lines indicate optical transitions and the dashed lines indicate non-radiative transitions. The non-radiative relaxation 4-3, 2-1, and 5-3 are much faster than the lifetime of the excited state 3.	17
Fig 1. 16 Energy gap versus lattice constant in InGaAs-InP-InAlAs system.	18
Fig 1. 17 Structure of periodic AlGaInAs QWs saturable absorbers. The periodic structure means the region of the saturable absorbers consist periodic groups of several QWs, spaced at half-wavelength intervals by barrier layers.	18

Chapter 2

Fig 2. 1 Transmittance spectrum at room temperature for the AR- coated AlGaInAs/InP saturable absorber. Inset, schematic diagram of a periodic AlGaInAs QW structure.	31
Fig 2. 2 Schematic diagram of the experimental setup. HR, high reflection; HT, high transmission.	31
Fig 2. 3 Average output powers at 1066 nm with respect to the incident pump power in cw and passively Q-switching operations.....	33
Fig 2. 4 Experimental results for the pulse repetition rate and the pulse energy versus incident pump power.....	33
Fig 2. 5 Expanded shape of a single pulse and (b) typical oscilloscope trace of a train of output pulses.....	34
Fig 2. 6 Saturation transmission of the AlGaInAs QWs and the Cr ⁴⁺ :YAG crystal. ...	37
Fig 2. 7 Schematic of diode-pumped PQS Yb-doped fiber lasers. (a) with Cr ⁴⁺ :YA crystal (b) with AlGaInAs QWs. HR: high reflection; HT: high transmission. ...	38
Fig 2. 8 Dependence of the average output power on the launched pump power for the cw and passive Q-switching operations.....	39
Fig 2. 9 (a) Pulse repetition rate and (b) pulse energy versus the launched pump power.	41
Fig 2. 10 Pulse energy versus the resonant wavelength.....	42
Fig 2. 11 Top: Oscilloscope traces of a typical Q-switched envelope; Bottom: Oscilloscope traces of a train of Q-switched pulses.	42

Chapter 3

Fig 3. 1 Schematic diagrams of three periodic AlGaInAs QWs structures.....	51
Fig 3. 2 ... Low-intensity transmittance spectrum of the three QW saturable absorbers.	51
Fig 3. 3 (a) Setup for the passively Q-switched PCF laser; (b) image of the cross section of PCF.	52
Fig 3. 4 Average output power with respect to launched pump power in CW and passive Q-switching operations.	53
Fig 3. 5 Pulse repetition rates in the passive Q-switching operation versus the	

launched pump power.	54
Fig 3. 6 Typical oscilloscope traces for the single Q-switched pulses of the lasers with the saturable absorbers of (a) 2×30 , (b) 3×30 , and (c) 3×50 QWs, respectively.	56
Fig 3. 7 Typical oscilloscope traces for a train of output pulses of the lasers with the saturable absorbers of (a) 2×30 , (b) 3×30 , and (c) 3×50 QWs, respectively.	57
Fig 3. 8 Schematic sketch of the external-cavity optical parametric oscillator pumped by the passively Q-switched photonic crystal fiber laser.	60
Fig 3. 9 Image of cross section of rod-type PCF.	62
Fig 3. 10 Transmission spectrum and structure of AlGaInAs saturable absorber.	63
Fig 3. 11 Output power of the passively Q-switched PCF laser versus the 976-nm launched pump power. Inset is the lasing spectrum obtained with 12.5 W of pump power.	63
Fig 3. 12 Typical oscilloscope traces of output pulses of the passively Q-switched PCF laser. (a) pulse shape with 6.3 W of pump power and (b) pulse shape with 13.1 W of pump power	64
Fig 3. 13 Schematic sketch of the OPO setup. A half-wave plate and polarization beam splitter cube were settled in front of OPO to control the input pump power.	65
Fig 3. 14 Output performance of external-cavity OPO. (a) averaged output power of signal wave versus averaged power of PCF laser and (b) temporal traces of pump and signal wave.	66
Fig 3. 15 Tuning curve of signal wavelength versus different operating temperature. Inset is the corresponding conversion efficiency with temperature.	66
Fig 3. 16 Setup for the passively Q-switched PCF laser with Cr^{4+} :YAG.	70
Fig 3. 17 (a) Average output power with respect to launched pump power in CW and passive Q-switching operations, the inset: typical lasing spectrum. (b) Pulse repetition rate and pulse energy versus launched pump power.	71
Fig 3. 18 Typical oscilloscope traces for (a) single Q-switched pulse and (b) Q-switched pulse train.	72
Fig 3. 19 Setup for the intracavity OPO pumped by the passively Q-switched PCF laser.	72
Fig 3. 20 (a) Average output power at 1515 nm with respect to launched pump power. (b) OPO pulse repetition rate and pulse energy versus launched pump	

power.....	74
Fig 3. 21 General oscilloscope traces for the fundamental (top) and OPO signal (bottom) output pulses.	74

Chapter 4

Fig 4. 1 Schematic diagram of the plano-concave cavity. (b) Equivalent cavity.....	88
Fig 4. 2 Dependence of the mode-to-pump size ratio ω_1/ω_{pa} on the pump power for different pumping spot radii.....	91
Fig 4. 3 Effective mode area ratio of A/A_s as a function of the pump power in the Nd:YVO ₄ /Cr ⁴⁺ :YAG PQS laser with $L = 0.9\rho_1$, $\rho_1 = 25$ mm, $\omega_p = 100$ μ m.	91
Fig 4. 4 Schematic diagram of a diode-pumped Nd:YVO ₄ laser PQS with a Cr ⁴⁺ :YAG as a saturable absorber. HR:high reflection. HT:high transmission.....	92
Fig 4. 5 (a) Dependence of the pulse repetition rate and the pulse energy on the initial transmission of Cr ⁴⁺ :YAG at the pump power of 5.4 W. (b) Dependence of the pulse width and the peak power on the initial transmission of Cr ⁴⁺ :YAG at the pump power of 5.4 W.....	93
Fig 4. 6 Oscilloscope traces of a single pulse of (a) PQS laser with Cr ⁴⁺ :YAG of $T_0 = 0\%$, (b) PQS laser with Cr ⁴⁺ :YAG of $T_0 = 40\%$	94
Fig 4. 7 (a) Scheme of the MOFA setup. HT: high transmission HR: high reflection. (b) Cross section of the PM Yb-doped fiber.....	95
Fig 4. 8 (a) Average output power and peak power of MOFA with the seed of repetition rate of 50 kHz as a function of the launched pump power. (b) Oscilloscope traces of a single pulse of the output pulse of the amplifier. (c) Oscilloscope traces of a train of amplified pulses.	96
Fig 4. 9 (a) Average output power and peak power of MOFA with the seed of repetition rate of 25 kHz as a function of the launched pump power. (b) Oscilloscope traces of a single pulse of the output pulse of the amplifier. (c) Oscilloscope traces of a train of amplified pulses.	97
Fig 4. 10 End view and side view of the damaged fiber.....	98
Fig 4. 11 Optical spectra of the MOFAs at the maximum output powers injected by the seed lasers with $T_0 =$ (a) 70 and (b) 40%.	98
Fig 4. 12 Schematic sketch of the extracavity harmonic generations pumped by a	

single-stage rod-like photonic crystal fiber amplifier. HR: high reflection; HT:
high 103

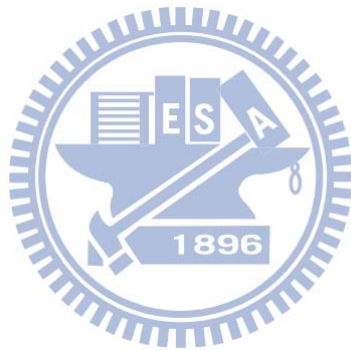
Fig 4. 13 Relevance of the average output power and the pulse energy with the..... 103

Fig 4. 14 Oscilloscope traces of a train of amplified pulses. (b) Oscilloscope trace . 104

Fig 4. 15 Schematic sketch of the setup of the SHG and THG. AR: anti-reflection. 106

Fig 4. 16 Dependences of the average output power at 532 nm and 355 nm on the . 106

Fig 4. 17 (a) Oscilloscope traces of a train of output pulses of 532 nm (top) and 355
..... 107



Chapter 1

Overview



1.1 Fiber lasers

The fiber lasers are a promising alternative to the conventional solid-state laser systems. They are a result of a merger between of the most innovative and advanced technologies in the laser world – active optical fibers and semiconductor diodes. Fiber lasers offer a superior beam quality and reliability, great output powers, high electrical efficiency, and smaller size.

1.1.1 History

The first fiber laser was demonstrated with erbium and neodymium doped glass lasers in 1960 by Snitzer and Koester [1-3]. It consisted of a coiled neodymium-doped fiber transversely pumped by a flash lamp, and emitted around 1060 nm with a multimode output. A few years later, the first longitudinally pumped fiber laser, pumped by a laser diode, was demonstrated by Stone and Burrus [4]. The breakthrough in the fabrication of rare-earth doped silica fiber came in 1985 thanks to the development of solution doping as a way to incorporate rare earths into performs fabricated through modified chemical vapour deposition (MCVD) [5]. Later, a Nd-doped silica single-mode fiber laser was demonstrated by Mears et al. [6]. Since then fiber lasers made with various rare-earth dopants including Nd, Er, Yb, Ho, Dy, and Eu have been investigated [7-8]. However, it is the erbium-doped fiber amplifier (EDFA) for optical telecommunications which catalyzes telecom research. The development of EDFAs, which was spurred by important telecommunication market demands and backed by the immense resources of the telecommunication industry, quickly led to the wide availability of knowledge, components, technologies, and equipment relevant to the development of optical fiber lasers. This, in turn, led to an extensive amount of research being conducted on rare-earth-doped fiber lasers covering continuous wave (CW) lasers, Q-switched lasers, mode-locked lasers, upconversion lasers, and single-frequency lasers in the late 1980s and early 1990s.

Two important technologies boost up the output power of fiber lasers. One is the invention of double-cladding fibers, and the other is rapid process in high power laser diodes.

Initially, the average power from a single-mode fiber laser pumped by the single-mode pump diode was too low for most industry applications. The pump diode can only be coupled into the core of the fiber, so just the single-mode pump diode

which has low-power output can do this work. Consequently the output power of a single-mode fiber laser was confined to the subwatt levels. Higher-power pump diodes with large diameter have multi-mode output, and they can't be coupled efficiently to the core of the fiber. Thus a double-cladding fiber scheme was proposed by Snitzer in 1988 to increase the coupling efficiency of multi-mode pump diodes[9]. The double-cladding fiber, which has a small rare-earth-doped single-mode core embedded in a much larger multimode pump guide, effectively behaves like a brightness converter, which allows conversion of high-power multi-mode pump light to a single-mode laser beam guided in the rare-earth doped single-mode core. The double-cladding fiber's configuration will be described in detail later.

In addition to continuous improvements in crystal growth technologies and the purity of materials sources, refinements in laser design, such as increased efficiency, improved facet passivation technology, robust die attach and advanced heat sinking, drive the growth in the output power of pump diodes [10]. As showed in Fig. 1.1 [11] , both single-mode and multi-mode laser diodes have about 15 percent increase on the output power every year. Nowadays kw-level commercial products of laser diodes are available [12].

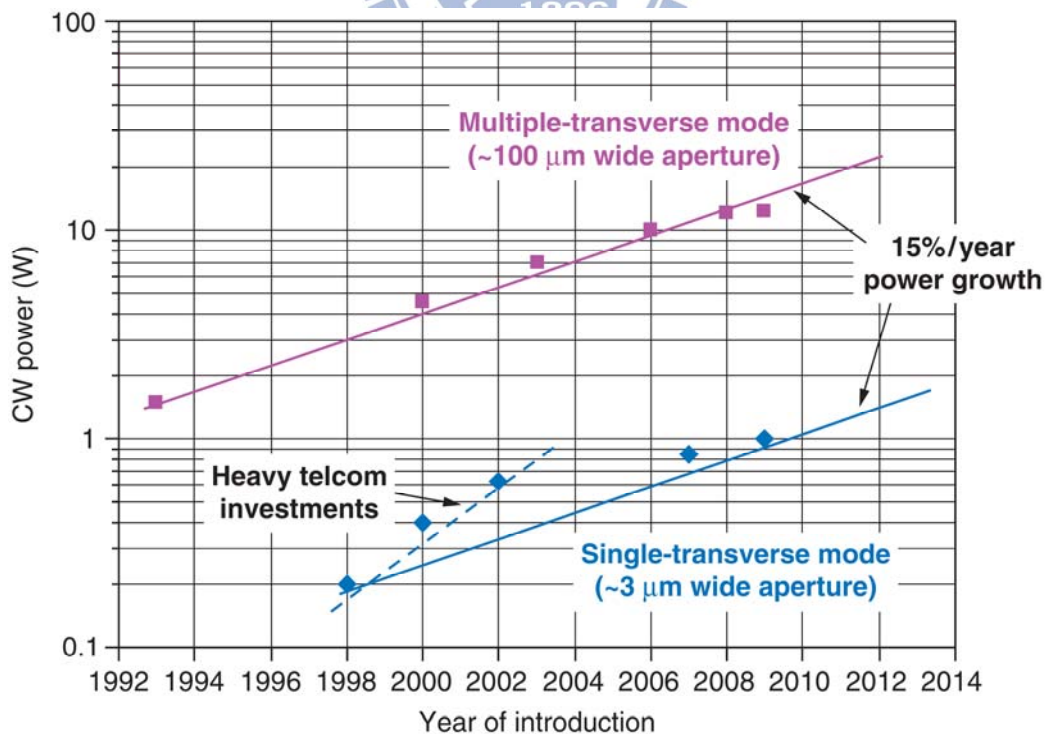


Fig 1. 1 Growth in multimode and single-mode reliable continuous waves power for 9XX-nm [11].

1.1.2 Advantages

An optical fiber is a cylindrical dielectric waveguide made of low-loss material such as a silica glass. It has a central core with refractive index n_1 in which the light is guided, embedded in an outer cladding of slightly lower refractive index n_2 (Fig. 1.2). Light rays, which incident the core at angles lower than the critical angle:

$$\theta_c = \arcsin NA \quad , \quad (1)$$

where NA, numerical aperture:

$$NA = (n_1^2 - n_2^2)^{1/2} \quad , \quad (2)$$

undergo total internal reflection and are guided through the core without the refraction. Rays of greater inclination to the fiber axis lose part of their energy into the cladding at each reflection and are not guided [13]. The V number:

$$V = \frac{2\pi r}{\lambda} NA = \frac{2\pi r}{\lambda} (n_1^2 - n_2^2)^{1/2} \quad , \quad (3)$$

depending on the wavelength λ , the fiber core radius r and the numerical aperture, determines the number of modes of a step-index fiber, and is related to n_1 and n_2 [14]. For single-mode guidance, the V number must be below 2.405 [15]. As showed in Fig. 1.3, thus an optical fiber can be designed properly to support only the lowest-order mode, fundamental LP_{01} mode, without the spatial mode control. So the fiber lasers have excellent beam quality which is very important in many applications [16].

Another significant benefit is the outstanding heat-dissipation capability [17-19], because the fiber has a long length with a large ratio of heat-dissipating surface to active volume, as showed in Fig. 1.4. It essentially does not have the active cooling so that the laser system can be simplified.

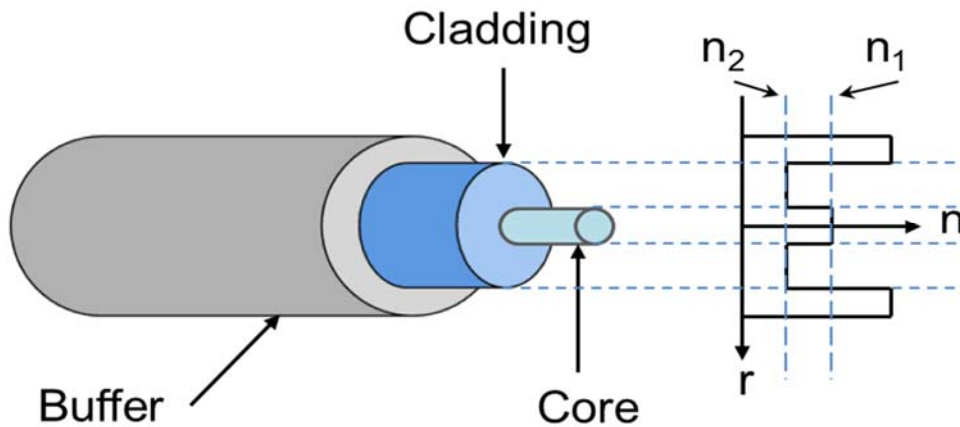


Fig 1. 2 The structure of an optical fiber.

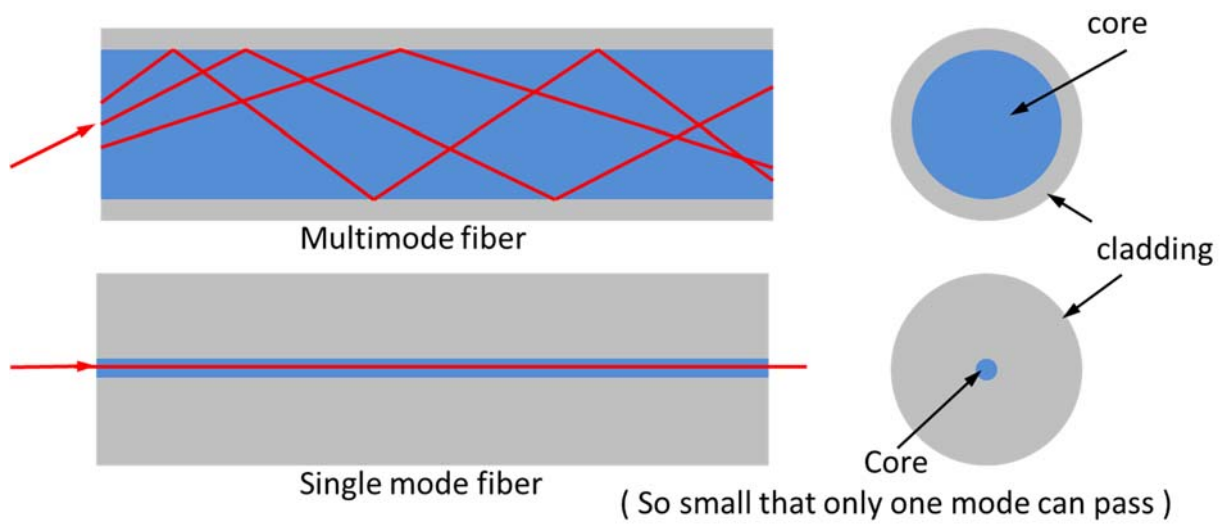


Fig 1. 3 The optical fiber can be designed to support multimode or single mode.

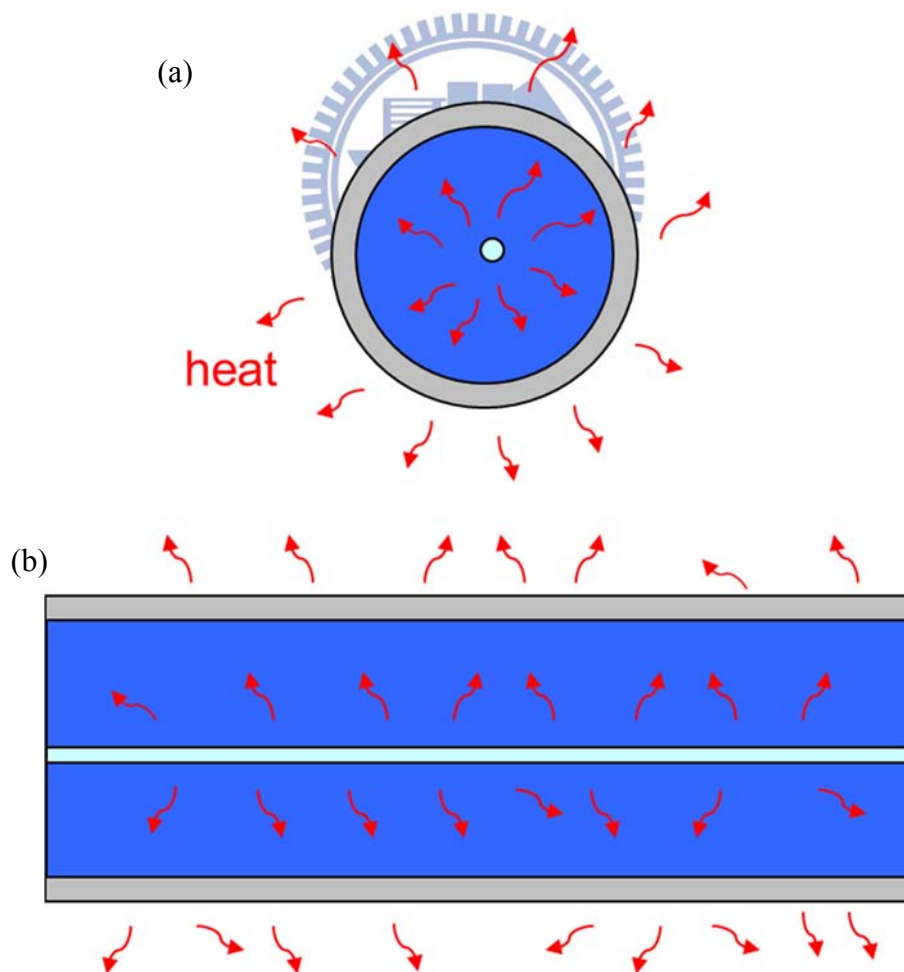


Fig 1. 4 An optical fiber has a good thermal dissipation due to (a) a large ratio of heat-dissipating surface to active volume and (b) a long length

1.2 Fiber concept

1.2.1 Ytterbium doped fiber

Ytterbium (Yb) is a chemical element belonging to the group of rare earth metals. In laser technology, it has acquired a prominent role in the form of the trivalent ion Yb^{3+} , which is used as a laser-active dopant in a variety of host materials, including both crystals and glasses. The energy level of Yb^{3+} ion which consists of two-manifolds; the ground manifolds ($^2F_{7/2}$) and a well separated excited manifolds ($^2F_{5/2}$), which include four and three Stark shifted levels respectively is shown in Fig. 1.5 [20]. Ytterbium doped fiber has a number of interesting properties for high-power fiber lasers. The first property is the Yb^{3+} ion's simple system with low quantum defect which means the pump wavelength is closer to the lasing wavelength. Low quantum defect equals less heat generation, which is a huge plus for high-power lasers. The simple system of ytterbium is also beneficial, because there is no need to worry too much about excited state absorption and cooperative upconversion, both of which are channels for power loss. The upconversion process can also lead to photodarkening, which compromises the long-term reliability of an optical fiber laser. Unlike for Er^{3+} ions, the manifolds of Yb^{3+} ion give distinct transitions in absorption and emission spectra. For a pump wavelength of 976 nm, $a \rightarrow e$ is used, especially for cladding pumped optical fibers due to high pump absorption. For pump wavelengths around 915 nm, $a \rightarrow f$ is sometimes used to provide more tolerance in pump wavelength control; this also allows higher gain per unit length due to the much higher inversion possible when pumped around 915 nm. Two transitions, one at 1025 nm, $e \rightarrow b$, and one at 1080 nm, $e \rightarrow c$, dominate the emission spectra.

The effective absorption and emission cross sections of Yb-doped fibers are shown in Figure 1.6 [21]. The gain bandwidth of the laser transitions is large due to the overlapping of Stark shifted levels which allows for wide wavelength tuning ranges (0.9 μm up to 1.2 μm), or for generating ultrashort pulses in mode-locked lasers. The upper-state lifetimes are relatively long, around 1.5 ms [21], which is beneficial for Q-switching.

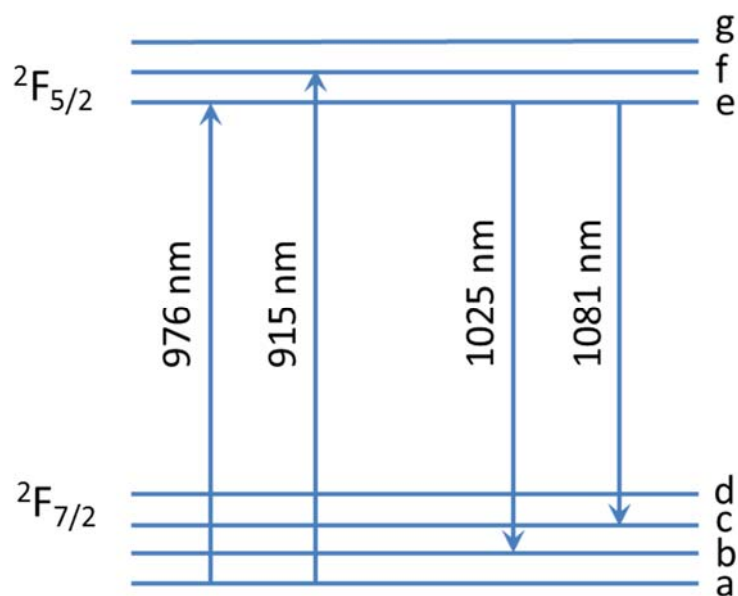


Fig 1. 5 Energy levels of Yb³⁺ ions.

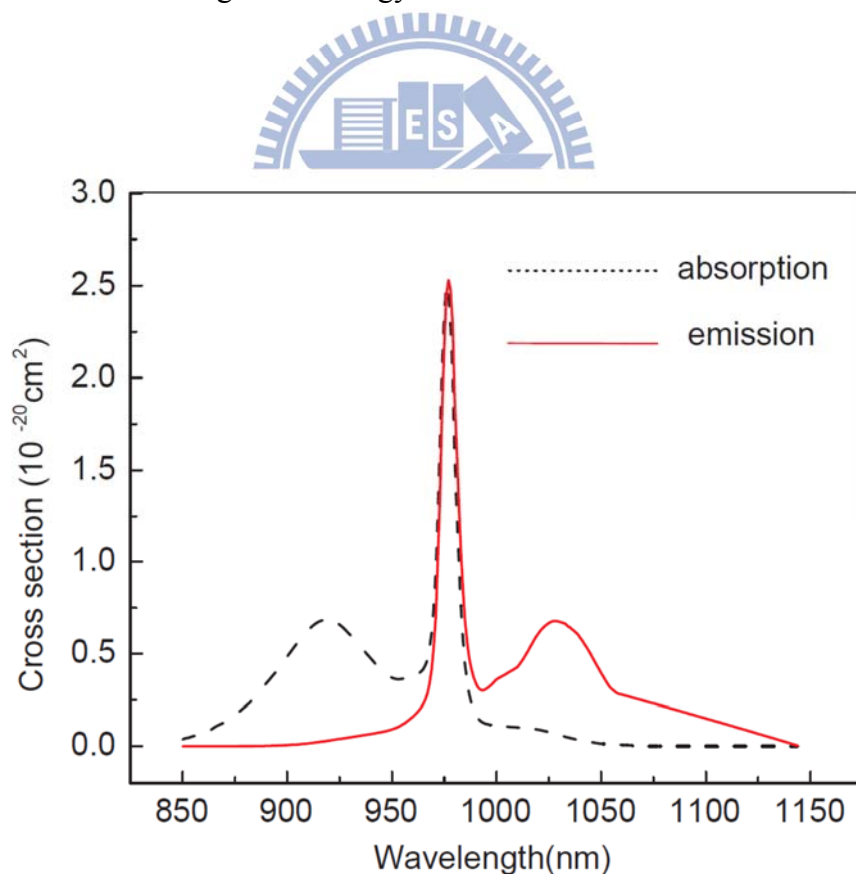


Fig 1. 6 Absorption and emission cross sections of Yb³⁺ in silica glass [21].

1.2.2 Double-cladding fibers(DCFs)

Double-cladding fibers are an important technology in the area of active fiber optics, particularly for high-power fiber lasers [22,23]. In the past a fiber laser based on an ordinary doped single-mode fiber can generate a diffraction-limited output, but it restricts the pump sources to those with diffraction-limited beam quality and thus normally to those with low power. On the other hand, the use of multimode fibers usually leads to poor beam quality. This problem can be solved with the invention of double-cladding fiber designs. These have a pump cladding (inner cladding) around the fiber core, which is itself surrounded by an outer cladding of even lower refractive index. The pump cladding, often having a substantially larger diameter than the fiber core and also a higher numerical aperture, constitutes a multimode waveguide into which high-power pump light can be launched easily and efficiently, even if the pump beam quality is not that great. The refractive index of the core is still higher than that of the pump cladding, so that it supports a single guided mode, or sometimes a few modes. Pump light launched into the inner cladding also gets into the fiber core, where it can be absorbed by laser-active ions. The pump light is gradually absorbed by active core during propagating in the undoped inner cladding. Figure 1.7 shows how pump light is injected into the inner cladding, while signal light is injected into the fiber core and remains there. Thus, the structure of DCF is absolutely a good brightness converter.

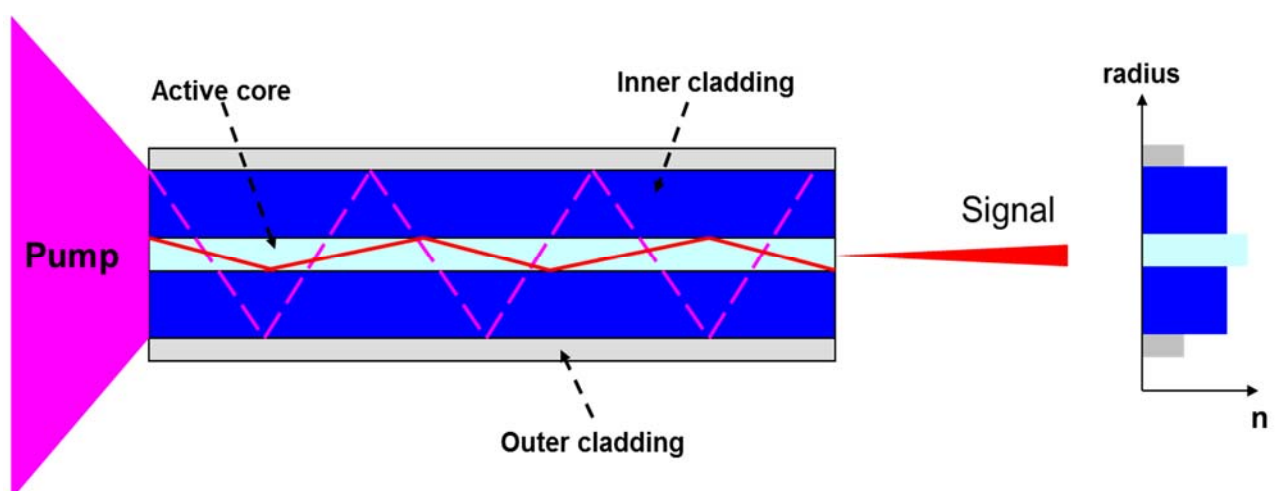


Fig 1.7 Double-cladding fiber structure

However, with increasing the diameter of the pump guide, the number of rays which do not interact with the absorbing core also increase. In particular, helical rays propagating in a meander-like path in the inner cladding have negligible overlap with the core and may be lost at the output side. Destroying the symmetry to make the rays irregular will be helpful to increase the absorption efficiency. Several shapes of inner cladding are proposed to solve the problem [24-26]. Fig. 1.8 shows the different inner cladding designs.

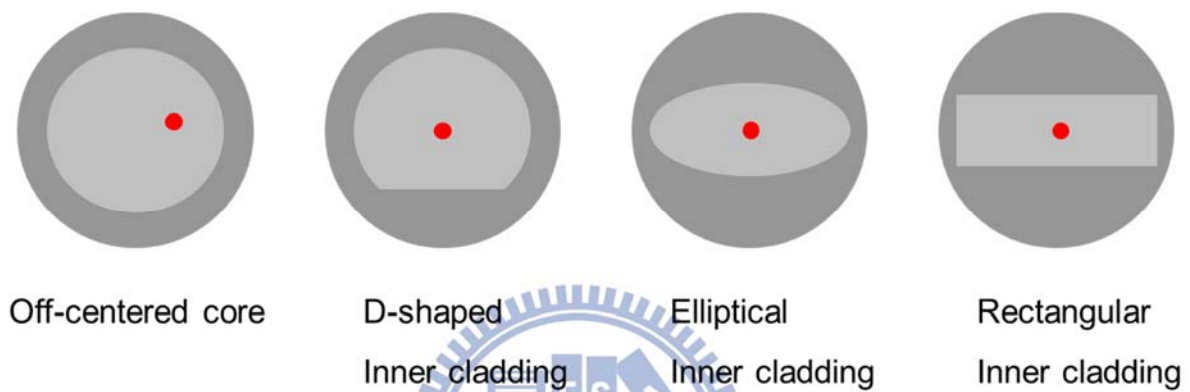


Fig 1. 8 Various designs of double-clad fibers

1.2.3 Photonic crystal fibers(PCFs)

Although DCF can be useful for scaling laser output power, there is some restriction. The limiting factor is the nonlinear effects such as stimulated Brillouin scattering (SBS), stimulated Raman scattering (SRS), self-phase modulation (SPM) and four-wave mixing (FWM) [27]. The nonlinearity of a fiber scales with the fiber length and is inversely proportional to mode-field area. To overcome this issue, specialty fiber of increasingly large diameter and high pump absorption is necessary in the reduction of fiber length. To date, with the development of the fabrication technology modern optical fibers are investigated. Photonic crystal fibers (PCFs), also known as microstructure fibers (MFS), are currently subject of intense research [28-30]. Photonic crystal fibers (PCFs) were first demonstrated in the late 1990s [31,32]. Its potential for achieving single-mode operation with large cores was realized very early on[33]. A photonic crystal fiber obtains its waveguide properties not from a spatially varying glass composition but from an arrangement of very tiny and closely spaced air holes

which go through the whole length of fiber. It is drawn from a hexagonal stack of capillaries, with typically one to seven capillaries replaced by rods in the center. Pressurization of the airholes is typically used to keep the holes from collapsing from surface tension during drawing. The center rods form the core. The composite cladding material of glass and air makes it easy to achieve a very low refractive index contrast between the core and the composite cladding, consequently providing much better control at achieving fibers with large mode field diameters and low NAs [34].

The pump cladding in PCFs is typically made with a layer of airholes with very thin glass webs (as showed in Fig. 1.9). This structure has been demonstrated to be capable of providing an effective pump NA of ~ 1 . In practice, the glass webs must be made thick enough to allow cleaving of the end face [35]. This typically limits pump NAs to ~ 0.6 , which is larger than what is possible with low-refractive index polymers. As a result, high power pump diodes with high NA can be used.

The combination of a large mode field diameter with low NA in the core and high NA in the pump cladding makes it possible to create single-mode lasers with very short fiber lengths, drastically reducing the nonlinear effects. When the nonlinear threshold is increasing, the output of fiber lasers can be scaled up significantly.

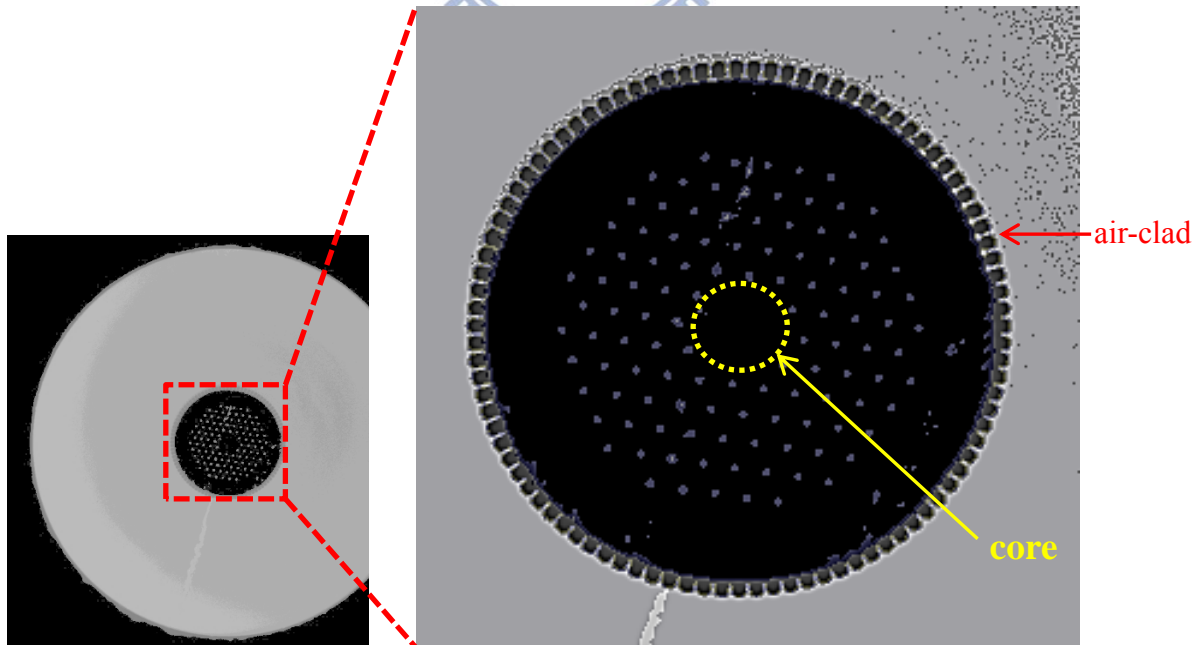


Fig 1. 9 Microscope picture of a 7-cell core Yb-doped air-clad PCF.

1.3 Q-switching

Q-switching is a technique for obtaining high pulse power [36]. The quality factor Q can be defined as the ratio of the energy stored in the cavity to the energy loss per cycle [37]. This technique is used to alter the quality factor of the resonant cavity. Hence the higher the quality factor, the lower the loss. While the laser pumping is in the process, it is necessary to keep the cavity itself from lasing by greatly increasing the loss. Then a large population inversion is developed, we restore, or “switch”, the cavity Q back to its usual large value. The result is a very short, intense burst of laser output which dumps all the accumulated population inversion in a single short laser pulse. The peak power of the resulting pulse exceeds that obtainable from the continuous-wave laser by several orders of magnitude. Lasers to which the Q-switching technique is applied are called Q-switched lasers. The possibility of Q-switched laser was first proposed by Hellwarth in 1961 [38]. The first experimental observation of Q-switched pulse behavior was made by McClung and Hellwarth in 1962 using an electrooptic Q-switch in a ruby laser [39]. A complete theoretical treatment was completed by Wagner and Lengyel in 1963 [40] and a simplified version was given by Wang in the same year [44]. A more elaborate treatment including numerical modeling was performed by Fleck in 1970 [42].

There are several methods that have been developed to achieve switching the Q of the resonator. A key requirement for all these methods is that the cavity Q is changed quickly enough that the population inversion remains nearly constant during the switching process. Generally, a switching time of ~ 10 ns is desirable. When the switching time is too long, multiple pulses may result as the population inversion oscillates above and below threshold. The Q-switching techniques can roughly divide into two categories, active Q-switching and passive Q-switching. For active Q-switching, the losses are modulated with an active control element, typically either an acousto-optic or electro-optic modulator [43,44]. Here, the pulse is formed shortly after an electrical trigger signal arrives. For passive Q-switching, the losses are automatically modulated with a saturable absorber [45,46]. Here, the pulse is formed as soon as the energy stored in the gain medium has reached a high enough level. In the following section, I will discuss the most commonly used methods, including mechanical switches, electro-optic switches, acousto-optic switches, and saturable absorbers.

1.3.1 Types of Q-switching

(a) Mechanical Q-switching

A simple mechanical Q-switching is illustrated in Fig. 1.10. One mirror in the laser cavity is fixed in place, and the other rotates at a high speed about a vertical axis. The Q of the cavity is then high only when the mirrors are parallel within some tolerance. Restricted to the nature of the mechanism, the switching time is so long that multiple pulses will be generated. Mechanical Q-switches are the simplest and least expensive of Q-switches, but they possess relatively short lifetimes and are not robust in harsh environments.

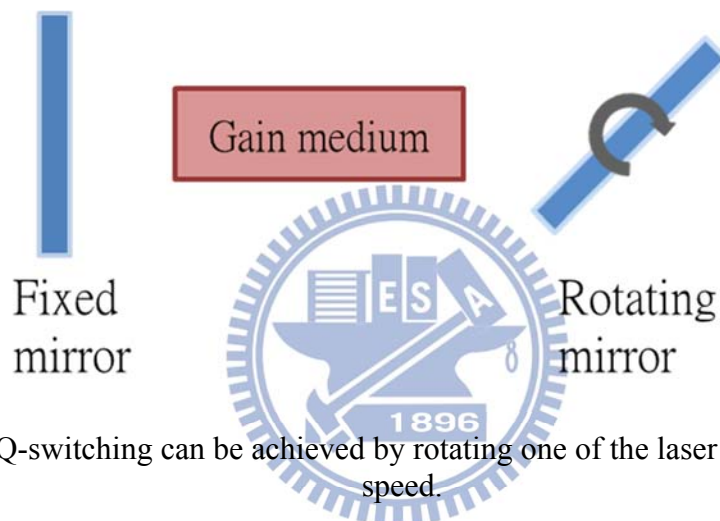


Fig 1. 10 Q-switching can be achieved by rotating one of the laser mirrors at a high speed.

(b) Electro-optics Q-switching

The electro-optics switch is formed by placing two optical elements in the path of the beam inside the cavity, as showed in figure 1.11. The first element is a polarizer, oriented to allow transmission of only one polarization of light. The second element is a Pockels cell, a nonlinear crystal that rotates the polarization of the light when a high voltage is applied. With no applied voltage, vertically polarized light is efficiently transmitted through both elements, and the cavity Q is high. When an appropriate voltage is applied, vertically polarized light is rotated to horizontal polarization in two passes through the nonlinear crystal, and this light is then blocked by the polarizer. The net result is a low Q value when the voltage is applied. The Q-switching process proceeds by initially applying a high voltage to the Pockels cell, and then rapidly removing the voltage, which switches the Q from low to high. This type of Q-switching is in common use, but requires attention to safety because of the high voltages involved.

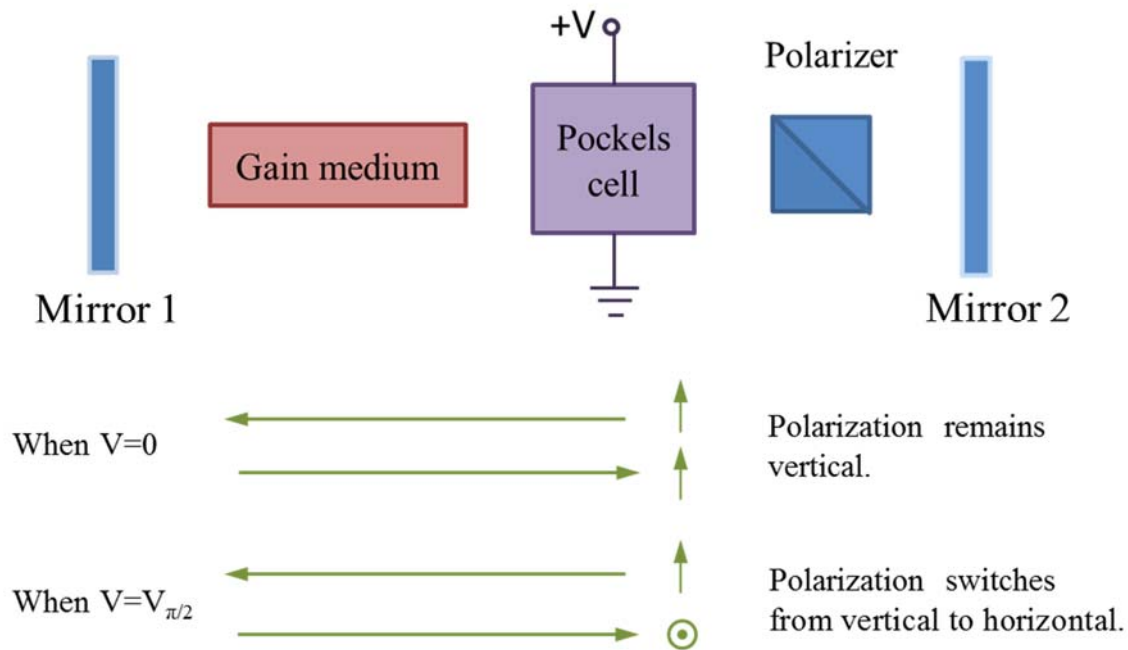


Fig 1. 11 Electrooptic Q-switching is achieved by placing a Pockels cell and polarizer in the laser cavity. Vertical polarization is maintained when $V = 0$. When a voltage $V = V_{\pi/2}$ is applied, the polarization is rotated from vertical to horizontal after passing through the Pockels cell twice.

(c) Acousto-optic Q-switching

In this method, a transparent crystal is inserted into the laser cavity, and high intensity acoustic waves are generated in the crystal by an attached piezoelectric transducer (PZT), as showed in figure 1.12. The acoustic waves create a periodic variation of the crystal's refractive index, which forms a volume-phase grating. Light that is diffracted from this grating increases the cavity loss and decreases Q . The Q-switching process starts with the acoustic waves turned on, such that Q is low enough to prevent lasing. The acoustic waves are then quickly turned off, which increases the Q and enables lasing.

(d) Passive Q-Switching

So far I have considered active Q-switching, in which the time and duration of the change in Q are under active control. The voltage pulse applied to the Pockels cell, or the RF power sent to the acousto-optic deflector, occurs with a timing and repetition rate determined by the user. An alternative approach is to let the laser cavity Q-switch itself, independently of actions by the user. Such a method is termed passive Q-switching.

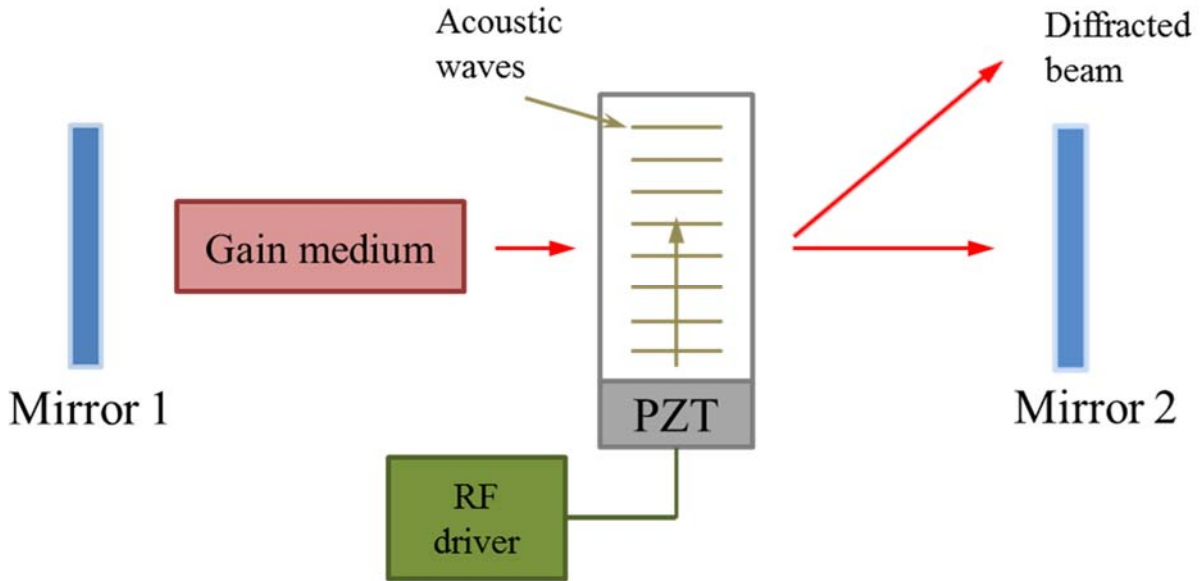


Fig 1. 12 In acousto-optic Q-switching, sound waves create a refractive-index grating that diffracts part of the beam, spoiling the Q of the cavity.

Figure 1.13 depicts that passive Q-switch consists of an optical element, such as a cell filled with organic dye or a doped crystal, which has a transmission characteristic as shown in Fig. 1.14 [47]. The material becomes more transparent as the fluence increases, and at high fluence levels the material saturates or bleaches, resulting in a high transmission. The bleaching process in a saturable absorber is based on saturation of a spectral transition. If such a material with high absorption at the wavelength is placed inside the laser resonator, it will initially prevent laser oscillation. As the gain increases during a pump pulse and exceeds the round-trip losses, the intracavity power density increases dramatically causing the passive Q-switch to saturate. Under this condition the losses are low and a Q-switch pulse builds up. Since the passive Q-switch is switched by the laser radiation itself, it requires no electro-optic driver, or RF generator. As an alternative to active methods, the passive Q-switch offers the advantage of an exceptional simple design, which leads to very small, robust, and low-cost systems.

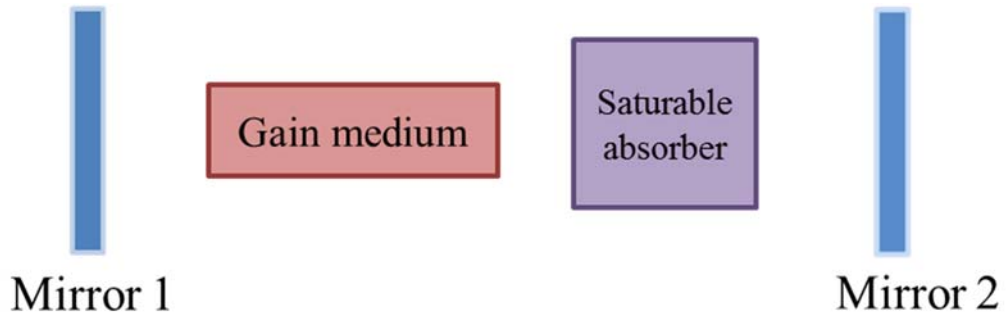


Fig 1. 13 Placing a saturable absorber inside the laser cavity causes the laser to self-Q-switch.

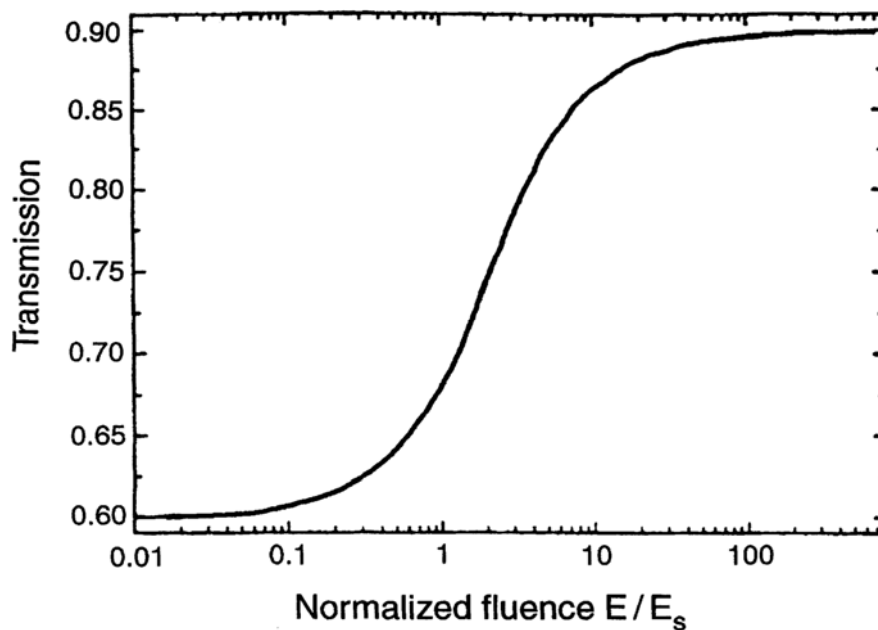


Fig 1. 14 Nonlinear transmission of a saturable absorber versus fluence normalized to the saturation fluence E_s of the absorber [47].

1.3.2 Passively Q-switching laser

Lasers which use the passively Q-switching technique are called passively Q-switching lasers, and so are actively Q-switching lasers. Compared with active Q-switching lasers, passively Q-switching lasers have not only the simplicity of implementation but also the advantages of the generation of a well-defined pulse energy and duration that is insensitive to pumping conditions as long as the pump energy is above the Q-switching threshold.

Originally, saturable absorbers used in passively Q-switching lasers were based on different organic dyes, either dissolved in an organic solution or impregnated in thin films of cellulose acetate [48,49]. The poor durability of dye-cell Q-switches, caused by the degradation of the light sensitive organic dye, and the low thermal limits of plastic materials severely restricted the applications of passive Q-switches in the past. The emergence of crystals doped with absorbing ions or containing color centers has greatly improved the durability and reliability of passive Q-switches. The first new material to appear was the F^{2-} :LiF color center crystal [50]. The color centers are induced in the crystal by irradiation with gamma, electron, or neutron sources. Today, the most common material employed as a passive Q-switch is Cr^{4+} : YAG [51].

In addition to own the desirable chemical, thermal, and mechanical properties required for long life, Cr^{4+} : YAG crystals have characteristics of large absorption cross section and long excited-state lifetime required for optical absorption. The optical energy-level of Cr^{4+} :YAG crystals is shown in Fig. 1.15. The Cr^{4+} :YAG crystal is a four-level system at the absorption band of 1.0~1.1 μm . The solid line and the dash line indicate radiative and non-radiative transitions respectively. The spontaneous emission occurs via transitions from level 3 to the metastable level 2 and the lifetime τ_{3-2} is in the order of 3~4 μs [52,53]. Excited-state absorption (ESA) is included in this figure and the lifetime for the corresponding decay is of the order of ps [54,55]. The ESA acts a loss in the absorption process and results in a degradation of final transmission of saturable absorbable. Fortunately the cross-section of ESA of Cr^{4+} : YAG is small compared to that of ground-state. However the excited cross section can not be neglected and they have been studied for years. The values of the cross sections for ground state absorption and excited state absorption are not known exactly so far and can vary by more than one order of magnitude due to measured cross section depending on the property of incident pump beam such as the pulse repetition rate and pulse duration, and concentration and homogeneity of Cr^{4+} :YAG crystals. Table 1.1 shows the reported results for the σ_{gs} and σ_{es} .

In addition to Cr^{4+} :YAG crystals, semiconductor-based saturable absorber is another most common material employed as a passive Q-switch recently. Semiconductor saturable absorbers offer more flexible parameters such as operating wavelength, modulation depth, unsaturated and saturated absorption, and recovery time. They are achieved by controlling band gap parameters, number of QWs, co-doping or growth technology [59,60]. To date semiconductors have proved to be one of the

excellent candidates for passively Q-switching fiber lasers [61,62]. The main advantage of taking semiconductor material as saturable absorber is their short recovery time in the time scale of ns to ps. Compared with Cr^{4+} : YAG crystals, semiconductors are able to provide large absorption cross section profit capturing photons in Q-switched lasers. Among the semiconductor saturable absorbers, InGaAs and AlGaInP materials are the most common ones in passively Q-switching lasers [61,63-64]. Recently AlGaInAs quaternary alloys semiconductors have been confirmed with the merits of larger conduction band offset [65] (meaning a better electron confinement than InGaAsP materials) and lattice-matching to the InP substrate. It is note that choice of InP based alloys provides higher thermal conductivity than GaAs or AlGaAs based alloys [66, 67]. Figure 1.16 shows the available range of operating wavelength of AlGaInAs. AlGaInAs can be alloyed with the ternary alloys of InAlAs and InGaAs. It is noted they are both lattice-matched to InP substrates with lattice constant of 5.87Å. The energy gap of AlGaInAs is determined by the composition of InAlAs and InGaAs and is tunable from 0.75eV to 1.37eV (1.65 μm to 0.9 μm). The advantages reveal that AlGaInAs quaternary alloys are potentially applicable as saturable absorbers in passively Q-switching lasers [68]. Figure 1.17 shows the structure of the AlGaInAs saturable absorber.

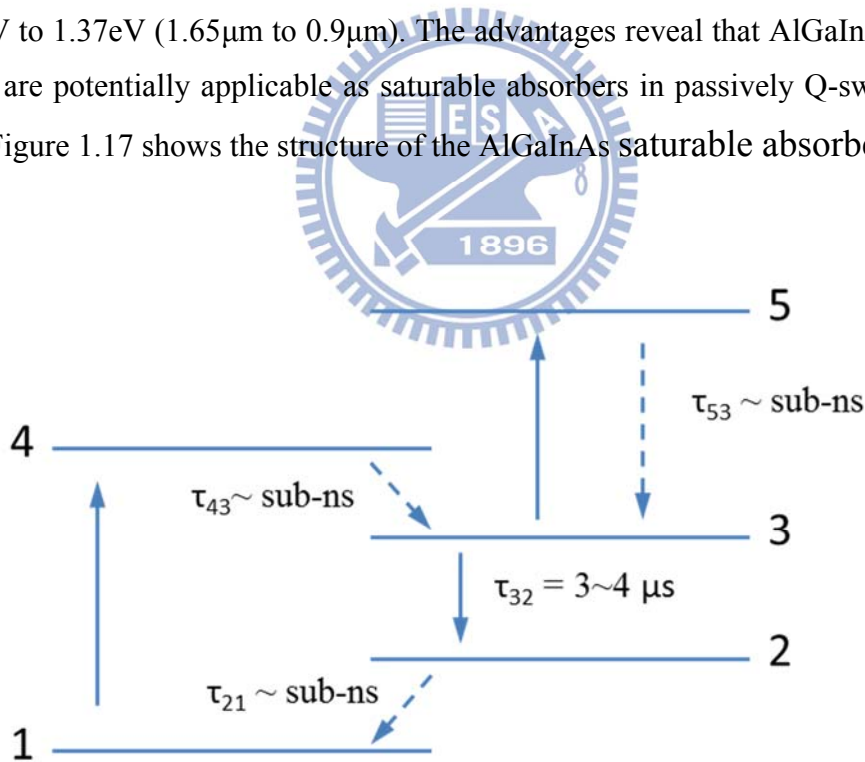


Fig 1. 15 Schematic energy-level diagram of Cr^{4+} : YAG with ESA. The solid lines indicate optical transitions and the dashed lines indicate non-radiative transitions. The non-radiative relaxation 4-3, 2-1, and 5-3 are much faster than the lifetime of the excited state 3.

σ_{gs} (10^{-18} cm ²)	7 ± 0.8	2 ± 0.4	0.87 ± 0.08
σ_{es} (10^{-19} cm ²)	2 ± 0.3	2 ± 0.4	2.2 ± 0.2
$\sigma_{es} / \sigma_{gs}$	0.286	0.1	0.25
Ref.	[56]	[57]	[58]

Table 1. 1 The reported values of σ_{gs} and σ_{es} of the Cr⁴⁺:YAG crystal

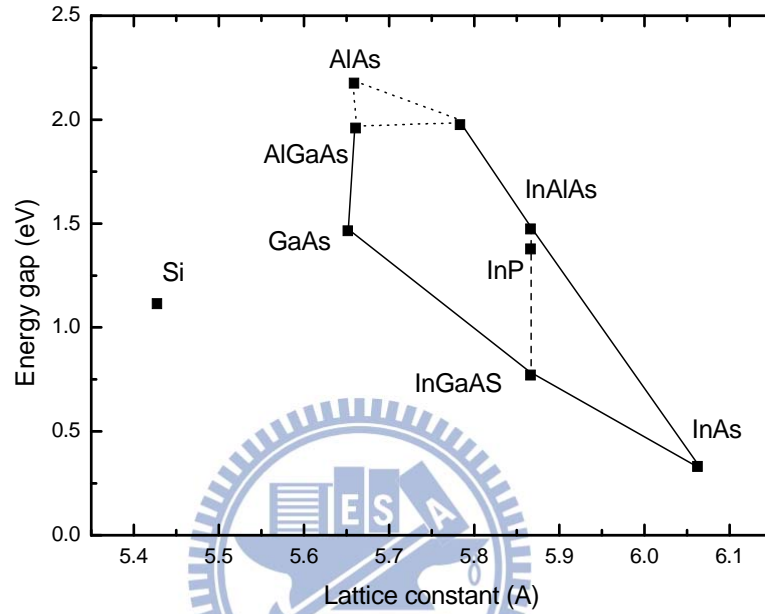


Fig 1. 16 Energy gap versus lattice constant in InGaAs-InP-InAlAs system

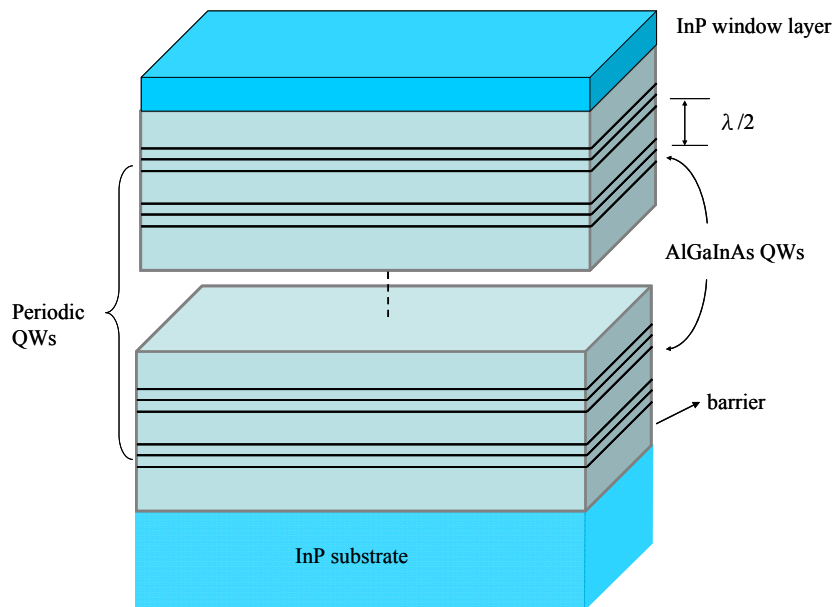


Fig 1. 17 Structure of periodic AlGaInAs QWs saturable absorbers. The periodic structure means the region of the saturable absorbers consist periodic groups of several QWs, spaced at half-wavelength intervals by barrier layers.

1.4 Motivation

Compared with conventional bulk solid-state lasers, fiber lasers have some intrinsic merits and have seen a tremendous growth in both industrial and research markets. Fiber lasers have excellent thermal properties. Their high ratio of heat-dissipating surface to active volume allows efficient thermal dissipation and usually they do not need active cooling. In addition, the property of wave guide tends to reduce thermal distortion of the beam and achieves excellent beam quality independent of the power. Fiber lasers can be fabricated robustly with long lifetime stability and reliability. The cladding pump scheme has enabled the coupling of high power LDs with large NA into the fiber lasers. A pulsed laser may be advantageous over a continuous one in some applications, such as remote sensing, material processing, and medical needs [69-71], due to its higher peak power.

Recently there has been considerable interest in studying Yb doped fiber lasers because of their beneficial properties for a number of applications. With a small quantum defect (difference in the energy of the pump photons and the emitted photons), Yb doped fiber lasers are suitable for high power operation with reduced thermal loading. The relatively long upper-state lifetime of Yb enables more efficient pumping from a given diode pump source and storage of a large amount of energy which is of benefit for Q-switching operation. Many actively and passively Q-switched DC Yb fiber lasers have been reported to date [72-77]. The emission spectrum of Yb is also broad which allows wide wavelength tuning or multi-wavelength lasing [78-81].

Passive Q-switching (PQS) is a sophisticated and an efficient technique to create high-pulse-energy and high-peak-power pulses. Besides, PQS lasers are more compact and lower cost than the active Q-switching cause of that they utilize saturable absorbers (SAs) in replace of acoustic-optic or electro-optic modulators as the Q-switch. Fiber-type SA [82-84] offers the in-line configuration, nevertheless they are restricted by modulation depth to deliver high-pulse-energy laser. Crystal-based and semiconductor-based SAs are other choices of passive Q-switch. Their high mechanical robustness and well-developed fabrication process make them more common in Q-switched fiber lasers [85-87]. In the spectral region of 1.0~1.1 μm , Cr^{4+} :YAG crystals [85] and InGaAs/GaAs quantum wells (QWs) [87] have been adopted to Q-switch fiber lasers. However, the output pulse energy with InGaAs SESAMs in passively Q-switched lasers are limited by the lattice mismatch with the substrate GaAs

for the spectral region of above 1.0 μm . As a consequence, the output pulse energies and the conversion efficiencies with InGaAs/GaAs QWs in passively Q-switched lasers are generally significantly lower than those with Cr^{4+} :YAG crystals. Recently, an AlGaInAs with a periodic QW/barrier structure has been exploited to be an efficient saturable absorber for a passively Q-switched Nd:YVO₄ laser [88]. Compared with InGaAsP materials, the AlGaInAs quaternary alloy with a larger conduction band offset is confirmed to offer a superior electron confinement in the 0.84-1.65 μm spectral region [89-91]. Nevertheless, AlGaInAs/InP QWs have not been employed to passively Q-switching Yb-doped fiber lasers. Therefore, it is interesting to study a passively Q-switching Yb-doped fiber laser with an AlGaInAs/InP QWs saturable absorber, and have a comparison between Cr^{4+} :YAG crystal and AlGaInAs QWs.

To achieve higher pulse energy, it is necessary to enlarge the active volume of the gain medium, corresponding to the doped core size of the fiber. However, the conventional double-cladding fibers suffer from mode-quality degradation and their long lengths usually lead to long pulse widths and low peak powers. For improving these deficiencies, photonic crystal fibers have been developed to provide large single-mode cores and high absorption efficiencies. So far passively Q-switching Yb-doped photonic crystal fiber lasers with AlGaInAs QWs or Cr^{4+} :YAG crystal as the saturable absorber have not been investigated, so I have some studies about these.

The configuration of master oscillator fiber amplifier (MOFA) consists of a seed laser and a fiber amplifier for boosting the output power. Because the output performance is affected by the low-power seed laser which can be easily modulated, shorter pulse width can be attained by shortening the cavity length of the seed laser. Therefore, it is necessary to use the MOFA to have higher-peak-power pulse lasers. Thus I use the MOFA to have some studies.

Reference

1. E. Snitzer, "Proposed fiber cavities for optical lasers", J. Appl. Phys. 32, 36-39 (1961).
2. E. Snitzer, "Optical maser action of Nd^{3+} in a barium crown glass", Phys. Rev. Lett. 7, 444-446 (1961).
3. C. J. Koester, and E. Snitzer, "Amplification in a fiber laser", Appl. Opt. 3, 1182-1186 (1964).
4. J. Stone, and C. A. Burrus, "Neodymium-Doped Silica Lasers in End-Pumped Fiber Geometry", Appl. Phys. Lett. 23(7), 388-389 (1973).
5. Hegarty, J., Broer, M. M., Golding, B., Simpson, J. R., and MacChesney, J. B., "Photon Echoes Below 1 K in a Nd^{3+} -Doped Glass Fiber," Phys. Rev. Lett. 51, 2033-2035 (1983).
6. R. J. Mears, L. Reekie, S. B. Poole, and D. N. Payne, "Neodymium-doped silica singlemode fibre laser", Electron. Lett. 21, 738-740 (1985).
7. S. B. Poole, D. N. Payne, R. J. Mears, M. E. Fermann, and R. I. Laming, "Fabrication and characterization of low-loss optical fibers containing rare earth ions", J. Lightwave Technol. LT-4 (7), 870-876 (1986)
8. J. E. Townsend et al., "Solution-doping technique for fabrication of rare earth doped optical fibres", Electron. Lett. 23, 329-331 (1987)
9. E. Snitzer, H. Po, F. Hakimi, R. Tumminelli, and B. C. McCollum, "Double-clad, offset core Nd fiber laser", in Proc. Opt. Fiber Sensors, New Orleans, 1988, post-deadline paper PD5.
10. Welch, D. F., "A Brief History of High-Power Semiconductor Lasers", IEEE J. Sel. Top. Quant. Electron. 6, 1470-1477 (2000).
11. H. Injeyan and G. D. Goodno, *High-Power Laser Handbook*, McGraw-Hill (2011).
12. Information available from DILAS Diodenlaser GmbH: <http://www.dilas.com/>
13. B. E. A. Saleh and M. C. Teich, *Fundamentals of photonics*, John Wiley & Sons, Inc. (1991).
14. A. W. Snyder and J. D. Love, *Optical Waveguide Theory*, Chapman and Hall, London (1983).
15. D. Gloge, "Weakly guiding fibers", Appl. Opt. 10 (10), 2252 (1971)
16. H. F. Zeng and F. H. Xiao, "The development of Yb-doped double-clad fiber laser

- and its application”, *Laser Tec.* 30(4), 438-441 (2006).
17. K. I. Ueda, "High power fiber lasers", in *Proc. Pacific Rim Conference on Lasers and Electro-Optics (CLEO)*, Chiba, 2001.
 18. L. Zenteno, "High power double clad fibre lasers", *J. Lightwave Technol.* 11(9), 1435-1447, (1993).
 19. D. C. Brown and H. J. Hoffman, "Thermal, stress, and thermo-optic effects in high average power double-clad silica fiber lasers", *IEEE J. Quantum Electron.* 37(2), 207 (2001).
 20. K. Lu and N. K. Dutta, "Spectroscopic properties of Yb-doped silica glass", *J. Appl. Phys.* 91,576–581 (2002).
 21. R. Paschotta, J. Nilsson, A. C. Tropper, and D. C. Hanna, "Ytterbium-doped fiber amplifiers," *IEEE J. Quantum Electron.* 33, 1049-1056 (1997).
 22. A. Tunnermann, T. Schreiber, F. Roser, A. Liem, S. Hofer, H. Zellmer, S. Nolte, and J. Limpert, "The renaissance and bright future of fibre lasers," *Journal of Physics B-Atomic Molecular and Optical Physics* 38, S681-S693 (2005).
 23. J. Limpert, F. Roser, S. Klingebiel, T. Schreiber, C. Wirth, T. Peschel, R. Eberhardt, and A. Tunnermann, "The rising power of fiber lasers and amplifiers," *Ieee Journal of Selected Topics in Quantum Electronics* 13, 537-545 (2007).
 24. V. Doya, O. Legrand, and F. Mortessagne, "Optimized absorption in a chaotic doubleclad fibre amplifier", *Opt. Lett.* 26(12), 872 (2001).
 25. P. Leproux, S. Février, "Modeling and optimization of double-clad fibre amplifiers using chaotic propagation of the pump", *Opt. Fibre Technol.* 7(4), 324 (2001).
 26. A. Liu, K. Ueda, "The absorption characteristics of circular, offset, and rectangular double-clad fibers," *Opt. Commun.* 132(5-6) 511 (1996).
 27. G. P. Agrawal, *Nonlinear Fiber Optics*, Academic, San Diego, Calif. (1995).
 28. A. Bjarklev, J. Broeng, A.S. Bjarklev, *Photonic crystal fibres*, Kluwer Academic Publishers (2003).
 29. P. Russell, "Photonic crystal fibers," *Science* 299, 358-362 (2003).
 30. J. C. Knight, "Photonic crystal fibres," *Nature* 424,847-851 (2003).
 31. J. C. Knight, T. A. Birks, P. Russell, and D. M. Atkin, "All-Silica Single-Mode Optical Fiber with Photonic Crystal Cladding," *Opt. Lett.* 21, 1547-1549 (1996).
 32. T. A. Birks, J. C. Knight, and P. Russell, "Endless Single-Mode Photonic Crystal Fiber," *Opt. Lett.* 22, 961-963 (1997).

33. J. C. Knight, T. A. Birks, R. F. Cregan, P. Russell, and J. P. de Sandro, "Large Mode Area Photonic Crystal Fiber," *Electron. Lett.* 34, 1347-1348 (1998).
34. J. Limpert, A. Liem, M. Reich, T. Schreiber, S. Nolte, H. Zellmer, A. Tunnermann, et al., "Low-Nonlinearity Single-Transverse-Mode Ytterbium-Doped Photonic Crystal Fiber Amplifier," *Opt. Express* 12, 1313-1319 (2004).
35. K. P. Hansen, J. Broeng, A. Petersson, M. D. Nielsen, P. M. W. Skovgaard, et al., "High-power photonic crystal fibers," *Proc. of SPIE*, 6102, 61020B-1 (2006).
36. C. C. Wang. "Optical giant pulses from a Q-switched laser," *Proc. of the IEEE*, 51 (12), 1767-1767 (1963).
37. J. T. Verdeyen, *Laser electronics*, Prentice-Hall third ed. (1995).
38. R. W. Hellwarth, "Control of Fluorescent Pulsations," *Advances in Quantum Electronics*, ed J. R. Singer, 334-341 (1961).
39. F. J. McClung and R. W. Hellwarth. "Giant Optical Pulsations from Ruby," *J. Appl. Phys.* 33, 828 (1962).
40. W. G. Wagner and B. A. Lengyel, "Evolution of the Giant Pulse in a Laser," *J. Appl. Phys.* 34, 2040(1963).
41. C. C. Wang, "Optical giant pulses from a Q-switched laser," *Proc. IEEE* 51(12), 1764 (1963).
42. J.A. Fleck, " Ultrashort-Pulse Generation by Q-Switched Lasers," *Phys. Rev. B* 1 (1), 84 (1970).
43. J. Limpert, N. Deguil-Robin, S. Petit, I. Manek-Hönninger, F. Salin, P. Rigail, C. Hönninger, and E. Mottay, "High power Q-switched Yb-doped photonic crystal fiber laser producing sub-10 ns pulses," *Appl. Phys. B* 81, 19 (2005).
44. O. Schmidt, J. Rothhardt, F. Röser, S. Linke, T. Schreiber, K. Rademaker, J. Limpert, S. Ermeneux, P. Yvernault, F. Salin, and A. Tünnermann, " Millijoule pulse energy Q-switched short-length fiber laser, " *Opt. Lett.* **32**, 1551 (2007).
45. J. Dong, P. Deng, Y. Liu, Y. Zhang, J. Xu, W. Chen and X. Xie, "Passively Q-switched Yb:YAG laser with Cr⁴⁺:YAG," *Appl. Opt.* 40, 4303 (2001).
46. G. J. Spuhler, R. Paschotta, M. P. Kullberg, M. Graf, M. Moser, E. Mix, G. Huber, C. Harder and U. Keller, "A passively Q-switched Yb:YAG microchip laser ," *Appl. Phys. B* 72, 285 (2001).
47. W. T. Rhodes, et al., *Solid-State Laser Engineering*, Springer sixth ed. (2006).
48. P. P. Sorokin and J. R. Lankard, "Stimulated emission observed from an organic dye, chloro-aluminum phthalocyanine," *IBM J. Res. Dev.* 10, 162 (1966)

49. F. P. Schäfer, et al., "Organic dye solution laser," *Appl. Phys. Lett.* 9 (8), 306 (1966)
50. V. A. Buchenkov, A. G. Kalintsev, A. A. Mak, L. N. Soms, A. I. Stepanov, and A. A. Tarasov, "Characteristics of YAG:Nd³⁺ lasers passively Q switched by LiF crystals containing color centers," *Sov.J. Quantum Electron.* 11(10), 1367-1368 (1981)
51. H. Ridderbusch and T. Graf, "Saturation of 1047- and 1064-nm absorption in Cr⁴⁺:YAG crystals," *IEEE J. Quantum Electron.* 43 (2), 168 (2007)
52. Y. Shimony, Z. Burshtein, and Y. Kalisky, "Cr⁴⁺ :YAG as passive Q-switch and brewster plate in a pulsed Nd:YAG laser," *IEEE J. Quantum Electron.* 31, 1738-1741 (1995).
53. Z. Burshtein, P. Blau, Y. Kalisky, Y. Shimony, and M. R. Kokta, "Excited-state absorption studies of Cr⁴⁺ ions in several garnet host crystals," *IEEE J. Quantum Electron.* 34, 292-299 (1998).
54. S. H. Yim, D. R. Lee, B. K. Rhee, and D. Kim, "Nonlinear absorption of Cr⁴⁺ :YAG studied with lasers of different pulsewidth," *Apl. Phys. Lett.* 73, 3193-3195 (1998).
55. N. I. Borodin, V. A. Zhitnyuk, A. G. Okhrimchuk, and A. V. Shestakov, "Oscillation of a Y₃Al₅O₁₂ : Cr⁴⁺ laser in wave length region of 1.34-1.6 μm," *Izvestiya Akademii Nauk SSSR* 54, 1500-1506 (1990).
56. Z. Burshtein, P. Blau, Y. Kalisky, Y. Shimony, M.R. Kokta, "Excited-State Absorption Studie of Cr⁴⁺ Ions in Several Garnet Host Crystals," *IEEE J. of Quantum Electron.* 34, 292–299 (1998).
57. R. Moncorge, H. Manna, F. Deghoul, Y. Guyot, Y. Kalisky, S.A. Pollack, E.V. Zharikov, M. Kokta, "Saturable and excited state absorption measurements in Cr⁴⁺:LuAG single crystals," *Optics Commun.* 132, 279–284 (1996).
58. Y. Shimony, Z. Burshtein and Y. Kalisky, "Cr⁴⁺:YAG as passive Q-switch and Brewster plate in a pulsed Nd:YAG laser," *IEEE J. Quantum Electron.* 31, 1738-1741 (1995).
59. M. Haiml, R. Grange, U. Keller, "Optical characterization of semiconductor saturable absorbers," *Appl. Phys. B* 79, 331 (2004).
60. U. Keller, K. J. Weingarten, F. X. Kärtner, D. Kopf, B. Braun, I. D. Jung, R. Fluck, C. Hönniger, N. Matuschek, J. Aus der Au, "Semiconductor saturable absorber mirrors (SESAMs) for femtosecond to nanosecond pulse generation in solid-state

- lasers," *IEEE J. Selected Topics in Quantum Electronics (JSTQE)* 2, 435-453 (1996).
61. T. Hakulinen and O. G. Okhotnikov, "8 ns fiber laser Q switched by the resonant saturable absorber mirror," *Opt. Lett.* 32, 2677-2679 (2007).
 62. S. Kivistö, R. Koskinen, J. Paajaste, S. D. Jackson, M. Guina, and O. G. Okhotnikov, "Passively Q-switched Tm^{3+} , Ho^{3+} -doped silica fiber laser using a highly nonlinear saturable absorber and dynamic gain pulse compression," *Opt. Express* 16, 22058-22063 (2008).
 63. J.Y. Huang, H.C. Liang, K.W. Su, H.C. Lai, Y.F. Chen and K.F. Huang, "InGaAs quantum-well saturable absorbers for a diode-pumped passively Q-switched Nd:YAG laser at 1123 nm," *Appl. Opt.* 46, 2, 239-242 (2007).
 64. A. Li, S.C. Liu, K.W. Su, Y.L. Liao, S.C. Huang, Y.F. Chen, K.F. Huang, "InGaAsP quantum-wells saturable absorber for diode-pumped passively Q-switched 1.3- μm lasers," *Appl. Phys. B* 84, 3, 429-431 (2006).
 65. K. Alavi, H. Temkin, W. R. Wagner, and A. Y. Cho, "Optically pumped 1.55- μm double heterostructure $Ga_xAl_yIn_{1-x-y}As/Al_uIn_{1-u}As$ lasers grown by molecular beam epitaxy," *Appl. Phys. Lett.* 42, 254-256 (1983).
 66. S.T. Huxtable, A. Shakouri, C. Labounty, X. Fan, P. Abraham, Y.J. Chiu, J.E. Bowers and A. Majumdar, "Thermal conductivity of indium phosphide based superlattices," *Microscale. Thermophys Eng* 4, 197–203 (2000).
 67. V. Spagnolo, M. Troccoli, C. Gmachl, F. Capasso, A. Tredicucci, A. M. Sergent, A. L. Hutchinson, D. L. Sivco, A. Y. Cho, and G. Scamarcio, "Temperature profile of GaInAs/AlInAs/InP quantum cascade-laser facets measured by microprobe photoluminescence," *Appl. Opt. Lett.* 78, 20952097 (2001).
 68. S. C. Huang, S. C. Liu, A. Li, K. W. Su, Y. F. Chen, and K. F. Huang, "AlGaInAs quantum-well as a saturable absorber in a diode-pumped passively Q-switched solid-state laser," *Opt. Lett.* 32, 1480–1482 (2007).
 69. S. D. Jackson, and A. Lauto, "Diode-pumped fiber lasers: a new clinical tool?" *Lasers Surg. Med.* 30(3), 184–190 (2002).
 70. L. Quintino, A. Costa, R. Miranda, D. Yapp, V. Kumar, and C. J. Kong, "Welding with high power fiber lasers – A preliminary study," *Mater. Des.* 28(4), 1231–1237 (2007).
 71. Z. J. Chen, A. B. Grudinin, J. Porta, and J. D. Minelly, "Enhanced Q switching in double-clad fiber lasers," *Opt. Lett.* 23(6), 454–456 (1998).
 72. J. A. Alvarez-Chavez, H. L. Offerhaus, J. Nilsson, W. A. Clarkson P. W. Turner, and D. J. Richardson. "High-energy, high-power ytterbium-doped Q-switched fiber laser," *Opt. Lett.*, 25, 37-39 (2000).
 73. C. C. Ranaud, H. L. Offerhaus, J. A. Alvarez-Chavez, C. J. Nilsson, W. A.

- Clarkson, P. W. Turner, D. J. Richardson, and A. B. Grudinin. "Characteristics of Q-switched cladding-pumped ytterbium-doped fiber lasers with different high-energy fiber designs," *IEEE J. Quantum Electron.* 37, 199-206 (2001).
74. A. Piper, A. Malinowski, K. Furusawa, and D. J. Richardson. "High power, high-brightness, mJ Q-switched ytterbium-doped fibre laser. *Electron. Lett.* 40, 928-929 (2004).
75. M. Laroche, H. Gilles, S. Girard, N. Passilly, and K. At-Ameur. "Nanosecond pulse generation in a passively Q-switched Yb-doped fiber laser by Cr⁴⁺:YAG saturable absorber." *IEEE Photon. Technol. Lett.* 18,764-766 (2006).
76. J. Y. Huang, H. C. Liang, K. W. Su, and Y. F. Chen. "High power passively Q-switched ytterbium fiber laser with Cr⁴⁺:YAG as a saturable absorber," *Opt. Express* 15, 473-479 (2007).
77. J. Y. Huang, H. C. Liang, K. W. Su, and Y. F. Chen. "Analytical model for optimizing the parameters of an external passive Q-switched in fiber laser," *Appl. Opt.* 47, 2297-2302 (2008).
78. R. Chi, K. Lu, and S. Chen. "Multi-wavelength Yb-doped fiber ring laser. *Microwave Opt., Technol. Lett.* 36, 170-172 (2003).
79. W. Guan and J. R. Marciante. "Dual-frequency operation in a shortcavity ytterbium-doped fiber laser," *IEEE Photon. Technol. Lett.* 19,261- 263 (2007).
80. L. R. Chen and X. J. Gu. "Dual-wavelength yb-doped fiber laser stabilized through four-wave mixing," *Opt. Express* 15, 5083–5088 (2007).
81. S. L. Hu, J. Yu, C. Q. Gao, G. H. Wei, and F. Y. L. "Dual-wavelength stable nanosecond pulses generation from cladding-pumped fiber laser," *Chin. Opt. Lett.* 4, 655-657 (2006).
82. A. Fotiadi, A. Kurkov, and I. Razdobreev, "All-fiber passively Q-switched ytterbium laser," *CLEO/Europe-EQEC 2005, Technical Digest, CJ 2-3, Munich, Germany* (2005).
83. T. Tordella, H. Djellout, B. Dussardier, A. Saïssy, and G. Monnom, "High repetition rate passively Q-switched Nd³⁺:Cr⁴⁺ all-fibre laser," *Electron. Lett.* 39(18), 1307–1308 (2003).
84. P. Adel, M. Auerbach, C. Fallnich, S. Unger, H.-R. Müller, and J. Kirchhof, "Passive Q-switching by Tm³⁺codoping of a Yb³⁺-fiber laser," *Opt. Express* 11(21), 2730–2735 (2003).
85. M. Laroche, H. Gilles, S. Girard, N. Passilly, and K. Aït-Ameur, "Nanosecond

- pulse generation in a passively Qswitched Yb-doped fiber laser by Cr⁴⁺:YAG saturable absorber," *IEEE Photon. Technol. Lett.* 18(6), 764–766(2006).
86. M. Laroche, A. M. Chardon, J. Nilsson, D. P. Shepherd, W. A. Clarkson, S. Girard, and R. Moncorgé, "Compact diode-pumped passively Q-switched tunable Er-Yb double-clad fiber laser," *Opt. Lett.* 27(22), 1980–1982 (2002).
87. T. Hakulinen, and O. G. Okhotnikov, "8 ns fiber laser Q switched by the resonant saturable absorber mirror," *Opt. Lett.* 32(18), 2677–2679 (2007).
88. S. C. Huang, S. C. Liu, A. Li, K. W. Su, Y. F. Chen, and K. F. Huang, "AlGaInAs quantum-well as a saturable absorber in a diode-pumped passively Q-switched solid-state laser," *Opt. Lett.* 32, 1480-1482 (2007).
89. K. Alavi, H. Temkin, W. R. Wagner, and A. Y. Cho, "Optically pumped 1.55- μ m double heterostructure Ga_xAl_yIn_{1-x-y}As/Al_uIn_{1-u}As lasers grown by molecular beam epitaxy," *Appl. Phys. Lett.* 42, 254-256 (1983).
90. W. T. Tsang and N. A. Olsson, "New current injection 1.5- μ m wavelength Ga_xAl_yIn_{1-x-y}As/InP double-heterostructure laser grown by molecular beam epitaxy," *Appl. Phys. Lett.* 42, 922-924 (1983).
91. N. Nishiyama, C. Caneau, B. Hall, G. Guryanov, M. H. Hu, X. S. Liu, M.-J. Li, R. Bhat, and C. E. Zah, "Long-wavelength vertical-cavity surface-emitting lasers on InP with lattice matched AlGaInAs–InP DBR grown by MOCVD," *IEEE J. Sel. Top. Quantum Electron.* 11, 990-998 (2005).

Chapter 2

Passively Q-switched double-cladding fiber lasers



2.1 Passively Q-switched double-cladding fiber laser with AlGaInAs quantum wells

2.1.1 Introduction

Fiber lasers have been confirmed to possess the merits of high efficiency, excellent beam quality, and good heat dissipation. High-pulse-energy Q-switched fiber lasers are practically useful in numerous applications, such as range finding, remote sensing, industrial processing, and coherent lidar systems [1–4]. Passively Q-switched lasers with saturable absorbers have attracted significant attention because of their compactness and simplicity in operation. Several saturable absorbers have been developed to replace the dyes used in solid-state lasers, such as Cr⁴⁺-doped crystals [5–9] and semiconductor saturable absorber mirrors (SESAMs) [10,11]. Currently, Cr⁴⁺:YAG crystals are the most recognized saturable absorbers in the spectral region of 0.9–1.2 μm. Passively Q-switched fiber lasers with Cr⁴⁺:YAG saturable absorbers have been recently demonstrated [12–14], among which the maximum pulse energy achieved with a large-mode-area Yb-doped fiber was 120 μJ.

Alternatively, InGaAs/GaAs quantum wells (QWs) have been used to develop the SESAMs for Nd-doped or Yb-doped lasers. The obtainable absorption change between low and high intensities, however, is hindered by the lattice mismatch for the spectral region of above 1.0 μm. As a consequence, the output pulse energies and the conversion efficiencies with InGaAs SESAMs in passively Q-switched lasers are generally significantly lower than those with Cr⁴⁺:YAG crystals. Recently, an AlGaInAs with a periodic QW/ barrier structure has been exploited to be an efficient saturable absorber for a passively Q-switched Nd:YVO₄ laser [15]. Compared with InGaAsP materials, the AlGaInAs quaternary alloy with a larger conduction band offset is confirmed to offer a superior electron confinement in the 0.84–1.65 μm spectral region [16–18]. Nevertheless, AlGaInAs/InP QWs have not been employed to passively Q switch Yb-doped fiber lasers.

We demonstrate a high-pulse-energy passively Q-switched Yb-doped fiber laser with an AlGaInAs/InP QWs saturable absorber. With an incident pump power of 7.6 W, an average output power of 3.8 W with a Q-switched pulse width of 30 ns at a pulse repetition rate of 12.5 kHz was obtained; consequently, the maximum pulse energy was up to 300 μJ. More importantly, the overall Q-switching efficiency could exceed 90% because of a low nonsaturable loss.

2.1.2 Characteristics of semiconductor saturable absorber

The structure of the semiconductor saturable absorber was essentially similar to that reported in [15]. The previous saturable absorber consisted of 30 groups of two QWs, spaced at half-wavelength intervals by InAlAs barrier layers with a bandgap wavelength around 805 nm. Here we fabricated a saturable absorber with 50 groups of three QWs to increase the modulation strength. The luminescence wavelength of the saturable absorber was designed to be near 1066 nm. An InP window layer was deposited on the QW/barrier structure to avoid surface recombination and oxidation. The backside of the substrate was mechanically polished after growth. Each side of the semiconductor saturable absorber was antireflection coated to reduce back reflections and the couplecavity effects. Figure 2.1 shows the measured result for the low-intensity transmittance spectrum of the QW saturable absorber. The initial transmission of the absorber at the wavelength of 1066 nm was found to be approximately 26%. The operation bandwidth of the absorber is approximately 8 nm. With the z-scan method, the absorption change between low and high intensities was observed to be approximately 70% in a single pass, and the total nonsaturable losses were lower than 5%. Furthermore, the saturation fluence of the saturable absorber was estimated to be in the range of 1 mJ/cm², and its relaxation time was on the order of 100 ns.

2.1.3 Experimental setup

Figure 2.2 depicts the schematic of the experimental setup for the passively Q-switched fiber laser, which is composed of a 1.5 m Yb-doped fiber and an external feedback cavity. The external cavity comprises a reimaging lens, a saturable absorber, a highly reflective mirror at 1.06 μm for feedback, and a Fabry–Perot thin film filter (FP filter) for controlling the lasing wavelength. The peak of the FP filter is at 1100 nm with a FWHM bandwidth of 5 nm at normal incidence. The end facets of the fiber were cut to be normal incident. The fiber has a peak cladding absorption coefficient of 10.8 dB/m at 976 nm and a double-clad structure with a diameter of 350 μm octagonal outer cladding, a diameter of 250 μm octagonal inner cladding with an NA of 0.46, and a 25 μm circular core with an NA of 0.07. Note that the robust single-mode output was achieved with a unique low NA feature of the core.

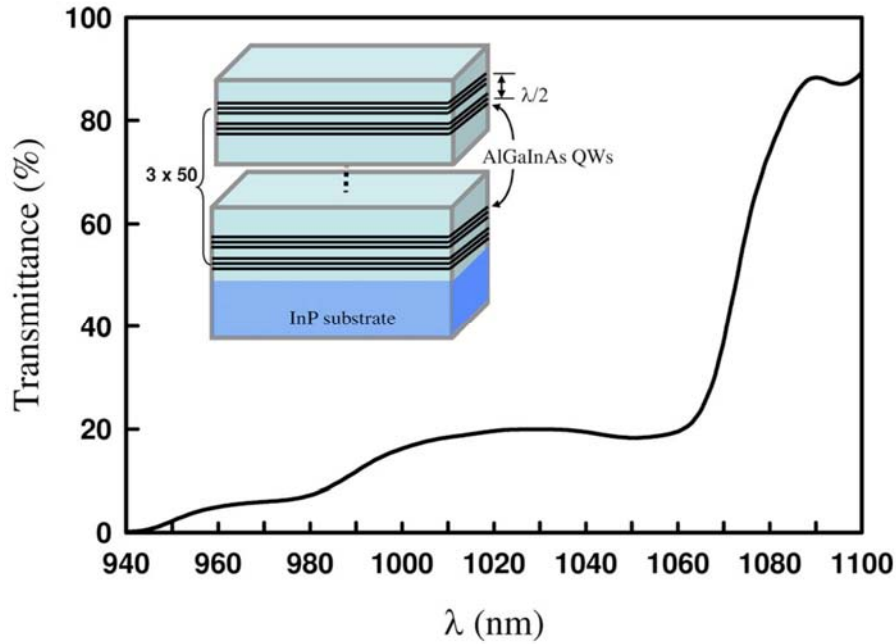


Fig 2. 1 Transmittance spectrum at room temperature for the AR- coated AlGaInAs/InP saturable absorber. Inset, schematic diagram of a periodic AlGaInAs QW structure.

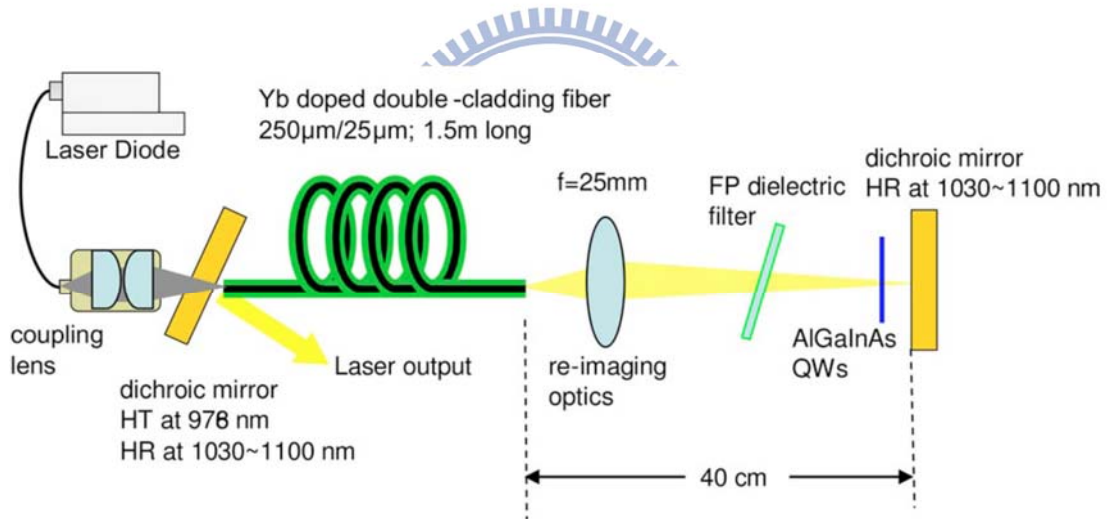


Fig 2. 2 Schematic diagram of the experimental setup. HR, high reflection; HT, high transmission.

The pump source was a 10 W 976 nm fiber-coupled laser diode with a core diameter of 400 μm and an NA of 0.22. A focusing lens with 25 mm focal length and 90% coupling efficiency was used to re-image the pump beam into the fiber through a dichroic mirror with high transmission ($>90\%$) at 976 nm and high reflectivity ($>98.8\%$) at 1066 nm. The pump spot radius was approximately 200 μm . With launching into an undoped fiber, the pump coupling efficiency was measured to be approximately 80%. The pulse temporal behavior was recorded with a digital oscilloscope (LeCroy

Wavepro 7100; 10G samples/s; 1 GHz bandwidth) and a fast InGaAs photodiode. The laser spectrum was measured by an optical spectrum analyzer with 0.1 nm resolution (Advantest Q8381A).

2.1.4 Results and discussions

Figure 2.3 shows the average output powers with respect to the incident pump power in cw and passive Q-switching operations. The cw operation was performed to make an evaluation for the passively Q-switched efficiency. Without the saturable absorber in the cavity, the laser had an output power of 4 W at an incident pump power of 7.6 W in a cw operation, and the corresponding slope efficiency was 66%. In the passive Q-switching operation, an average output power of 3.8 W was obtained at an incident pump power of 7.6 W. The Q-switching efficiency, which is defined as ratio of the Q-switched output power to the cw power, at the same pump power, can be found to exceed 90%. This Q-switching efficiency is considerably better than the results obtained with the Cr⁴⁺:YAG saturable absorber [13]. The superior Q-switching efficiency confirms that the AlGaInAs QW material can be exploited to be an efficient absorber with a large modulation change and a quite low nonsaturable loss. The lasing linewidth was narrower than 1.0 nm with the help of a dielectric bandpass filter, as shown in the inset of Figure 2.3. The M² factor was also measured to be less than 1.5 over the complete output power range, owing to the low-NA feature of the fiber. Furthermore, we also detuned the resonant wavelength (by tilting the FP filter) to investigate the bandwidth of comparable Q-switching performance. It is found that the output pulse energy of >280 μJ with the identical Q-switching efficiency could be obtained within 1066±4 nm.

Figure 2.4 shows the pulse repetition rate and the pulse energy versus the incident pump power. It can be seen that the pulse repetition rate increases monotonically with the pump power up to 12.5 kHz and that the pulse energy is approximately 300 μJ for all pump power range. The pulse duration, as shown in Figure 2.5(a), was found to be almost constant at 30 ns for all pump powers. As a consequence, the maximum peak power reaches approximately 10 kW. A typical oscilloscope trace of a train of output pulses is shown in Figure 2.5(b). Under the optimum alignment condition, the pulse-to-pulse amplitude fluctuation was found to be within 10%. In passively Q-switched Yb-doped fiber lasers, on the whole, the performances with AlGaInAs QWs saturable absorbers are superior to the results obtained with Cr⁴⁺:YAG crystals [12–14].

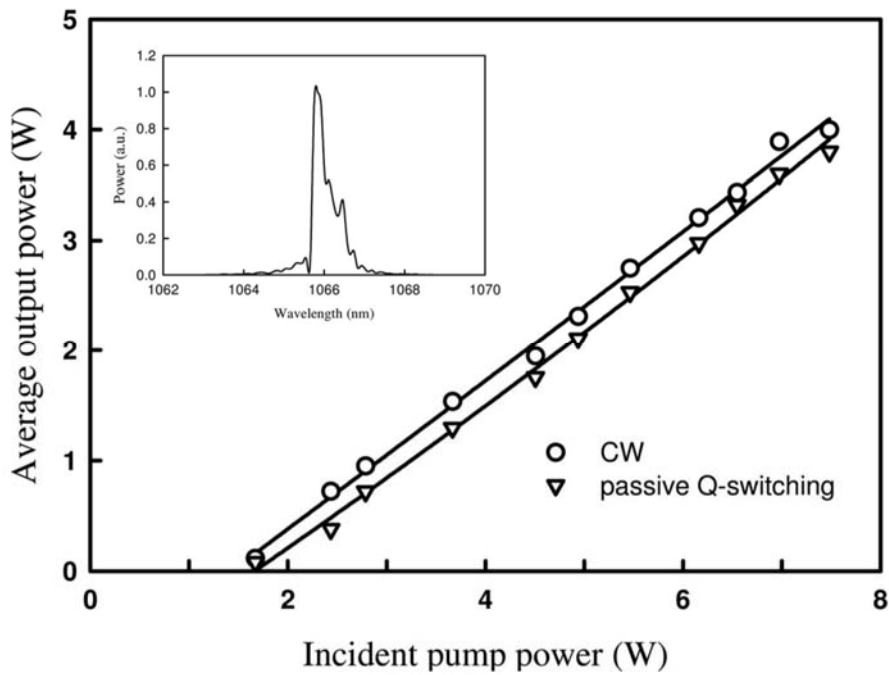


Fig 2. 3 Average output powers at 1066 nm with respect to the incident pump power in cw and passively *Q*-switching operations.

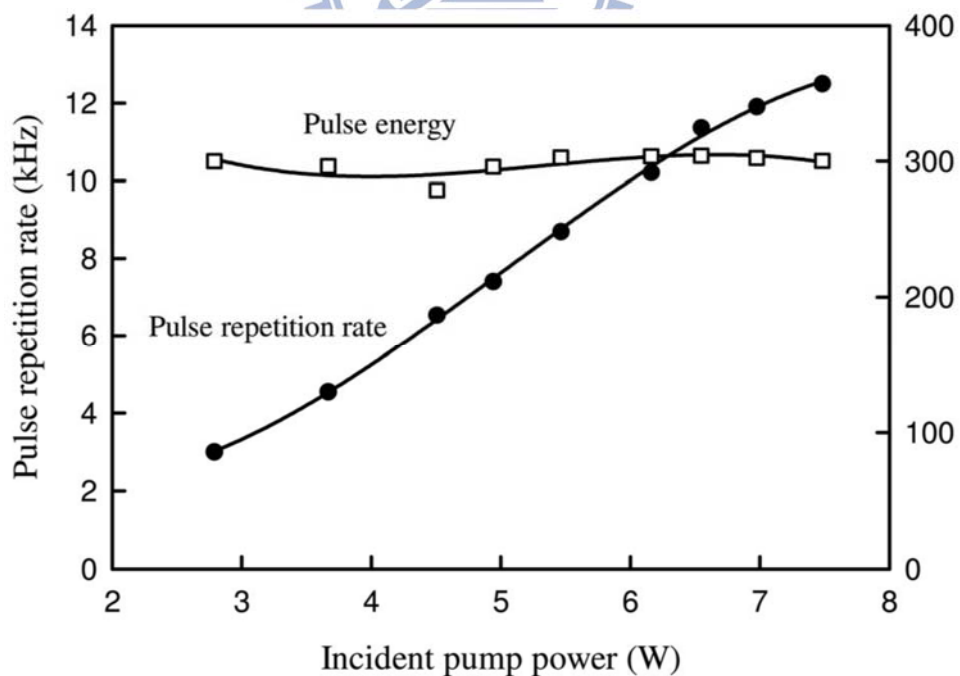


Fig 2. 4 Experimental results for the pulse repetition rate and the pulse energy versus incident pump power.

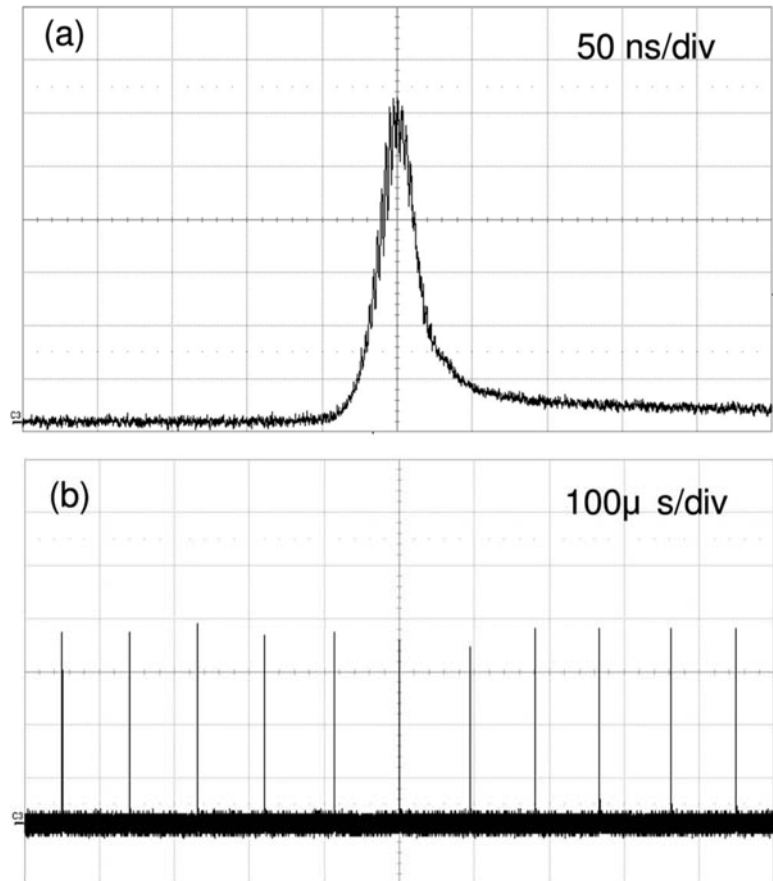


Fig 2. 5 Expanded shape of a single pulse and (b) typical oscilloscope trace of a train of output pulses.

2.1.5 Conclusion

In summary, a high-pulse-energy passively Q-switched Yb-doped fiber laser was developed with an AlGaInAs/InP QW saturable absorber. Stable Q-switched pulses of 30 ns duration with an average output power of 3.8 W and a repetition rate of 12.5 kHz were obtained at an incident pump power of 7.6 W. The overall Q-switching efficiency was found to exceed 90%. Excellent results confirm that the AlGaInAs QW material can be exploited to be an efficient absorber with a large modulation change and a quite-low nonsaturable loss.

2.2 Comparative studies for Cr⁴⁺:YAG crystal and AlGaInAs quantum wells in passively Q-switched double-cladding fiber lasers

2.2.1 Introduction

The rapid development of double-clad rare-earth doped fibers and high-power laser diodes spirits the generation of high-power and high-brightness light sources [19-21]. Pulsed fiber lasers have attracted a great deal of attentions in applications owing to their higher peak power than in CW operation. Passive Q-switching (PQS) is a sophisticated and an efficient technique to create high-pulse-energy and high-peak-power pulses. Besides, PQS lasers are more compact and lower cost than the active Q-switching cause of that they utilize saturable absorbers (SAs) in replace of acoustic-optic or electro-optic modulators as the Q-switch.

Fiber-type SA [22-24] offers the in-line configuration, nevertheless they are restricted by modulation depth to deliver high-pulse-energy laser. Crystal-based and semiconductor-based SAs are other choices of passive Q-switch. Their high mechanical robustness and well-developed fabrication process make them more common in Q-switched fiber lasers [25-29]. In the spectral region of 1.0~1.1 μm , Cr⁴⁺:YAG crystals [25] and InGaAs/GaAs quantum wells (QWs) [28] have been adopted to Q-switch fiber lasers. However, the output pulse energy with InGaAs SESAMs in passively Q-switched lasers are limited by the lattice mismatch with the substrate GaAs for the spectral region of above 1.0 μm . Alternatively, AlGaInAs material has the advantages of lattice match with the substrate InP and better electron confinement in the 0.84-1.65 μm spectral region than AlGaInP materials [16,17]. We have recently utilized AlGaInAs periodic QWs to Q-switch a Nd:YVO₄ laser [15] and an Yb fiber laser [30], they could emit pulse energy up to 40 and 300 μJ , respectively. Furthermore both of them delivered pulse peak power ≥ 10 kW. Consequently, AlGaInAs semiconductor QWs is comparable with Cr⁴⁺:YAG crystal in the region of 1.0~1.1 μm .

We will report on comparative studies for Cr⁴⁺:YAG crystal and AlGaInAs semiconductor used as a SA in Q-switched Yb-doped fiber lasers. The two SAs were designed to be possessed of nearly identical small-signal transmission of ~28%. Experimental results reveal that the maximum transmissions are 85% and 96% for the Cr⁴⁺:YAG crystal and the AlGaInAs QWs, respectively. Under a pump power of 24 W, the average output powers were up to 14.4 W and 13.8 W obtained with the AlGaInAs

QWs and with the Cr⁴⁺:YAG crystal, respectively. The maximum pulse energies obtained with the AlGaInAs QWs and with the Cr⁴⁺:YAG crystal were found to be 0.45 mJ and 0.35 mJ, respectively.

2.2.2 Characteristics of saturable absorbers

The Cr⁴⁺:YAG crystal has thickness of 3 mm and was highly doped with a small signal transmission of 28%. Both sides of the Cr⁴⁺:YAG crystal were coated for antireflection at 1030 ~1080 nm (R<0.2%). The AlGaInAs absorber was designed with 50 groups of three QWs as described in Ref [30]. Both sides of the semiconductor SA were coated for anti-reflecting to reduce back reflections and the couple-cavity effects. Figure 2.6 shows the saturation transmission of the SAs, where the pump source was a nanosecond Nd:YAG Qswitched laser. The saturation energy density of AlGaInAs QWs and Cr⁴⁺:YAG crystal are estimated to about 1 mJ/cm² and 300 mJ/cm², respectively. The deduced absorption cross-section of the Cr⁴⁺:YAG crystal is in the order of 10⁻¹⁹ cm² and agrees approximately with Ref. [31-33]. Besides, the cross-section for the AlGaInAs QWs was obtained in the order of 10–15 cm². The 95% final transmission of AlGaInAs reveals the low nonsaturable loss induced by the facet reflection and absorption by the substrate. On the other hand, the final transmission of the Cr⁴⁺:YAG was only 85%, the lossy phenomenon was attributed mainly to the excited-state absorption (ESA) [34]. The final transmission influenced by the ESA effect could be express approximately as $T_f = T_i^\beta$, where T_f and T_i are the final and initial transmission, respectively, and the parameter β is the ratio of the absorption cross-section of the excited-state and the ground-state, i.e. $\beta = \sigma_{es} / \sigma_{gs}$. The values of β derived from Ref [31-33]. ranges from 0.1~0.28 and is 0.128 in our experiment. The modulation depth could be found to be 68% for AlGaInAs QWs and 57% for the Cr⁴⁺:YAG crystal. Furthermore, the relaxation time of the AlGaInAs QWs the Cr⁴⁺:YAG crystal were estimated to be on the order of 100 ns and 3 μ s respectively.

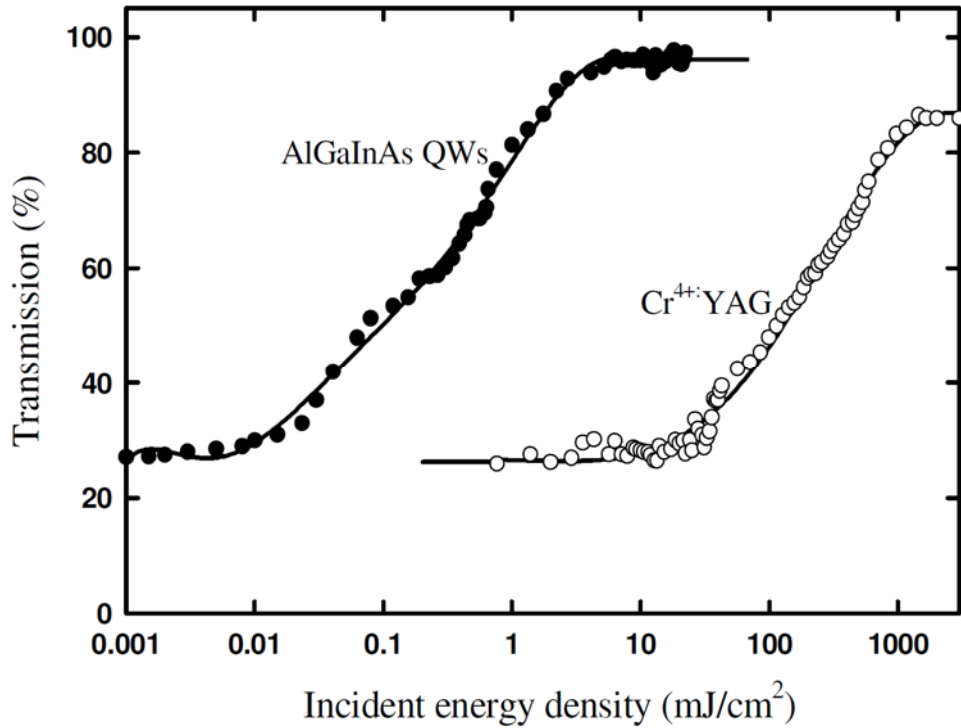


Fig 2. 6 Saturation transmission of the AlGaInAs QWs and the Cr⁴⁺:YAG crystal.

2.2.3 Experimental setup

The cavity consists of a 3-m Yb-doped fiber and an external feedback cavity with a SA. Figures 2.7 (a) and (b) show the setups for PQS fiber lasers by use of a Cr⁴⁺:YAG crystal and a AlGaInAs semiconductor, respectively. The fiber has an absorption coefficient of 10.8 dB/m at 976 nm and a double-clad structure with a 350 μm octagonal outer cladding, a 250 μm inner cladding with a numerical aperture (NA) of 0.46, and 30μm circular core with a NA of 0.07. The use of the large-mode-area fiber with low NA is beneficial for storing higher pulse energies and sustaining excellent beam quality simultaneously. The external cavity in Fig. 2.7 (a) consists of a focusing lens of 25-mm focal length to focus the fiber output into the Cr⁴⁺:YAG crystal, a re-imaging lens to re-image the beam on a highly reflective mirror for feedback, and a thin film filter for controlling the resonant wavelength. The SA was wrapped with indium foil and mounted in a copper block without active cooling. Here we used a tight focusing configuration to enhance the energy inside the Cr⁴⁺:YAG crystal. The beam waist was about 20 μm and a translation stage was used to adjust the longitudinal position of the Cr⁴⁺:YAG saturable absorber for minimizing the beam volume inside the crystal and achieving the lowest Q-switching threshold. On the other hand, the low saturation energy density of the AlGaInAs QWs could allow a simple external cavity,

as shown in Fig. 2.7 (b), where the beam spot diameter was approximately 300 μm . And the peak optical intensity allowed on the AlGaInAs QWs is estimated to be 300 MW/cm^2 without damage. The SA was tilted slightly to avoid facet reflection back to the gain fiber, which usually incurs parasitic fluctuation in pulse stability in high gain fiber lasers.

The pump source was a 35-W 976-nm fiber-coupled laser diode with a core diameter of 400 μm and a NA of 0.22. Focusing lens with 25 mm focal length and 92% coupling efficiency was used to re-image the pump beam into the fiber through a dichroic mirror with high transmission ($>90\%$) at 976 nm and high reflectivity ($>99.8\%$) within 1030~1100 nm. The pump spot radius was approximately 200 μm . With launching into an undoped fiber, the pump coupling efficiency was measured to be approximately 80%.

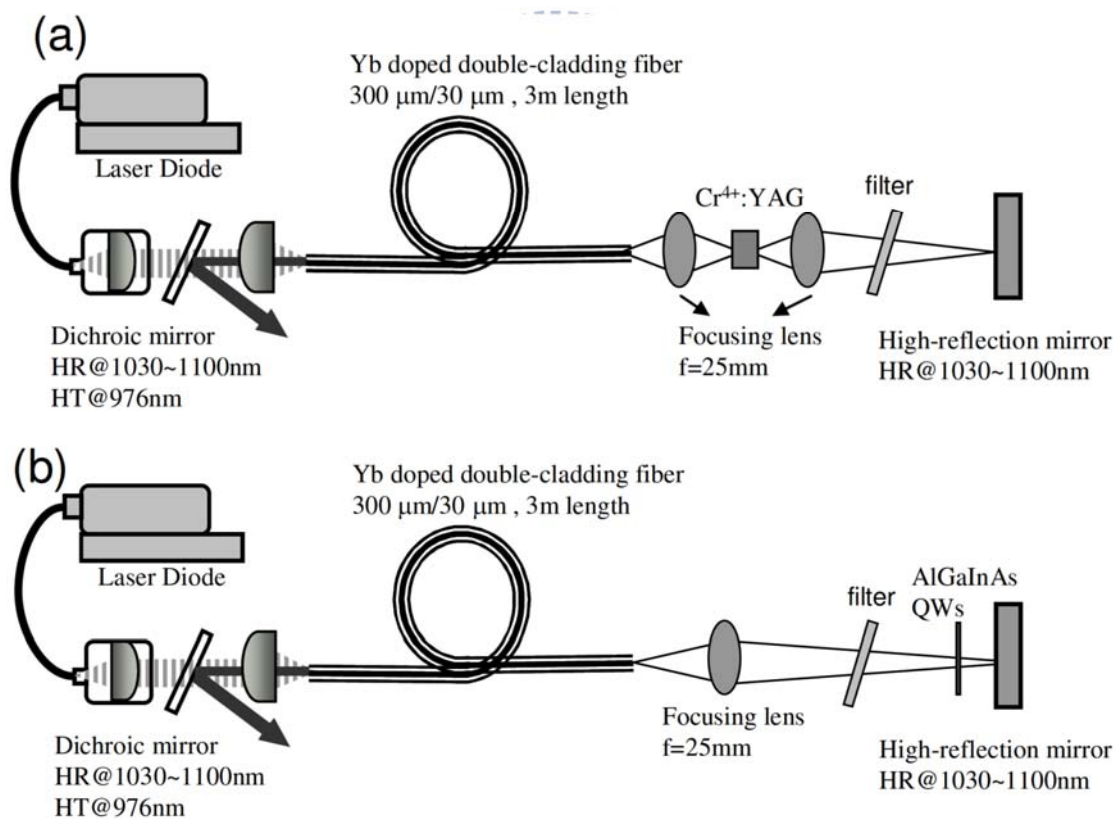


Fig 2. 7 Schematic of diode-pumped PQS Yb-doped fiber lasers. (a) with Cr⁴⁺:YA crystal (b) with AlGaInAs QWs. HR: high reflection; HT: high transmission.

2.2.4 Results and discussions

Figure 2.8 shows the average output powers with respect to the launched pump power in cw and PQS operations. The cw operation was performed with an external cavity only comprising a re-imaging lens and a reflective mirror. In the cw regime, the laser had a slope efficiency of 74% and the output power reached 15.8 W at a launched pump power of 24 W. In the PQS regime, the maximum average output powers at a launched pump power of 24 W were up to 14.4 W and 13.8 W with the AlGaInAs QWs and with the Cr⁴⁺:YAG crystal, respectively. The Q-switching efficiencies were 91% and 87% for the lasers with with the AlGaInAs QWs and with the Cr⁴⁺:YAG crystal, respectively.

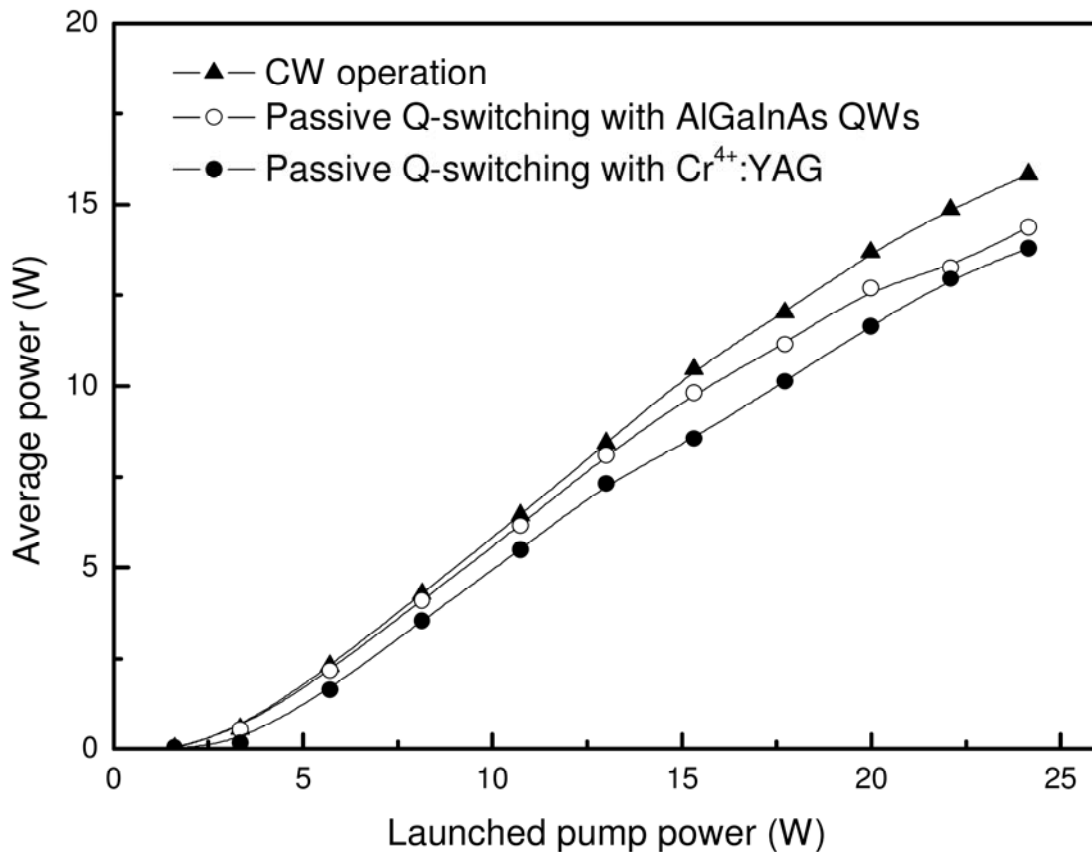


Fig 2. 8 Dependence of the average output power on the launched pump power for the cw and passive Q-switching operations.

The pulse temporal behavior was recorded by a Leroy digital oscilloscope (Wavepro 7100; 10G samples/sec; 4 GHz bandwidth) with a fast InGaAs photodiode. Figure 2.9 shows the pulse characteristics including the pulse repetition rate and the pulse energy. Figure 2.9 (a) shows the pulse repetition rate versus the launched pump power. The repetition rates of both lasers increased monotonically with the pump power. At a launched pump power of 24 W, the repetition rates were 38 kHz and 30 kHz for using the Cr⁴⁺:YAG crystal and the AlGaInAs QWs, respectively. Figure 2.9 (b) shows the pulse energy versus the launched pump power. The pulse energy with the Cr⁴⁺:YAG crystal was almost constant at 0.3 mJ for the pump power less than 20 W and slightly increased up to 0.35 mJ at a pump power of 24 W. On the other hand, the pulse energy with the AlGaInAs QWs increases gradually, from 0.25 mJ at the threshold to 0.45 mJ at a pump power of 24 W.

Another interesting characteristic of saturable absorbers is the wavelength-dependent absorption. In this investigation the thin film filter was tilted for controlling the lasing wavelength from 1055 nm to 1083 nm. Figure 2.10 shows the pulse energy versus the lasing wavelength at a pump power of 24 W. Since the absorption bandwidth of the AlGaInAs QWs was rather narrower, the variation of the pulse energy with the AlGaInAs QWs was more significant than that with the Cr⁴⁺:YAG crystal. Therefore, the Cr⁴⁺:YAG crystal is more suitable than the AlGaInAs QWs for using in tunable operation.

The temporal shapes of the Q-switched pulses for the maximum pulse energy were depicted in Fig. 2.11. The top of Fig. 2.11 shows the single Q-switched envelopes. The pulse durations were 70 ns and 60 ns for using the Cr⁴⁺:YAG crystal and the AlGaInAs QWs, respectively. The bottom of Fig. 2.11 shows the typical oscilloscope traces of Q-switched pulse train with the optimum alignment. The pulse-to-pulse stability was found to be noticeably better with the AlGaInAs QWs than with the Cr⁴⁺:YAG crystal under 30 °C because of the proper cooling ability by the copper sink. Without any cooling mechanism, the pulse-to-pulse stability and the laser output energy will be reduced.

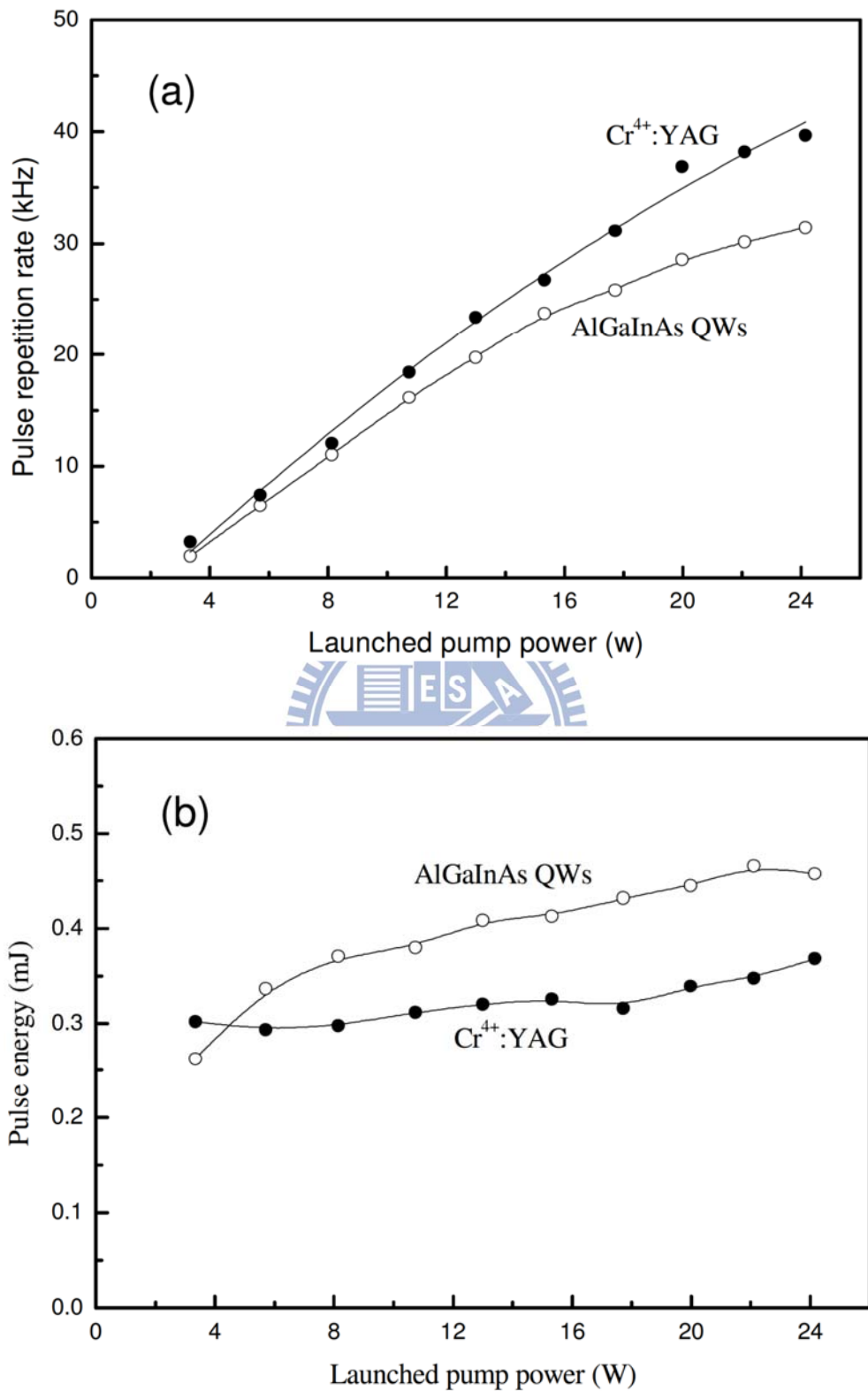


Fig 2. 9 (a) Pulse repetition rate and (b) pulse energy versus the launched pump power.

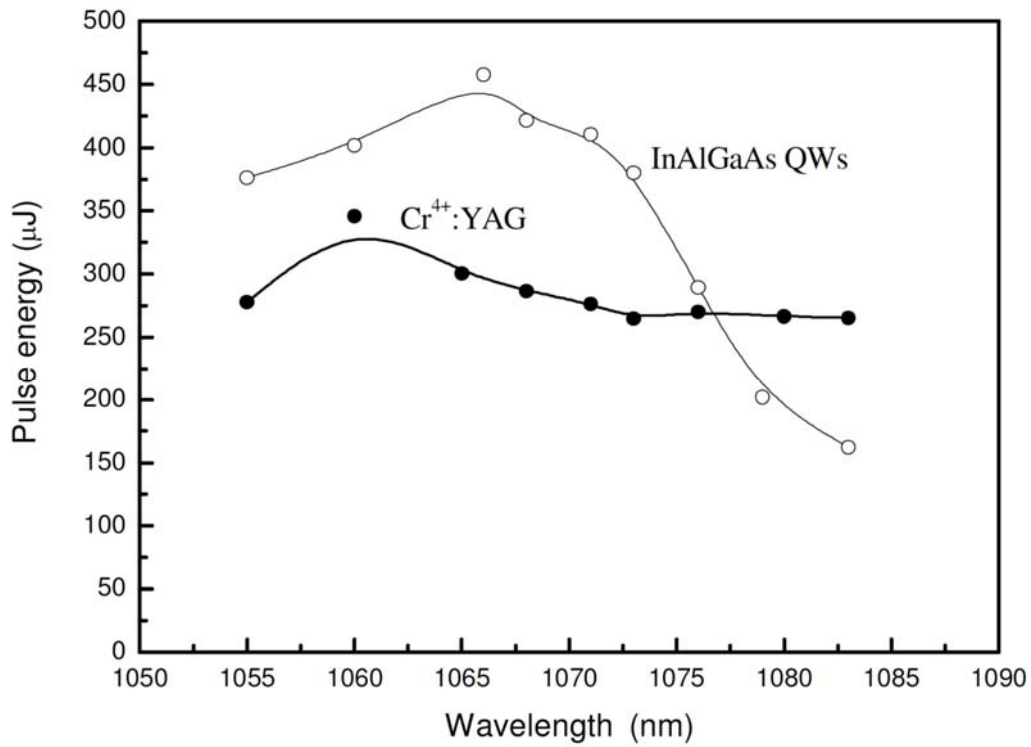


Fig 2. 10 Pulse energy versus the resonant wavelength.

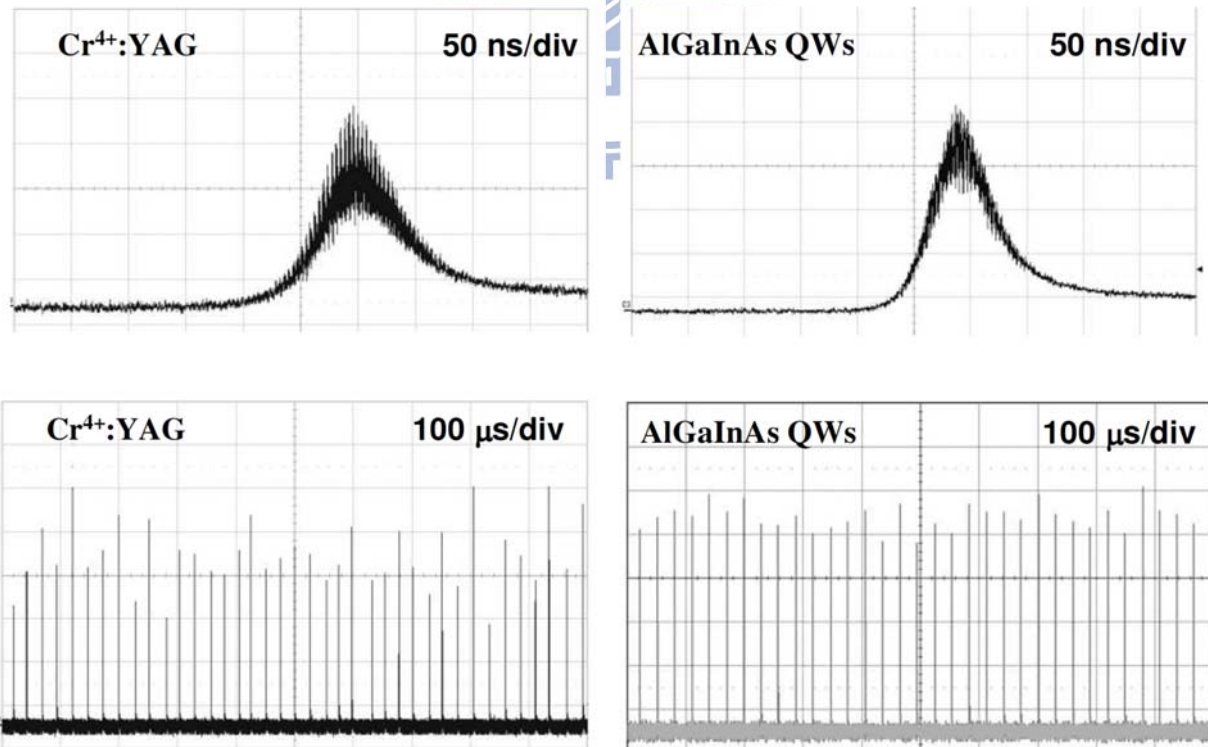


Fig 2. 11 Top: Oscilloscope traces of a typical Q-switched envelope; Bottom: Oscilloscope traces of a train of Q-switched pulses.

2.2.5 Conclusion

In conclusion, we have demonstrated comparative studies for the Cr⁴⁺:YAG crystal and the AlGaInAs QWs used as a SA in efficient high-pulse-energy PQS Yb-doped fiber lasers. The two SAs were designed to exhibit nearly identical small-signal transmission of ~28%. Under a pump power of 24 W, the average output powers were up to 14.4 W and 13.8 W obtained with the AlGaInAs QWs and with the Cr⁴⁺:YAG crystal, respectively. The maximum pulse energies obtained with the AlGaInAs QWs and with the Cr⁴⁺:YAG crystal were 0.45 mJ and 0.35 mJ, respectively. The pulse-to-pulse stability was found to be noticeably better with the AlGaInAs QWs than with the Cr⁴⁺:YAG crystal. Nevertheless, the Cr⁴⁺:YAG crystal has a broader absorption band that is beneficial to the tunable operation. It is believed that the efficient Q-switched fiber lasers should be useful light sources for technical applications because of its high average power as well as high pulse energy.



Reference

1. Z. J. Chen, A. B. Grudinin, J. Porta, and J. D. Minelly, "Enhanced Q switching in double-clad fiber lasers," *Opt. Lett.* 23, 454-456 (1998).
2. Y. X. Fan, F. Y. Lu, S. L. Hu, K. C. Lu, H. J. Wang, X. Y. Dong, J. L. He, and H. T. Wang, "Tunable high-peak-power, high-energy hybrid Q-switched double-clad fiber laser," *Opt. Lett.* 29, 724-726 (2004).
3. O. Schmidt, J. Rothhardt, F. Röser, S. Linke, T. Schreiber, K. Rademaker, J. Limpert, S. Ermeneux, P. Yvernault, F. Salin, and A. Tünnermann, "Millijoule pulse energy Q-switched short-length fiber laser," *Opt. Lett.* 32, 1551-1553 (2007).
4. J. A. Alvarez-Chavez, H. L. Offerhaus, J. Nilsson, P. W. Turner, W. A. Clarkson, and D. J. Richardson, "High-energy, high-power ytterbium-doped Q-switched fiber laser," *Opt. Lett.* 25, 37-39 (2000).
5. J. J. Zayhowski and C. Dill III, "Diode-pumped passively Q-switched picosecond microchip lasers," *Opt. Lett.* 19, 1427-1429 (1994).
6. X. Zhang, S. Zhao, Q. Wang, Q. Zhang, L. Sun, and S. Zhang, "Optimization of Cr⁴⁺-doped saturable-absorber Q-switched lasers," *IEEE J. Quantum Electron.* 33, 2286-2294 (1997).
7. A. Agnesi and S. Dell'acqua, "High-peak-power diode-pumped passively Q-switched Nd:YVO₄ laser," *Appl. Phys. B* 76, 351-354 (2003).
8. Y. Kalisky, "Cr⁴⁺-doped crystals: their use as lasers and passive Q-switches," *Prog. Quantum Electron.* 28, 249-303 (2004).
9. A. Sennaroglu, U. Demirbas, S. Ozharar, and F. Yaman, "Accurate determination of saturation parameters for Cr⁴⁺-doped solid-state saturable absorbers," *J. Opt. Soc. Am. B* 23, 241-249 (2006).
10. G. J. Spühler, R. Paschotta, R. Fluck, B. Braun, M. Moser, G. Zhang, E. Gini, and U. Keller, "Experimentally confirmed design guidelines for passively Q-switched microchip lasers using semiconductor saturable absorbers," *J. Opt. Soc. Am. B* 16, 376-388 (1999).
11. R. Häring, R. Paschotta, R. Fluck, E. Gini, H. Melchior, and U. Keller, "Passively Q-switched microchip laser at 1.5 μm," *J. Opt. Soc. Am. B* 18, 1805-1812 (2001).
12. M. Laroche, H. Gilles, S. Girard, N. Passilly, and K. Aït-Ameur, "Nanosecond pulse generation in a passively Q-switched Yb-doped fiber laser by Cr⁴⁺: YAG saturable absorber," *IEEE Photon. Technol. Lett.* 18, 764-766 (2006).

13. J. Y. Huang, H. C. Liang, K. W. Su, and Y. F. Chen, "High power passively Q-switched ytterbium fiber laser with Cr⁴⁺:YAG as a saturable absorber," *Opt. Express* 15, 473-479 (2007).
14. L. Pan, I. Utkin, R. J. Lan, Y. Godwal, and R. Fedosejevs, "High-peak-power subnanosecond passively Q-switched ytterbium-doped fiber laser," *Opt. Lett.* 35, 895-897 (2010).
15. S. C. Huang, S. C. Liu, A. Li, K. W. Su, Y. F. Chen, and K. F. Huang, "AlGaInAs quantum-well as a saturable absorber in a diode-pumped passively Q-switched solid-state laser," *Opt. Lett.* 32, 1480-1482 (2007).
16. K. Alavi, H. Temkin, W. R. Wagner, and A. Y. Cho, "Optically pumped 1.55- μ m double heterostructure Ga_xAl_yIn_{1-x-y}As/Al_uIn_{1-u}As lasers grown by molecular beam epitaxy," *Appl. Phys. Lett.* 42, 254-256 (1983).
17. W. T. Tsang and N. A. Olsson, "New current injection 1.5- μ m wavelength Ga_xAl_yIn_{1-x-y}As/InP double-heterostructure laser grown by molecular beam epitaxy," *Appl. Phys. Lett.* 42, 922-924 (1983).
18. N. Nishiyama, C. Caneau, B. Hall, G. Guryanov, M. H. Hu, X. S. Liu, M.-J. Li, R. Bhat, and C. E. Zah, "Long-wavelength vertical-cavity surface-emitting lasers on InP with lattice matched AlGaInAs-InP DBR grown by MOCVD," *IEEE J. Sel. Top. Quantum Electron.* 11, 990-998 (2005).
19. Y. Jeong, J. K. Sahu, R. B. Williams, D. J. Richardson, K. Furusawa, and J. Nilsson, "Ytterbium-doped large-core fibre laser with 272 W output power," *Electron. Lett.* 39(13), 977-978 (2003).
20. Y. Jeong, J. K. Sahu, D. N. Payne, and J. Nilsson, "Ytterbium-doped large-core fibre laser with 1 kW of continuous-wave output power," *Electron. Lett.* 40(8), 470-471 (2004).
21. A. Liem, J. Limpert, H. Zellmer, A. Tünnermann, V. Reichel, K. Mörl, S. Jetschke, S. Unger, H.-R. Müller, J. Kirchhof, T. Sandrock, and A. Harschak, "1.3 kW Yb-doped fiber laser with excellent beam quality," in *Proc. Conference on Lasers and Electro-Optics 2004*, San Francisco, USA, May 16-21, 2004, postdeadline paper CPDD2.
22. A. Fotiadi, A. Kurkov, and I. Razdobreev, "All-fiber passively Q-switched ytterbium laser," *CLEO/Europe-EQEC 2005*, Technical Digest, CJ 2-3, Munich, Germany (2005).
23. T. Tordella, H. Djellout, B. Dussardier, A. Saïssy, and G. Monnom, "High

- repetition rate passively Q-switched Nd³⁺:Cr⁴⁺ all-fibre laser,” *Electron. Lett.* 39(18), 1307–1308 (2003).
24. P. Adel, M. Auerbach, C. Fallnich, S. Unger, H.-R. Müller, and J. Kirchhof, “Passive Q-switching by Tm³⁺ codoping of a Yb³⁺-fiber laser,” *Opt. Express* 11(21), 2730–2735 (2003).
25. M. Laroche, H. Gilles, S. Girard, N. Passilly, and K. Aït-Ameur, “Nanosecond pulse generation in a passively Q-switched Yb-doped fiber laser by Cr⁴⁺:YAG saturable absorber,” *IEEE Photon. Technol. Lett.* 18(6), 764–766 (2006).
26. M. Laroche, A. M. Chardon, J. Nilsson, D. P. Shepherd, W. A. Clarkson, S. Girard, and R. Moncorgé, “Compact diode-pumped passively Q-switched tunable Er-Yb double-clad fiber laser,” *Opt. Lett.* 27(22), 1980–1982 (2002).
27. F. Z. Qamar and T. A. King, “Passive Q-switching of the Tm-silica fiber laser near 2 mm by Cr²⁺:ZnSe saturable absorber crystal,” *Opt. Commun.* 248, 501–505 (2005).
28. T. Hakulinen, and O. G. Okhotnikov, “8 ns fiber laser Q switched by the resonant saturable absorber mirror,” *Opt. Lett.* 32(18), 2677–2679 (2007).
29. S. Kivistö, R. Koskinen, J. Paajaste, S. D. Jackson, M. Guina, and O. G. Okhotnikov, “Passively Q-switched Tm³⁺, Ho³⁺-doped silica fiber laser using a highly nonlinear saturable absorber and dynamic gain pulse compression,” *Opt. Express* 16(26), 22058–22063 (2008).
30. J. Y. Huang, W. C. Huang, W. Z. Zhuang, K. W. Su, Y. F. Chen, and K. F. Huang, “High-pulse-energy, passively Q-switched Yb-doped fiber laser with AlGaInAs quantum wells as a saturable absorber,” *Opt. Lett.* 34(15), 2360–2362 (2009).
31. H. Ridderbusch, and T. Graf, “Saturation of 1047- and 1064nm absorption in Cr⁴⁺:YAG crystals,” *IEEE J. Quantum Electron.* 43(2), 168–173 (2007).
32. V. G. Shcherbitsky, S. Girard, M. Fromager, R. Moncorgé, N. V. Kuleshov, V. I. Levchenko, V. N. Yakimovich, and B. Ferrand, “Accurate method for the measurement of absorption cross sections of solid-state saturable absorbers,” *Appl. Phys. B* 74, 367–374 (2002).
33. Y. Kalisky, “Cr⁴⁺-doped crystals: their use as lasers and passive Q-switches,” *Prog. Quantum Electron.* 28(5), 249–303 (2004).
34. Z. Burshtein, P. Blau, Y. Kalisky, Y. Shimony, and M. R. Kokta, “Excited-state absorption studies of Cr⁴⁺ ions in several garnet host crystals,” *IEEE J. Quantum Electron.* 34(2), 292–299 (1998).

Chapter 3

Passively Q-switched photonic crystal fiber lasers



3.1 Passively Q-switched photonic crystal fiber laser with AlGaInAs quantum wells

3.1.1 Introduction

High-power diode-pumped double-clad rare-earth doped fiber lasers have been proved to be efficient and compact with excellent beam quality, high efficiency, and good thermal management [1-3]. Q-switched fiber lasers are practically useful in a variety of applications in virtue of their high pulse energy, such as remote sensing, industrial processing, and medical needs [4-6]. Compared with active Q-switching techniques, passive Q-switching methods that employ saturable absorbers can considerably enhance the compactness and simplify the operation [7-10]. By enlarging the active volume of the gain medium, corresponding to the doped core size of the fiber, one can achieve the merit of the high pulse energy. However, the conventional large-core fibers suffer from mode-quality degradation and their long lengths usually lead to long pulse widths and low peak powers. For improving these deficiencies, photonic crystal fibers (PCFs) have been developed to provide large single-mode cores and high absorption efficiencies. The PCF was recently employed to demonstrate a passively Q-switched laser with a Cr⁴⁺:YAG crystal as a saturable absorber in which under a pump power of 14.2 W, an average output power of 3.4 W with a repetition rate of 5.6 kHz was generated, corresponding to a pulse energy of 630 μJ [11]. However, the scale-up of the pulse energy is hindered by the nonsaturable loss of the Cr⁴⁺:YAG crystal [9].

In recent years, an AlGaInAs semiconductor material with a periodic quantum-well (QW) structure grown on a Fe-doped InP structure has been successfully used as a saturable absorber in an Yb-doped fiber laser to produce pulse energy up to 450 μJ [9]. It was found that the saturation fluence of the AlGaInAs QW absorber was two orders of magnitude smaller than that of Cr⁴⁺:YAG crystal. This property enables the AlGaInAs QW devices to be appropriate saturable absorbers for high-gain lasers. More importantly, experimental results also revealed that the AlGaInAs QW absorber has a lower nonsaturable loss than the Cr⁴⁺:YAG crystal with the same initial transmission. This result indicates that AlGaInAs QW absorbers have a potential to generate much higher pulse energies. So far, AlGaInAs QWs have not been employed to passively Q-switch Yb-doped PCF lasers.

We demonstrate a millijoule-level passive Q-switched Yb-doped photonic crystal

fiber laser with AlGaInAs QWs as a saturable absorber. We fabricate three types of AlGaInAs devices with different QW numbers to investigate the performance of passively Q-switched PCF lasers. With 50 groups of three AlGaInAs QWs as a saturable absorber and under a pump power of 16 W, the PCF laser generates an average power of 7.1 W at the pulse repetition rate of 6.5 kHz, corresponding to a pulse energy of approximately 1.1mJ. The overall pulse-to-pulse amplitude fluctuation and the temporal jitter are found to be well below 10% in root mean square (rms). I also calculated the peak power by integrating the photodiode traces and found its maximum value to reach 110 kW.

3.1.2 AlGaInAs QWs absorber and experimental setup

Similar to the previous structure [9] the saturable absorbers that offered by TrueLight Corporation were AlGaInAs QW/barrier structures grown on a Fe-doped InP substrate by metalorganic chemical-vapor deposition. The saturable absorbers were designed to consist of many groups of several QWs, spaced at half-wavelength intervals by InAlAs barrier layers with the band-gap wavelength around 806 nm and with the luminescence wavelength near 1064 nm. The thickness of the saturable absorbers was approximately 400 μm . Compared with other similar QWs devices, AlGaInAs material has the advantages of lattice match with the substrate InP over InGaAs/GaAs that output pulse energy of the passive Q-switch and the conversion efficiency are limited as a result of the lattice mismatch. AlGaInAs materials is also superior to InGaAsP material which can be grown on InP substrate because of its better electron confinement covering the wavelength range in 0.84-1.65 μm provided by the larger conduction band offset [12,13]. In this work we fabricated three types of AlGaInAs QWs that possess 50 groups of three QWs (3×50 QWs), 30 groups of three QWs (3×30 QWs), and 30 groups of two QWs (2×30 QWs). Figures 3.1(a)–(c) depict the schematic diagrams of three periodic AlGaInAs QWs structures. Figure 3.2 shows the measured results for the low-intensity transmittance spectrum of the three QW saturable absorbers. The initial transmissions of the absorbers near the wavelength of 1030 nm can be seen to be 18%, 36%, and 48% for the devices of 3×50 QWs, 3×30 QWs, and 2×30 QWs, respectively. With the z-scan method [9], I found that the modulation depths between low and high intensities were approximately 77%, 59%, and 47% for the absorbers of 3×50 QWs, 3×30 QWs, and 2×30 QWs, respectively. We also found that the

nonsaturable losses for three devices were less than 5%. The low nonsaturable losses indicate the quality of the QW devices to be rather high. Furthermore, the saturation fluence of the QW absorbers was measured to be in the range of 1 mJ/cm² and the relaxation time to be on the order of 100 ns [14]. The damage threshold for the AlGaInAs QWs was found to be approximately 300 MW/cm². Both sides of the semiconductor absorber have a simple single layer coating to reduce back reflections and the couple-cavity effects. The scheme of the experimental setup is shown in Fig. 3.3 (a). The cavity is composed of a 0.55 m polarization maintaining Yb-doped PCF (NKT photonics) that is the same one described in Ref. 11 and an external feedback cavity with a saturable absorber. Figure 3.3 (b) depicts the image of the cross section of the PCF pumped by a 532 nm light source. Since the absorption coefficient of the PCF was approximately 30 dB/m at 976 nm, the overall absorption efficiency could reach 95%. The rod-type PCF has a mode field diameter of 55 μm and a low numerical aperture (NA) of 0.02 to sustain the excellent beam quality. The pump cladding of the PCF has a diameter of 200 μm and an air-cladding to maintain a high NA of 0.6. The PCF was surrounded with a 1.7-mm thick outer cladding and was sealed with end-caps for protection. The boron doped stress-applying parts near the core were adopted to induce birefringence that produces diverse spectral losses to form a linearly polarization state for the fundamental mode.

The external cavity incorporates with a focusing lens of 50-mm focal length to focus the fiber output into the AlGaInAs QW absorber and a high reflective mirror behind the absorber for feedback. The AlGaInAs QW absorber was mounted in a copper block as a heat sink and with water cooling. The mode diameter on the saturable absorber was approximately 200 μm. The pump source was a 20-W 976-nm fiber-coupled laser diode with a core diameter of 200 μm and a numerical aperture of 0.2. Focusing lens with 25-mm focal length as one of the lens pairs depicted in Fig. 3.3 (a) and 90% coupling efficiency was used to re-image the pump beam into the fiber through the dichroic mirror with high transmission (HT, T>90%) at 976 nm and high reflectivity (HR, R>99.8%) within 1030~1100 nm. The pump spot radius was approximately 100 μm, and the pump coupling efficiency was estimated to be around 80%. The laser spectrum was measured by an optical spectrum analyzer with 0.1 nm resolution (Advantest Q8381A). The pulse temporal behavior was recorded by Leroy digital oscilloscope (Wavepro 7100; 10G samples/sec; 4 GHz bandwidth) with a fast InGaAs photodiode.

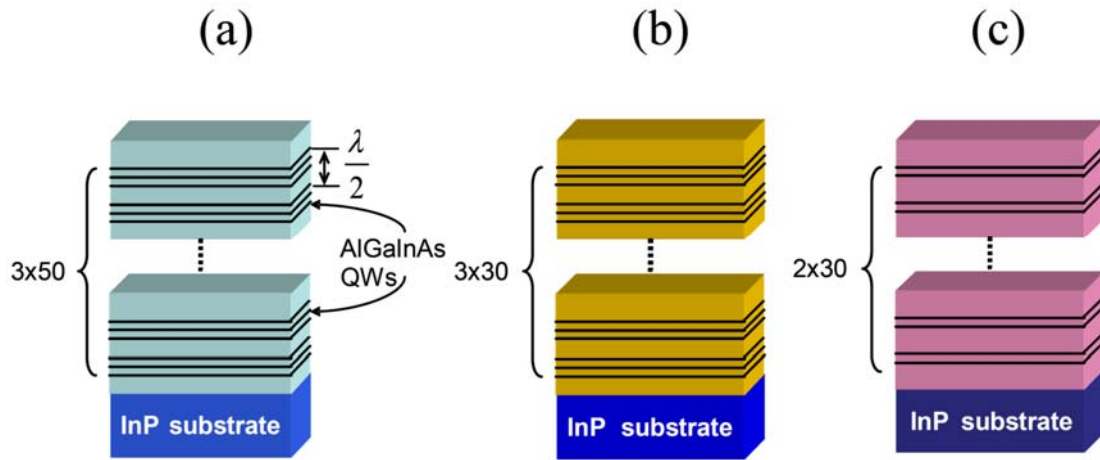


Fig 3. 1 Schematic diagrams of three periodic AlGaInAs QWs structures.

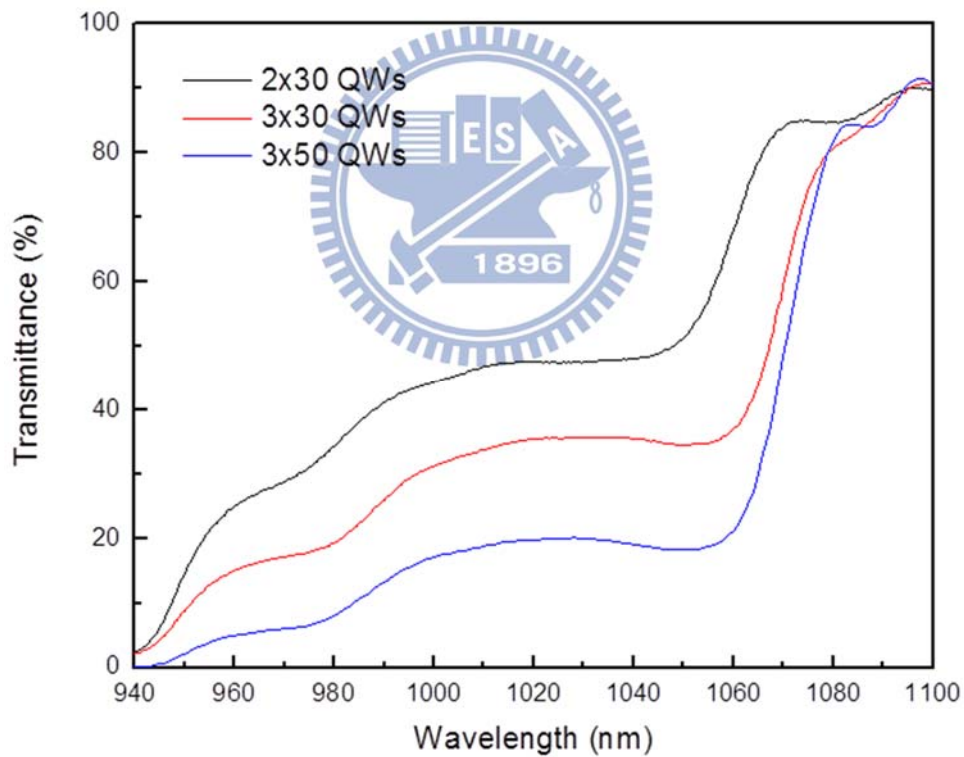


Fig 3. 2 Low-intensity transmittance spectrum of the three QW saturable absorbers.

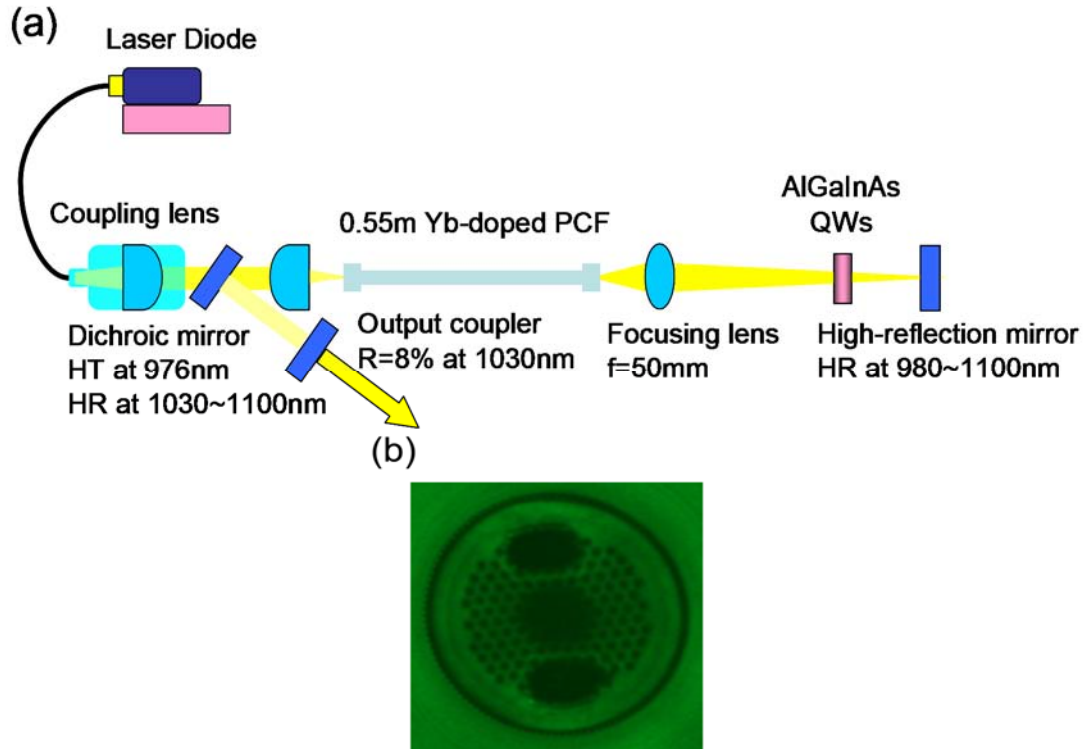


Fig 3. 3 (a) Setup for the passively Q-switched PCF laser; (b) image of the cross section of PCF.

3.1.3 Experimental results and discussions

Figure 3.4 depicts the average output power versus the launched pump power in CW and passive Q-switching operation. The external cavity in the CW operation contained only a re-imaging lens and a reflective mirror without the saturable absorber. At a launched pump power of 16 W, the CW PCF laser was found to generate an output power of 8.7 W, corresponding to a slope efficiency of 78%. In the passive Q-switching operation, the average output powers at a launched pump power of 16 W were 7.1 W, 7.7 W, and 8.0 W for the lasers with the saturable absorbers of 3×50 , 3×30 , and 2×30 QWs, respectively. The signal intensity of the amplified spontaneous emission (ASE) is 40 dB below the lasing signal of 1030 nm measured by the optical spectrum analyzer, so the fraction of the ASE output power can be neglected. As a result, the Q-switching efficiency (the ratio of the average power of Q-switched operation to that of CW one) were approximately 82%, 89%, and 92% for the lasers with the saturable absorbers of 3×50 , 3×30 , and 2×30 QWs, respectively. The overall Q-switching efficiency was significantly superior to the results obtained with Cr^{4+} :YAG crystals as saturable absorbers [11]. The lasing spectra for CW and passive Q-switching operations were quite similar with the peaks near 1030 nm and bandwidths

to be approximately 0.4 nm. The laser output was found to be linearly polarized with an extinction ratio of approximately 100:1, evidencing the function of the polarization maintaining in PCF. The M2 factor was found to be generally smaller than 1.3 over the entire output power range, owing to the low-NA feature of the PCF.

Figure 3.5 shows the pulse repetition rates in the passive Q-switching operation versus the launched pump power. Experimental results reveal that the pulse repetition rates for all cases increase monotonically with the pump power. At a launched pump power of 16 W, the pulse repetition rates were found to be 6.5 kHz, 16 kHz, and 23 kHz for the lasers with the saturable absorbers of 3×50 , 3×30 , and 2×30 QWs, respectively. With the experimental results of the average output power and the pulse repetition rate, we calculated the pulse energies versus the launched pump power. It was found that the pulse energies were nearly independent of the pump power and their average values were 1.1 mJ, 0.49 mJ, and 0.35 mJ for the lasers with the saturable absorbers of 3×50 , 3×30 , and 2×30 QWs, respectively. Fiber laser systems with energy of millijoule-class had been demonstrated with either actively Q-switched oscillator [15-17] or the master oscillator power fiber amplifier scheme [18-20]. To the best of our knowledge, this is the first time that the millijoule-level energy output was achieved with the passive Q-switching scheme in a PCF laser.

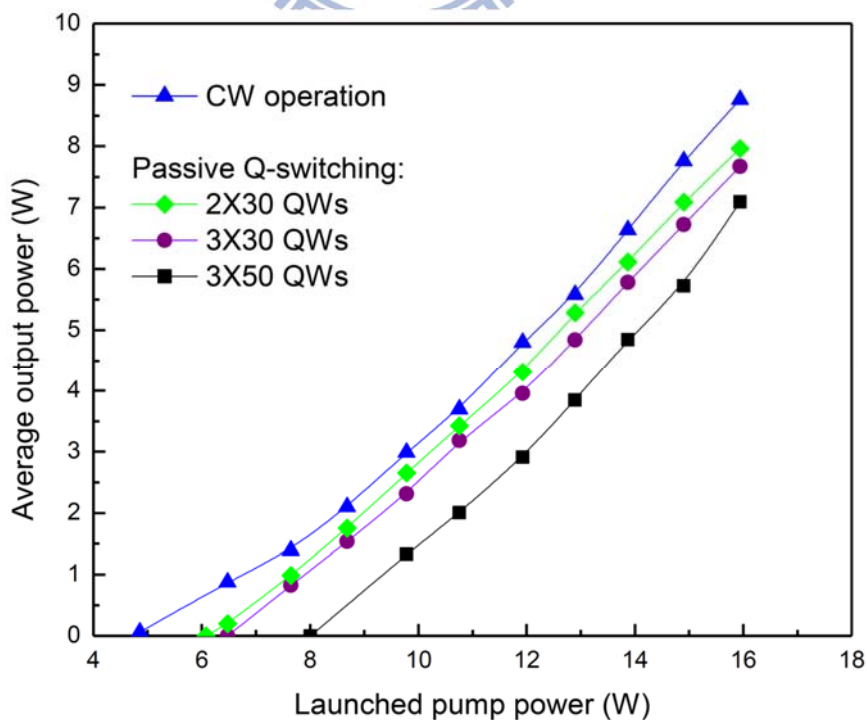


Fig 3. 4 Average output power with respect to launched pump power in CW and passive Q-switching operations.

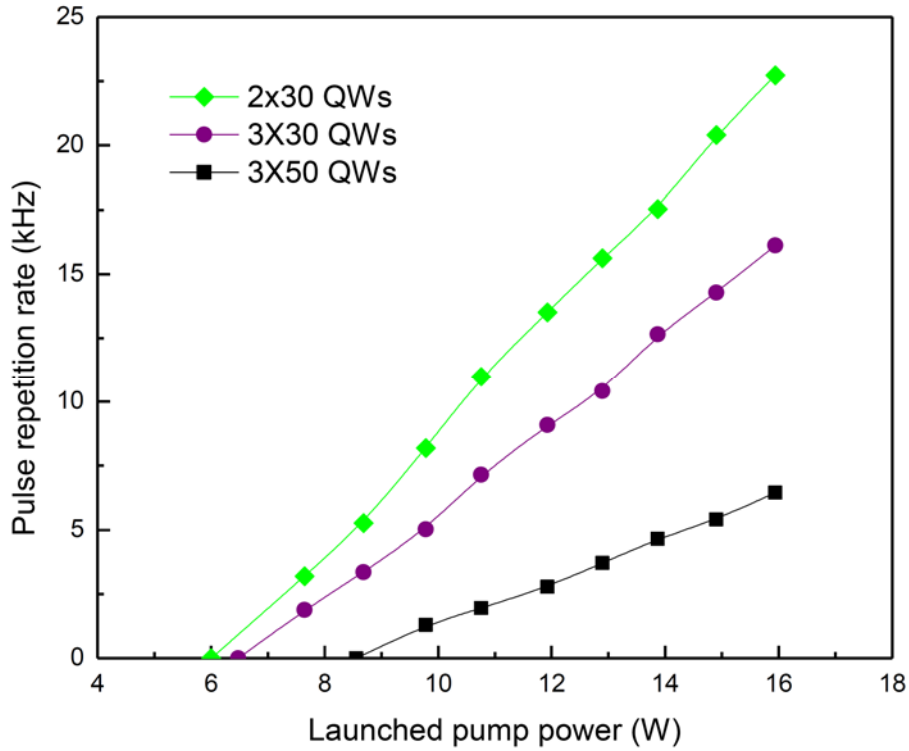
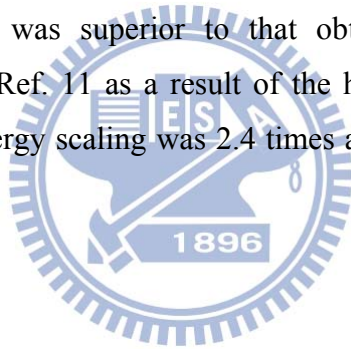


Fig 3. 5 Pulse repetition rates in the passive Q-switching operation versus the launched pump power.

Figures 3.6(a)–3.6(c) depict typical oscilloscope traces for the single Q-switched pulses of the lasers with the saturable absorbers of 2×30 , 3×30 , and 3×50 QWs, respectively. It can be seen that the temporal shape of the single Q-switched pulse obtained with the absorber of 2×30 QWs is a simple pulse, whereas the temporal shape obtained with the absorber of 3×50 QWs reveal conspicuous modulation whose period is nearly equal to the round trip time. The self-modulation phenomenon inside the Q-switched envelope has been frequently observed in pulsed fiber lasers. This phenomenon is generally considered to arise from the stimulated Brillouin scattering (SBS) which can provide strong feedback to the cavity together with pulse compression. The SBS-related pulses have been demonstrated in different fiber laser designs, such as self-Q switched [21-23], actively Q-switched [24,25], and passively Q-switched [26,27] fiber lasers. Note that another self-modulation phenomenon was found in passively Q-switched Nd-doped crystal lasers with Cr^{4+} :YAG crystals as saturable absorbers [28-31]; however, the origin is attributed to the excited-state absorption of the absorber and the fluctuation mechanism [32,33]. Our results reveal that the pulse energy obtained with the absorber of 3×30 QWs is just above the SBS threshold. As seen in Fig. 3.6(b), the rear end of the pulse exhibits a fast transient dynamics. On the other

hand, the intense SBS effect leads to the pulse to be strongly modulated, as seen in Fig. 3.6(c). With the numerical integration, we found the maximum peak powers were 7.4 kW, 12.8 kW, and 110 kW for the lasers with the saturable absorbers of 2×30 , 3×30 , and 3×50 QWs, respectively. The corresponding optical intensity on the 3×50 QWs was 350 MW/cm^2 which is quite close to the damage threshold of the saturable absorber, but no optical damage was observed. Figures 3.7(a)–3.7(c) show typical oscilloscope traces of a train of output pulses obtained with the saturable absorbers of 2×30 , 3×30 , and 3×50 QWs, respectively. It can be seen that for the laser with the absorber of 2×30 QWs the pulse-to-pulse amplitude fluctuation was generally less than 4% in rms. Even for the case of 3×30 QWs, just above the SBS threshold, the pulse-to-pulse amplitude fluctuation was also smaller than 4% in rms. Although the strong SBS effect might deteriorate the pulse stability to some extent, the pulse-to-pulse amplitude fluctuation could still be maintained to be 8.5% in rms for the laser with the saturable absorber of 3×50 QWs, as shown in Fig. 3.7(c). Compared with the previous results, the pulse stability was superior to that obtained in Ref. 9 and slightly diminished with respect to Ref. 11 as a result of the high pulse energy induced SBS effect. The overall pulse energy scaling was 2.4 times as high as the one in Ref. 9 and 1.8 times as that in Ref. 11.



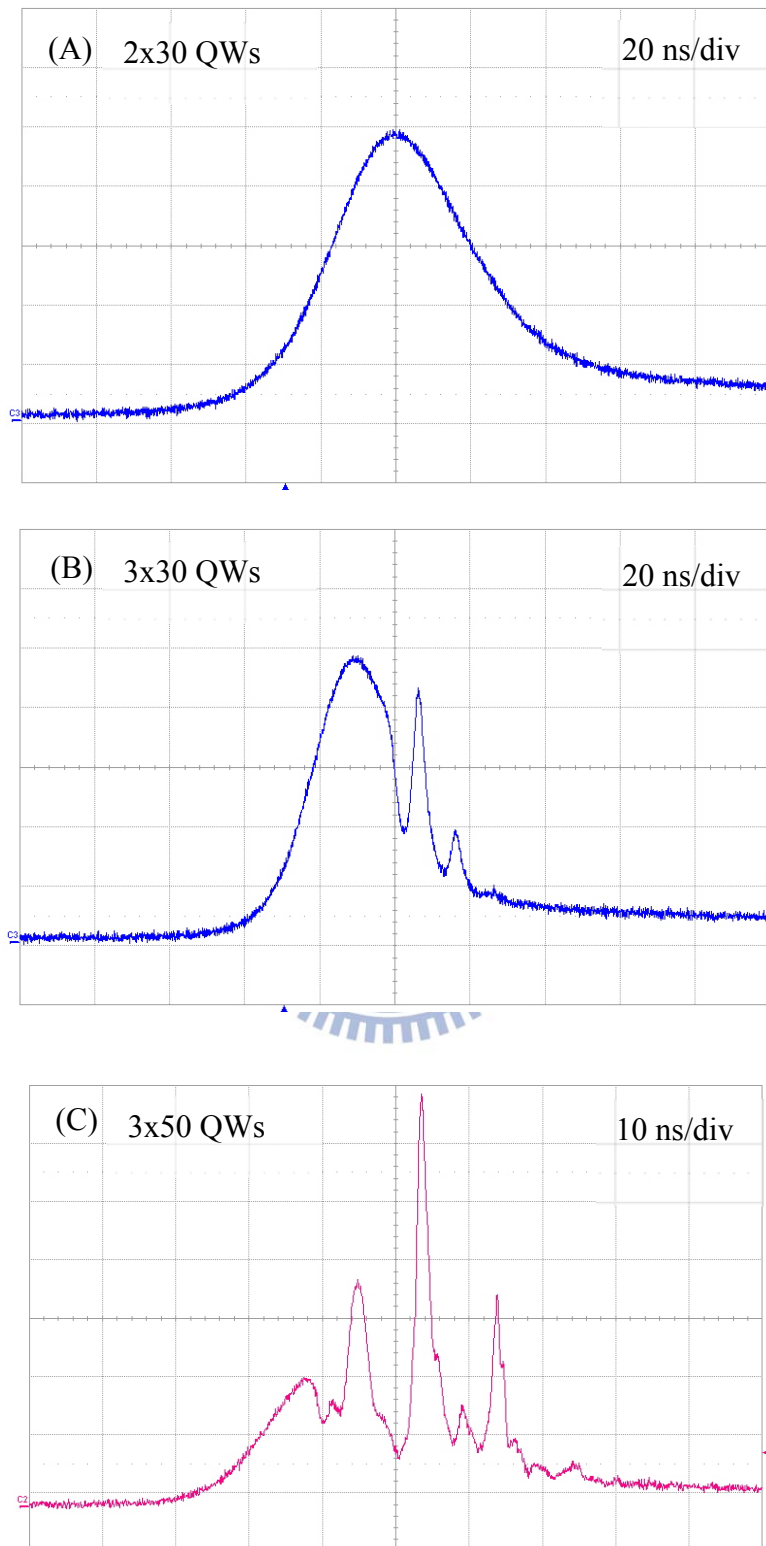


Fig 3. 6 Typical oscilloscope traces for the single Q-switched pulses of the lasers with the saturable absorbers of (a) 2×30 , (b) 3×30 , and (c) 3×50 QWs, respectively.

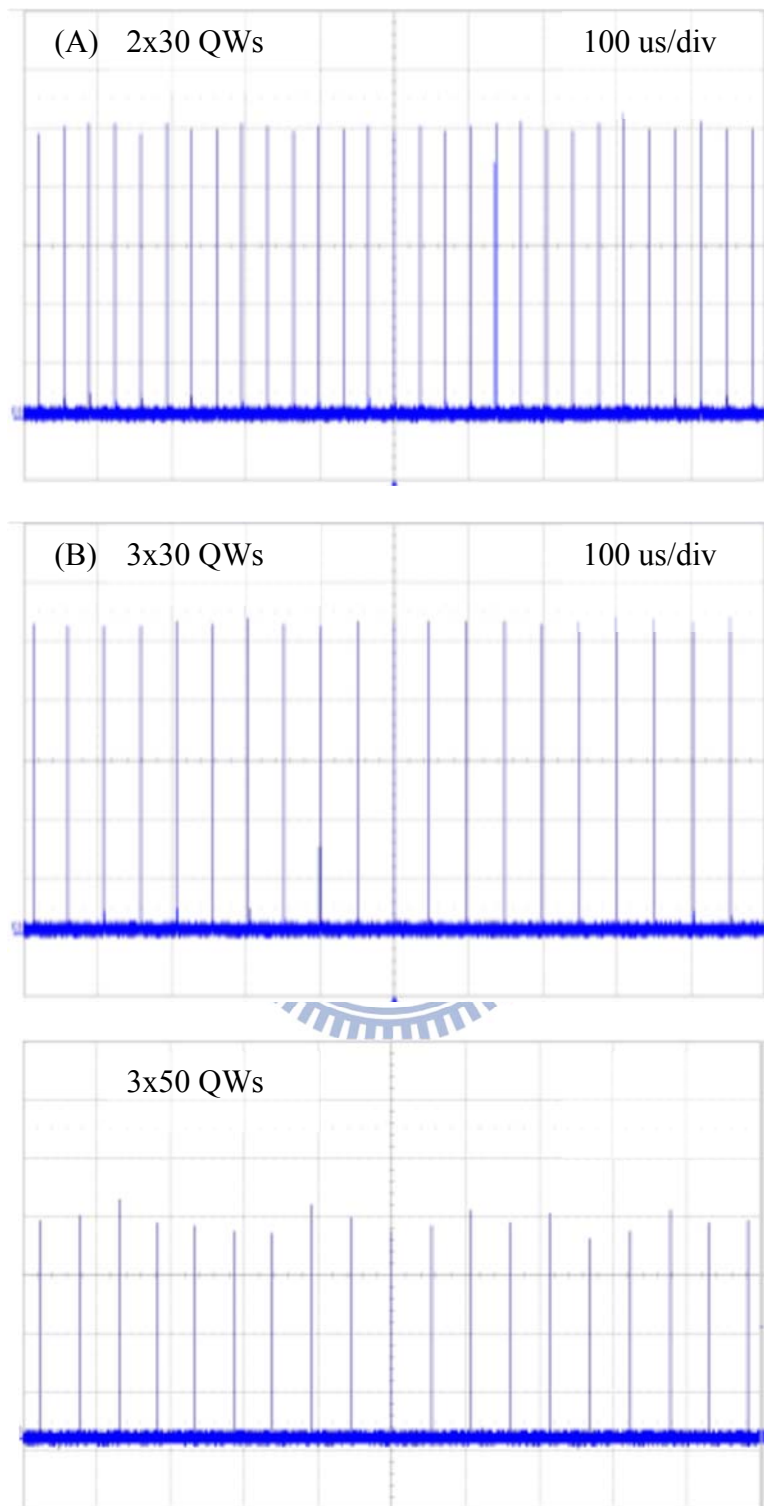


Fig 3. 7 Typical oscilloscope traces for a train of output pulses of the lasers with the saturable absorbers of (a) 2×30 , (b) 3×30 , and (c) 3×50 QWs, respectively.

3.1.4 Conclusion

In conclusions, we have, for the first time to my knowledge, demonstrated a millijoule-level passively Q-switched Yb-doped photonic crystal fiber laser with AlGaInAs QWs as a saturable absorber. At a launched pump power of 16 W, the average output powers were 7.1 W, 7.7 W, and 8.0 W for the lasers with the saturable absorbers of 3×50 , 3×30 , and 2×30 QWs, respectively. The pulse energies were found to be 1.1 mJ, 0.49 mJ, and 0.35 mJ for the lasers with the saturable absorbers of 3×50 , 3×30 , and 2×30 QWs, respectively. The maximum peak power could be up to 110 kW. The overall pulse-to-pulse amplitude fluctuation and the temporal jitter could be maintained to be well below 10% in rms. These high-pulse-energy high-peak-power passively Q-switched PCF lasers are potentially useful light sources for many technical applications.



3.2 A widely tunable eye-safe based on a passively Q-switched PCF laser

3.2.1 Introduction

High-peak-power tunable laser sources have been in demand for the applications in the eye-safe wavelength regime near 1.55- μm such as free-space communication, gas sensing, spectroscopy, and medical treatment [34-37]. In recent years, double-cladding rare-earth doped fiber lasers are of great interest due to their good beam confinement, excellent heat dissipation, spatial beam quality, and high efficiency [38-47]. Because of the broad bandwidth resulted from the amorphous nature of the glass host, directly utilizing erbium doped fiber (EDF) lasers or erbium-ytterbium-codoped double-clad fiber lasers (EYDFL) possess the potential of wavelength tunability [48-52]. However, traditionally a wavelength-selective element such as grating or etalon is desired in the cavity and thus increases the complexity of laser cavity [53-56]. An alternative method for flexibility in tuning wavelength is an optical parametric oscillator (OPO) pumped by a laser source with shorter wavelength [57-61]. Based on the phase matching condition, the signal output wavelength could be controlled by adjusting the temperature of nonlinear crystal, pump incident direction, or pump wavelength.

For pulsed OPO operation, the passively Q-switch gives the advantage of simplification and compactness in experimental setup. In addition to the mostly used transition metal-doped crystals, semiconductor material with a periodic quantum-well (QW) structure has been demonstrated as a saturable absorber in the EYDFL to achieve a 105- μJ passively Q-switched 1.54- μm laser [62] and in the ytterbium doped photonic crystal fiber (PCF) laser to achieve an 1.1-mJ passively Q-switched 1.03- μm laser [63]. In 2010, the performance of eye-safe laser with a passively Q-switched PCF laser in an intracavity OPO was firstly reported [64]. In the published work, the fundamental wavelength is fixed at the maximum gain peak and a temperature-insensitive x-cut KTiOPO (KTP) was used in the OPO, this makes it inflexible to realize a broadly tunable laser. Periodically poled lithium niobate (PPLN) is a powerful quasi-phase-matching (QPM) nonlinear crystal in OPOs for generating near-infrared (NIR) to midinfrared (MIR) radiation because of its advantages of high nonlinear coefficient ($\sim 15 \text{ pm/V}$) and broad transmission spectrum (up to 4.5 μm) [61,65-67]. In addition, the high refractive-index-temperature coefficient makes a signal wavelength shift up to 0.5 $\text{nm}/^\circ\text{C}$ at a pump source of 1030 nm for a grating period of 28-30 μm . Therefore, it is

well worthy of investigation to utilize the QPM nonlinear crystal in an OPO pumped by a passively Q-switched ytterbium-doped PCF laser to generate broadly tunable eye-safe wavelength radiation.

Here we report, for the first time to my knowledge, on a widely tunable eye-safe laser based on a PCF. An optical parametric oscillator was pumped by a passively Q-switched PCF laser with AlGaInAs QWs as a saturable absorber. First, the 1029-nm PCF laser with pulse energy of 750 μJ at a pulse repetition rate of 6.5 kHz was established under a pump power of 13.1 W at 976 nm. The PCF laser was used to pump an OPO to generate eye-safe signal wave. By tuning the temperature of PPLN in the OPO cavity from 20 to 140°C, the tuning range of signal wavelength was over 80 nm from 1513 to 1593 nm. A maximum peak power of 19 kW and pulse energy of 138 μJ was obtained under the pump energy of 390 μJ .

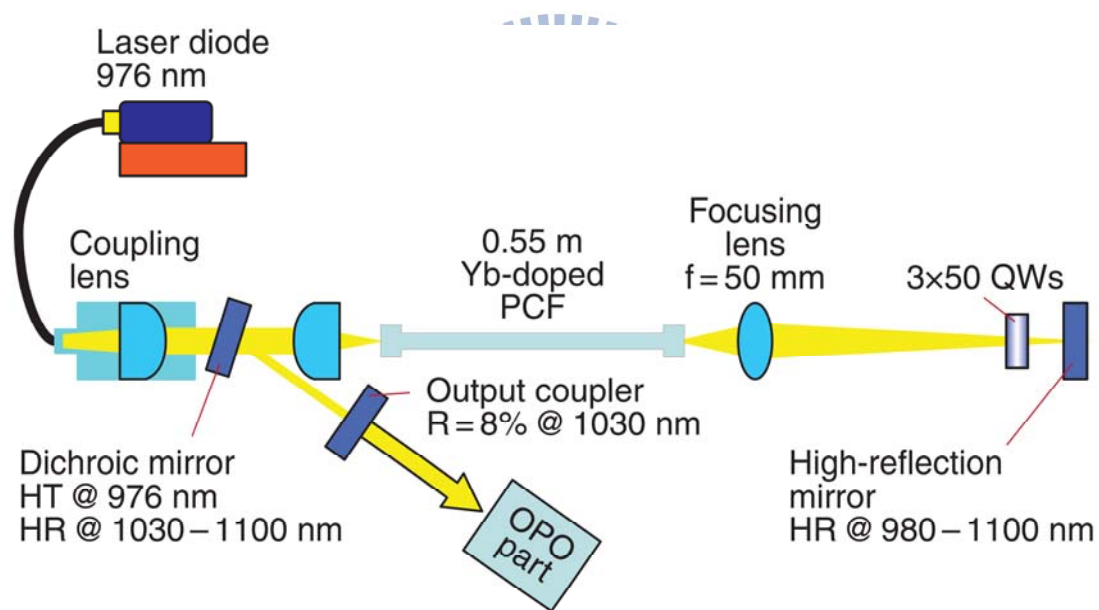


Fig 3. 8 Schematic sketch of the external-cavity optical parametric oscillator pumped by the passively Q-switched photonic crystal fiber laser.

3.2.2 Diode pumped PCF laser with AlGaInAs semiconductor absorber

The schematic of external-cavity OPO pumped by a passively Q-switched PCF laser is depicted as Fig. 3.8. The experimental setup could be separated into two major parts, one is a diode pumped passively Q-switched PCF laser and the other one is a

singly resonating OPO. The PCF laser cavity consists of a 55-cm polarization maintaining (PM) Yb-doped PCF and an external feedback cavity with a saturable absorber. The external cavity incorporates with a focusing lens of 50-mm focal length to focus the fiber output into the saturable absorber and a high reflective mirror behind the saturable absorber for feedback. The rod-type PCF has a large mode field diameter of 55 μm to push the nonlinear threshold up to higher level than conventional single mode fiber. And a low numerical aperture value of 0.02 permits to sustain the operation in single transverse mode and excellent beam quality. The pump cladding of the PCF has a diameter of 200 μm and an air-cladding to maintain a high numerical aperture of 0.6. The image of the cross section of the PCF is depicted as Fig. 3.9. The small ratio between the inner pump cladding and 70- μm core diameters brings about the pump absorption coefficient to be 30 dB/m at 976 nm. The PCF was surrounded with a 1.7-mm thick outer cladding and was sealed with end-caps for protection. The boron doped stress-applying parts were adopted to induce birefringence that produces diverse spectral losses to form a linearly polarization state for the fundamental mode. The saturable absorber is a structure of AlGaInAs QW/barrier grown on a Fe-doped InP substrate by metalorganic chemical-vapor deposition, as depicted in Fig. 3.10. The structure consists of 50 groups of AlGaInAs QW/barrier. Each group contains three 8-nm-thick QWs and 10-nm-thick barriers. In order to increase the damage threshold, each group of quantum wells is designed to be located at the nodes of the pumping mode, or to have intervals of half-wavelength separated by barriers. A window layer of InP was deposited on the gain structure to prevent surface recombination and oxidation. Both surfaces of the saturable absorber were coated to have anti-reflection coating at 1030 nm ($R < 0.2\%$). The initial transmission of the saturable absorber was measured to be 19%. The mode diameter on the saturable absorber was estimated to be approximately 400 μm . The pump source was a 20-W 976-nm fiber-coupled laser diode with a core diameter of 200 μm and a numerical aperture of 0.2. Focusing lens with 25-mm focal length and 90% coupling efficiency was used to re-image the pump beam into the fiber through the dichroic mirror with high transmission (HT, $T > 90\%$) at 976 nm and high reflectivity (HR, $R > 99.8\%$) within 1030 - 1100 nm. The pump spot radius was approximately 100 μm , and the pump coupling efficiency was estimated to be around 80%. The pulse temporal behavior was recorded by Leroy digital oscilloscope (Wavepro 7100, 10 G samples/sec, 4 GHz bandwidth) with a fast InGaAs photodiode.

The output power, pulse energy and output spectrum are shown in Fig. 3.11. The maximum output power was obtained to be 4.9 W under the 13.1 W of pump power and it turns out conversion efficiency over 37%. The central peak of wavelength is dependent on the pump power and distributes from 1031 to 1029 nm with increasing the pump power. The inset of Fig. 3.11 shows the output spectrum of PCF laser with the 13.1 W of pump power. The full width at half maximum FWHM of bandwidth is around 0.5 nm and the M² factor was measured to be less than 1.3 over the complete output power range, owing to the low-NA feature of the fiber. The laser output was measured to be linearly polarized with an extinction ratio of approximately 100:1. Fig. 3.12(a) and Fig. 3.12(b) show the traces of output pulses under a lower and higher pump power level, 6.3 and 13.1 W, respectively. A self-modulation phenomenon inside the Q-switched envelope was obviously observed in pulsed fiber lasers for high pump power. This phenomenon is generally considered to arise from the stimulated Brillouin scattering (SBS) which can provide strong feedback to the cavity together with pulse compression [68-71]. The SBS-related pulses have been demonstrated in different fiber laser designs, such as self-Q switched [35-37], actively Q-switched [71,72], and passively Q-switched [73,74] fiber lasers. Although the strong SBS effect might deteriorate the pulse stability to some extent, the pulse-to-pulse amplitude fluctuation could still be maintained to be less than 8.0% in rms at the maximum pump power of 13.1 W. The output repetition rate ranges from 1.5 to 6.5 kHz and is related to pump power. The pulses with maximum peak power of 170 kW and pulse energy up to 750 μ J were obtained.

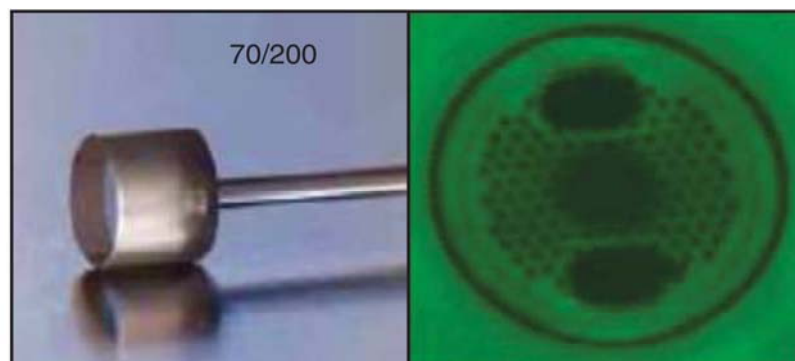


Fig 3. 9 Image of cross section of rod-type PCF.

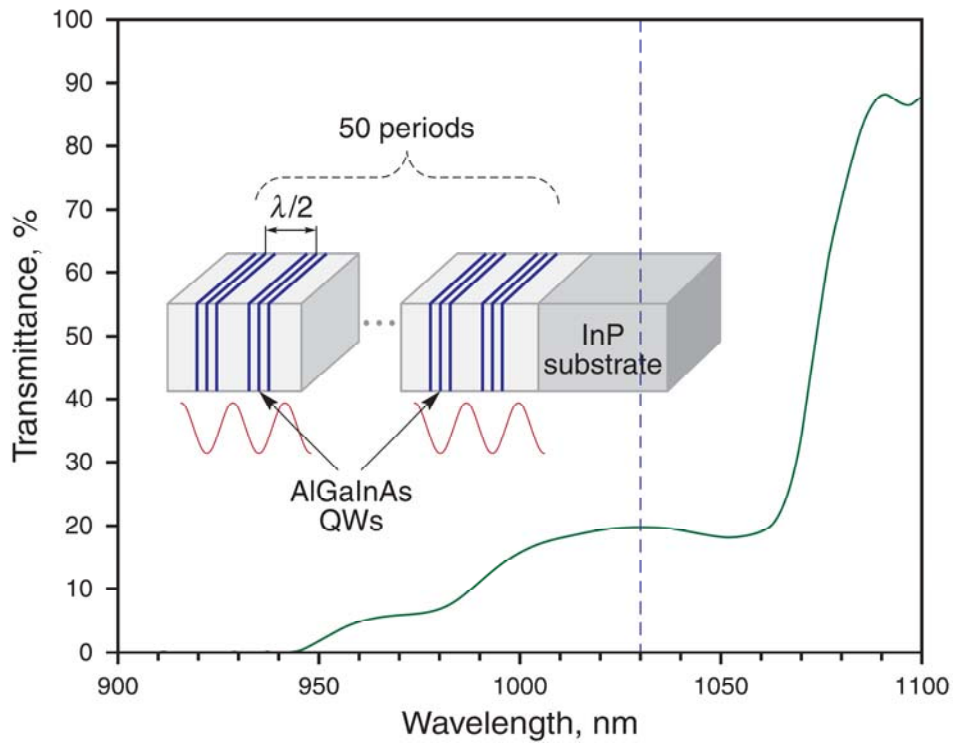


Fig 3. 10 Transmission spectrum and structure of AlGaInAs saturable absorber.

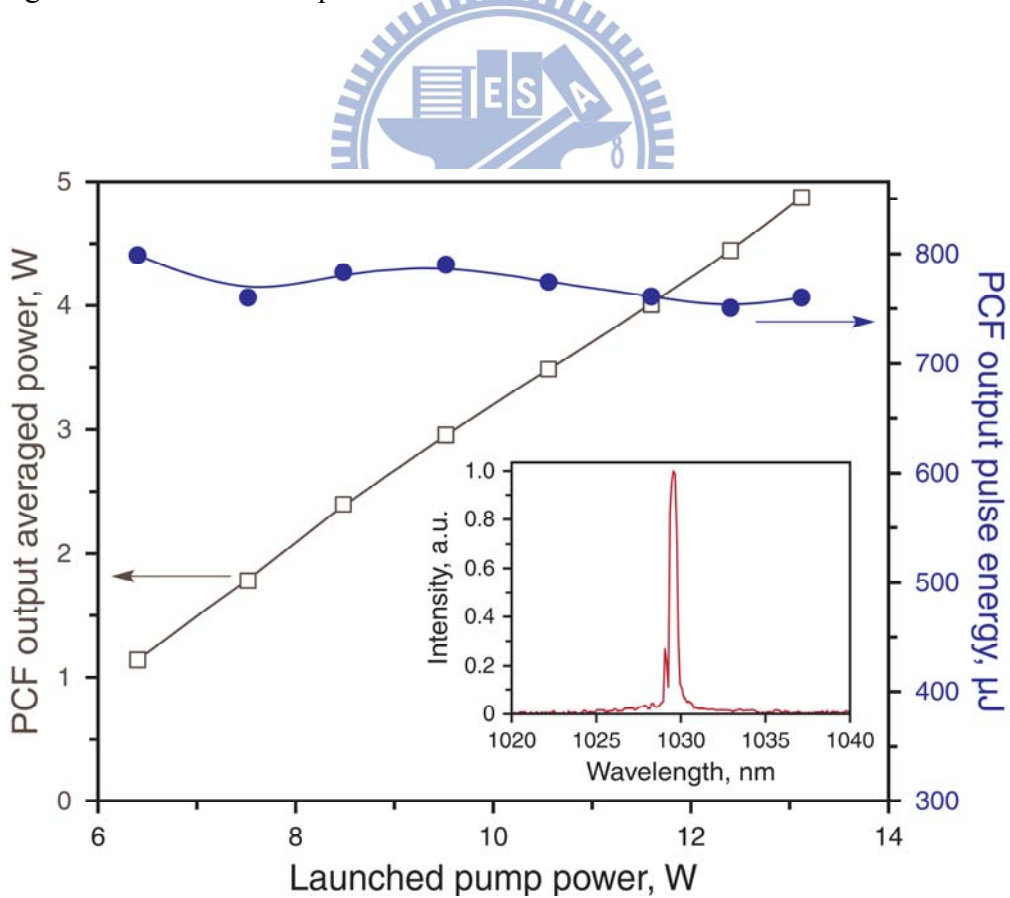


Fig 3. 11 Output power of the passively Q-switched PCF laser versus the 976-nm launched pump power. Inset is the lasing spectrum obtained with 12.5 W of pump power.

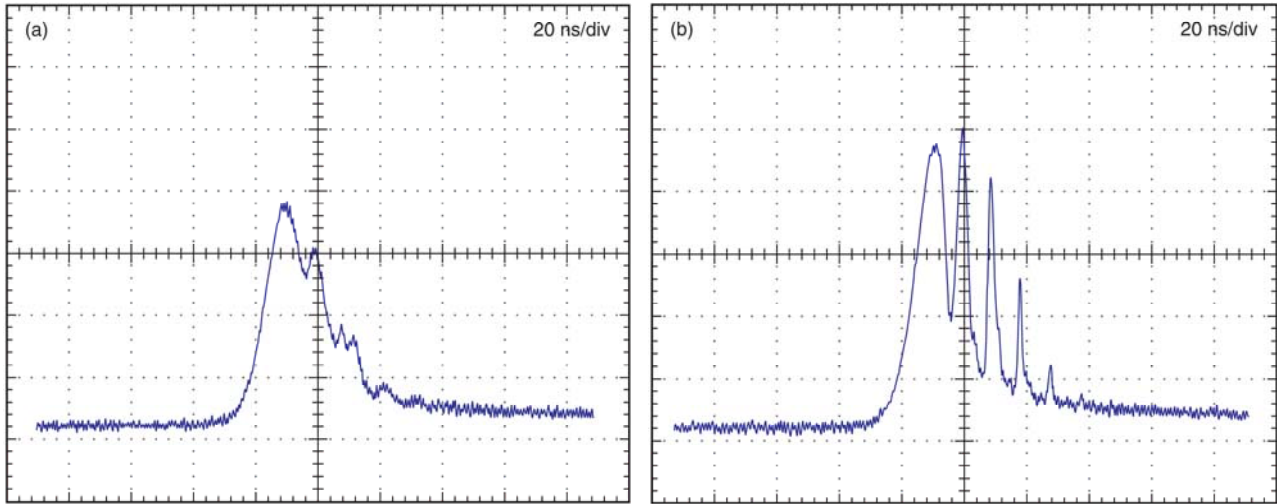


Fig 3. 12 Typical oscilloscope traces of output pulses of the passively Q-switched PCF laser. (a) pulse shape with 6.3 W of pump power and (b) pulse shape with 13.1 W of pump power

3.2.3 Tunable eye-safe laser with an external-cavity OPO

The 750- μ J passively Q-switched PCF laser at a repetition rate of 6.5 kHz was used as a pump source in the external-cavity OPO, as depicted in Fig. 3.13. The nonlinear crystal in is a 0.76-mm thick and 2-cm long congruent PPLN with a poling period of 29.6- μ m. The singly-resonant OPO cavity consists of two BK7 plane mirrors, the front mirror and output coupler. The front mirror is coated with high transmission at pump wavelength ($T > 90\%$) and high reflectivity from 1500 to 1600 nm ($R > 99\%$). The output coupler is coated with high transmission at pump wavelength ($T > 90\%$) and partial reflectivity from 20 to 90% corresponding to the wavelength from 1510 to 1590 nm. A focusing lens with 75-mm focal length was used to focus the pump source into the PPLN crystal. The pump spot size inside PPLN was measured to be around 300 μ m. Between the PCF laser and external-cavity OPO, a half-wave plate and a polarization cube were bundled together to control the pump incident power. The maximum average pump incident power was limited to 2.6 W, or the pulse energy limited to 390 μ J for the consideration of photorefractive effect and damage threshold of PPLN. The PPLN was temperature controlled from 20 to 140 $^{\circ}$ C by an oven to adjust the phase matching wavelength.

The performance of output power of external-cavity OPO pumped by passively Q-switched PCF laser is shown in Fig. 3.14. The temperature of PPLN was controlled at 100 $^{\circ}$ C. Under the pump power of 2.6 W, the output average power of 0.9 W at signal

wave was obtained and corresponds to pulse energy of 138 μJ . The conversion is about 35% and the slope efficiency is up to 37.5%. From the temporal pulse traces of pump and signal wave shown in Fig. 6b, the signal pulse shape possesses several spikes which were resulted from SBS effect in pump source as mentioned above. Such an effect can be reduced for lower operating power of PCF laser as depicted in Fig. 3.12(a). The maximum output peak power of signal wave was estimated to be 19 kW with an effective pulse width of 7.3 ns.

The temperature of PPLN was tuned from 20 to 140 $^{\circ}\text{C}$ in an interval of 20 $^{\circ}\text{C}$. The output wavelength of signal wave shifts from 1513 to 1593 nm and total 80-nm tuning range was obtained. Fig. 3.15 shows the wavelength of output signal in different operating temperature. The experimental data with empty circles is in good agreement with theoretical data calculated from Selmier's equations [75,76]. Higher temperature and larger wavelength is possible. However, the reflectivity of output coupler used is not uniform within the tuning range of wavelength. Besides, with increasing the temperature higher than 140 $^{\circ}\text{C}$, the idler phase-matching wavelength gradually approaches 2.8 μm , which locates at the peak absorption of lithium niobate [77]. As a result, higher loss will be induced in the cavity for operating temperature higher than 140 $^{\circ}\text{C}$. On the other hand, for lower operating temperature, the photorefractive effect of congruent PPLN will get stronger and limit the output performance. Therefore, there is an optimum efficiency for a specific temperature, as depicted in the inset of Fig. 3.15. In this experiment, the conversion efficiency varies from 11 to 35% and the optimum temperature is found to be around 100 $^{\circ}\text{C}$. At the optimum point, the phase-matching signal wavelength is 1559 nm with a corresponding output reflectivity of 65%.

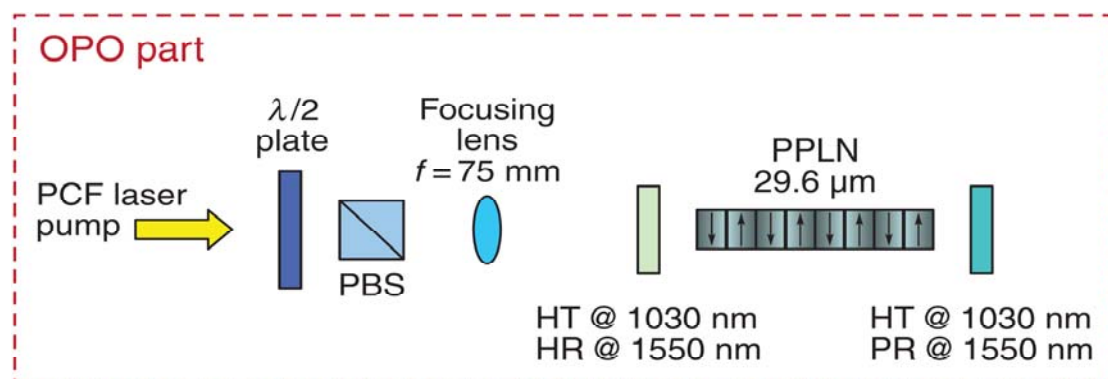


Fig 3. 13 Schematic sketch of the OPO setup. A half-wave plate and polarization beam splitter cube were settled in front of OPO to control the input pump power.

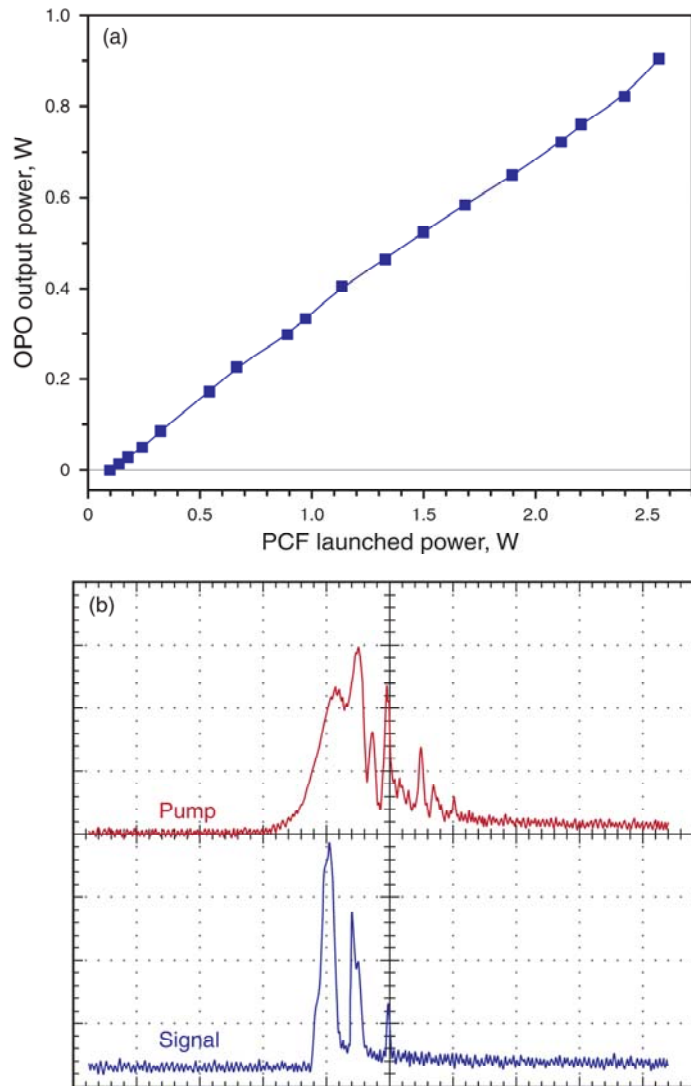


Fig 3. 14 Output performance of external-cavity OPO. (a) averaged output power of signal wave versus averaged power of PCF laser and (b) temporal traces of pump and signal wave.

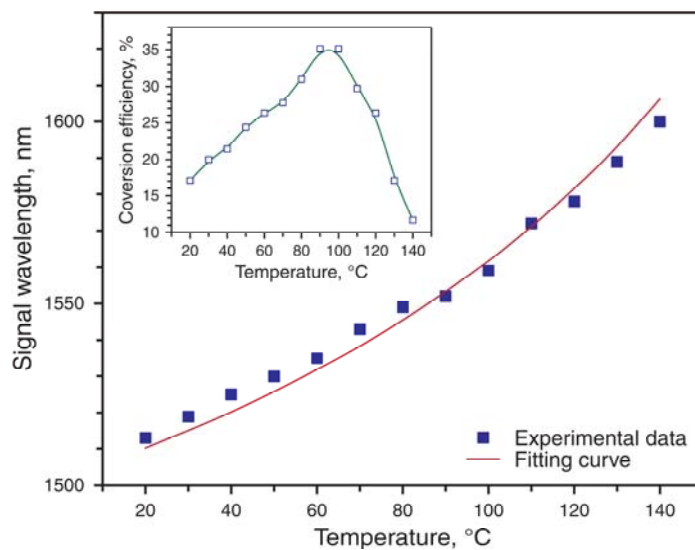


Fig 3. 15 Tuning curve of signal wavelength versus different operating temperature. Inset is the corresponding conversion efficiency with temperature.

3.2.4 Conclusion

We achieved a widely tunable passively Q-switched photonic crystal fiber laser by means of an external-cavity optical parametric oscillator. With an AlGaInAs QW/barrier structure as a saturable absorber in the 1029-nm PCF laser, the fundamental pulse with energy up to 750 μJ was obtained and was incident into the OPO cavity. Under the pump energy of 390 μJ , the maximum output energy and peak power of signal wave was found to be 138 μJ and 19 kW, respectively. By tuning the temperature of nonlinear nonlinear crystal, PPLN, over 80-nm tuning range of the signal output wavelength from 1513 to 1593 nm was obtained.



3.3 Passively Q-switched photonic crystal fiber laser with Cr⁴⁺:YAG and its application

3.3.1 Introduction

In recent years, double-cladding rare-earth doped fiber lasers have attracted a lot of attention due to their good beam confinement, excellent heat dissipation, spatial beam quality, and high efficiency [78–84]. Q-switched lasers have many applications on industrial processing, measurements of positions, and medical treatments owing to their high peak power than in CW operation [85–87]. By enlarging the active volume of the gain medium, corresponding to the doped core size of the fiber, one can achieve the merit of the high pulse energy [88,89]. However, the conventional large core fibers suffer from mode-quality degradation and their long lengths usually lead to long pulse widths and low peak powers.

Recently, a novel technology [90] has been developed to provide photonic crystal fibers (PCFs) with large single mode core and high absorption efficiency. The PCF laser was lately employed to perform an actively Q-switched operation in which the pulse energy was up to 2 mJ with a pulse width shorter than 10 ns at a repetition rate of 10 kHz. Compared to the active Q-switching, passive Q-switching lasers are more compact and lower cost because they use saturable absorbers in replace of acoustic-optic or electro-optic modulators as the Q-switch. Crystal-based [91–94] saturable absorbers have been well developed to replace the dye-cells used in solid-state lasers. Cr⁴⁺:YAG crystals have been exploited as saturable absorbers in large-mode-area Yb-doped fibers [95–98], among which the maximum pulse energy was 350 μJ. Nevertheless, the passive Q-switching in a PCF laser has not been investigated so far. In this paper, we report, for the first time to our knowledge, on the performance of a single-polarization passively Q-switched Yb-doped PCF laser and its application to intracavity optical parametric oscillator (OPO). With a Cr⁴⁺:YAG crystal as a saturable absorber and under a pump power of 14.2 W, the PCF laser generates an average output power of 3.4 W at 1030 nm at the repetition rate of 5.6 kHz, corresponding to the pulse energy up to 630 μJ. The pulse width and the peak power are 36 ns and 17.4 kW, respectively. Experimental results revealed that since the Yb-doped PCF provokes a narrow linewidth and a high polarization extinction ratio, the pulse-to-pulse amplitude fluctuation and the temporal jitter were well below 5% for the pump power greater than 8 W. The overall quality of the output pulses is noticeably

superior to that obtained in conventional passively Q-switched fiber lasers. With the passively Q-switched PCF laser to pump an intracavity OPO, the output pulse energy of 140 μJ can be generated for the signal wave at 1515 nm at a repetition rate of 3.3 kHz. Owing to the efficient cavity-dumping effect, the signal pulse width is found to be as short as 1.0 ns; consequently, the peak power can reach 140 kW.

3.3.2 Experiment setup

Figure 3.16 shows the setup of the passively Q-switched PCF laser with a Cr^{4+} :YAG as the saturable absorber. The cavity consists of a 55 cm polarization maintaining (PM) Yb-doped PCF and an external feedback cavity with a saturable absorber. The external cavity incorporates with a focusing lens of 50-mm focal length to focus the fiber output into the Cr^{4+} :YAG crystal and a high reflective mirror behind the saturable absorber for feedback. The rod-type PCF has a mode field diameter of 55 μm and a low numerical aperture of 0.02 to sustain the excellent beam quality. The pump cladding of the PCF has a diameter of 200 μm and an air-cladding to maintain a high numerical aperture of 0.6. The small ratio between the inner pump cladding and core diameters brings about the pump absorption coefficient to be approximately 30dB/m at 976nm. The PCF is surrounded with a 1.7-mm thick outer cladding and is sealed with end-caps for protection. The boron doped stress-applying parts were adopted to induce birefringence that produces diverse spectral losses to form a linearly polarization state for the fundamental mode. The Cr^{4+} :YAG saturable absorber has a thickness of 3 mm and was highly doped with a small signal transmission of 28%. Both sides of the saturable absorber are coated for antireflection at 1030 nm ($R < 0.2\%$) and the mode diameter on the saturable absorber is approximately 400 μm . The pump source is an 18-W 976-nm fiber-coupled laser diode with a core diameter of 100 μm and a numerical aperture of 0.2. Focusing lens with 25-mm focal length and 90% coupling efficiency is used to re-image the pump beam into the fiber through the dichroic mirror with high transmission (HT, $T > 90\%$) at 976 nm and high reflectivity (HR, $R > 99.8\%$) within 1030~1100 nm. The pump spot radius is approximately 50 μm , and the pump coupling efficiency is estimated to be around 80%. The pulse temporal behavior is recorded by Leroy digital oscilloscope (Wavepro 7100; 10G samples/sec; 4 GHz bandwidth) with a fast InGaAs photodiode.

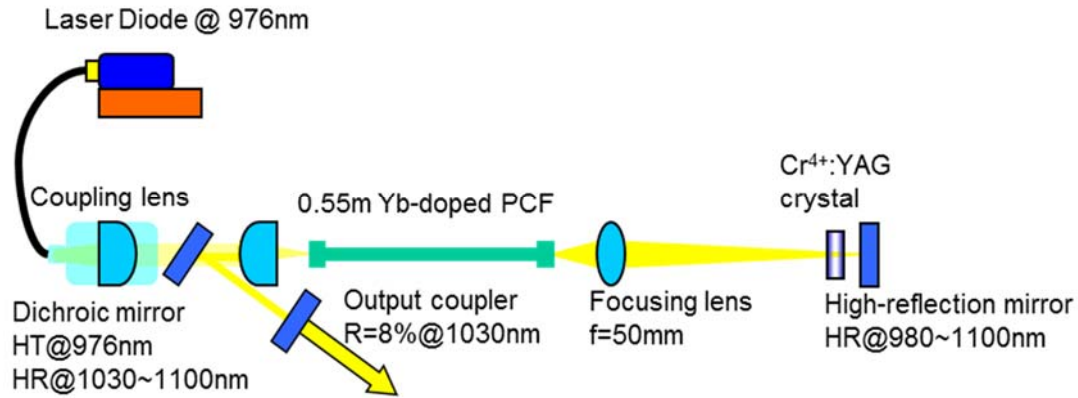


Fig 3. 16 Setup for the passively Q-switched PCF laser with Cr⁴⁺:YAG.

3.3.3 Experimental results and discussions

Figure 3.17(a) shows the average output power with respect to the launched pump power in the CW and passive Q-switching operations. The external cavity in the CW operation only included a re-imaging lens and a reflective mirror. At a launched pump power of 14.2 W, the average output power in the CW and passive Q-switching operations were 5.4 W and 3.4 W, respectively. The slope efficiency seemed to decrease slightly above 12.5 W of pump power which was due to temperature lifting induced wavelength shift of the pumping laser diode. The lasing spectra for both operations were quite similar with the peaks near 1030 nm and bandwidths to be approximately 0.4 nm, as shown in the inset of Fig. 3.17(a). The M^2 factor was also measured to be less than 1.3 over the complete output power range, owing to the low-NA feature of the fiber. The laser output was found to be linearly polarized with an extinction ratio of approximately 100:1, evidencing the function of the polarization maintaining in PCF. The pulse repetition rate and the pulse energy versus the launched pump power are shown in Fig. 3.17(b). The pulse repetition rate increased monotonically with the pump power up to 5.6 kHz at a pump power of 14.2 W. The pulse energy was maintained to be nearly constant at 630 μ J for all the pump power range. Figures 3.18(a) and 3.18(b) show typical oscilloscope traces for a single Q-switched pulse and a Q-switched pulse train, respectively. The temporal shape of the single pulse reveals a self-mode-locking (SML) phenomenon that has been observed in conventional fiber lasers and the possible mechanisms for its origin have been discussed in Refs [96,99,100]. During the early research on mode-locking, the SML phenomenon was observed on different types of lasers including He-Ne [101], ruby

[102], Nd:glass [103], and argon ion [104] laser systems. Based on the statistical analysis, it has been shown that the mode-locked behavior will always be observed in a multimode laser except when a systematic phase fluctuation over 2π is introduced [105,106]. Although a systematic phase fluctuation is usually caused by dispersion effects, theoretical studies on the SML mechanism have confirmed that the combination tones of the third order nonlinear polarization terms can help in compensating the dispersion-induced phase shift [107-109]. Consequently, the SML typically occurs in a multimode laser without employing an extra nonlinearity except the gain medium. Recently, fairly stable SML pulses have been observed in the experiments of Nd-doped double clad fiber lasers [109] and Nd-doped vanadate crystal lasers [110]. On the other hand, Laroche et al [96] found that the SML phenomenon can be eliminated by setting the Cr^{4+} :YAG crystal exactly at the focal point of the lens. However, we did not attempt to eliminate the SML phenomenon because this phenomenon did not deteriorate the pulse stability in the present PCF laser. Moreover, putting the Cr^{4+} :YAG crystal at the focal position may cause damage due to the high pulse energy and peak power. Experimental results revealed that both the pulse-to-pulse amplitude fluctuation and the temporal jitter were well below 5% for the pump power greater than 8 W because of the narrow linewidth and the high polarization extinction ratio of the PCF. More importantly, the pulse width of the Q-switched pulse envelope was as short as 36 ns. In short, the overall quality of the output pulses is significantly superior to that obtained in conventional passively Q-switched fiber lasers [111].

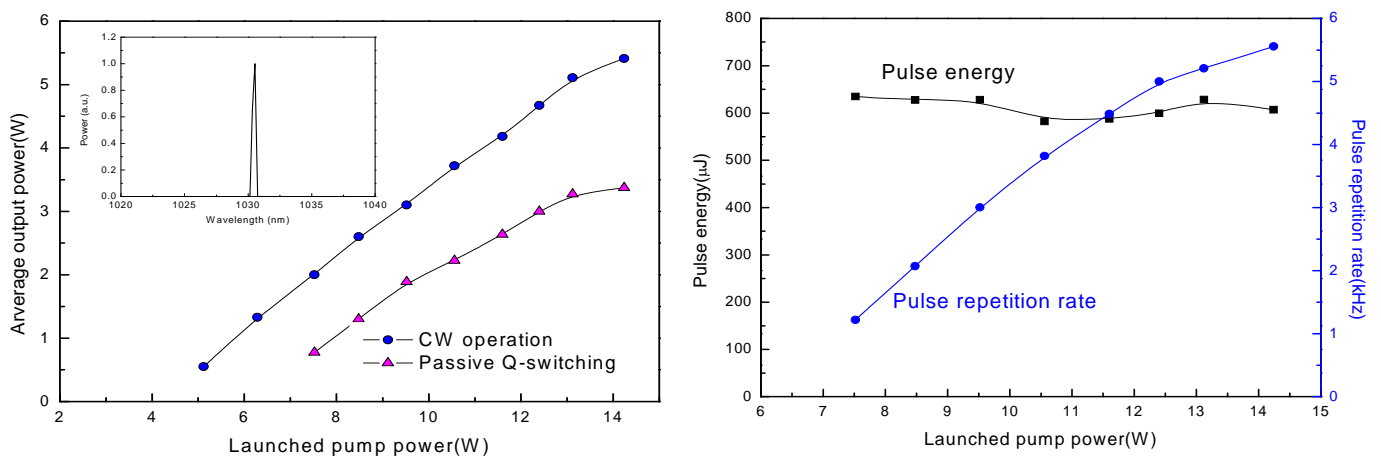


Fig 3. 17 (a) Average output power with respect to launched pump power in CW and passive Q-switching operations, the inset: typical lasing spectrum. (b) Pulse repetition rate and pulse energy versus launched pump power.

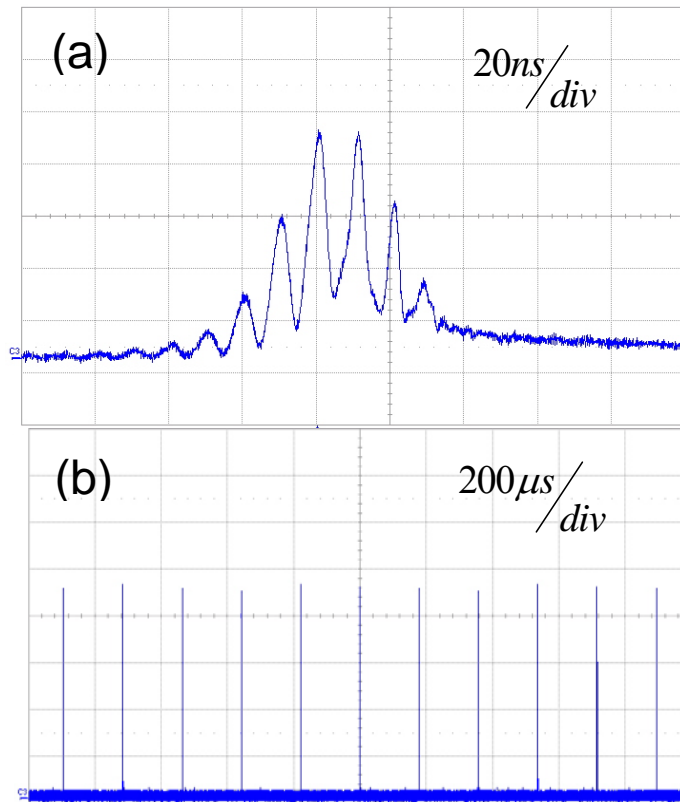


Fig 3. 18 Typical oscilloscope traces for (a) single Q-switched pulse and (b) Q-switched pulse train.

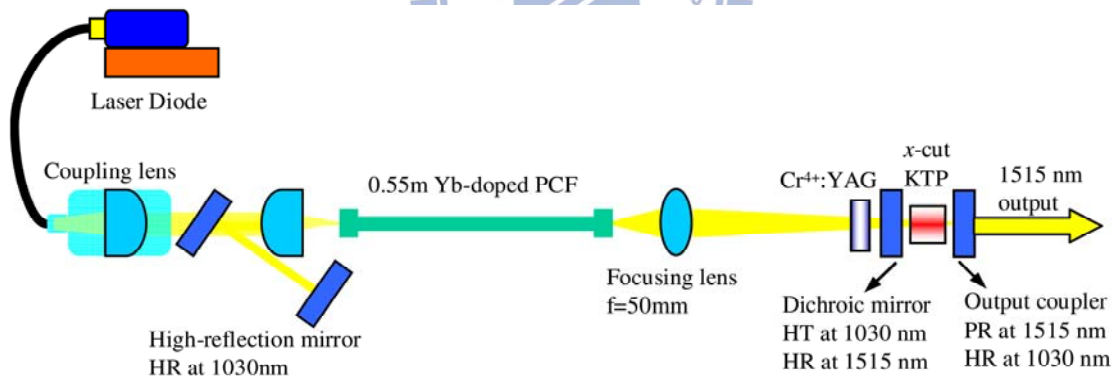


Fig 3. 19 Setup for the intracavity OPO pumped by the passively Q-switched PCF laser.

3.3.4 The application for OPO

To construct an intracavity OPO, the output coupler in the passively Q-switched PCF laser was replaced with a high-reflection mirror at 1030 nm and inserting a singly resonant OPO cavity behind the Cr⁴⁺:YAG crystal. Figure 3.19 shows the experimental setup for the intracavity OPO pumped by the passively Q-switched PCF laser. The OPO cavity is composed of a dichroic front mirror (HT at 1030 nm and HR at 1515 nm), a KTP nonlinear crystal, and an output coupler with partial transmission (PR) of $R = 38\%$

at 1515 nm and high reflectivity at 1030 nm. The nonlinear crystal KTP was x-cut with the dimension of $4 \times 4 \times 20 \text{ mm}^3$ and both sides of the KTP crystal were coated for antireflection at 1030 nm and 1515 nm ($R < 0.5\%$). The KTP crystal was mounted on a water-cooled copper heat sink with an indium thermal contact. The length of the OPO cavity was approximately 3 cm. The Cr^{4+} :YAG crystal was placed very close ($\sim 1.0 \text{ mm}$) to the front mirror of the OPO cavity to control the mode diameter on the Cr^{4+} :YAG crystal in the range of $400 \mu\text{m}$.

The average output power of the signal wave at 1515 nm with respect to the launched pump power is shown in Fig. 3.20(a). Under a pump power of 14.2 W, the average output power of the signal wave was found to be approximately 470 mW. No idler signal was detected because of the high absorption of the idler radiation in the KTP crystal and the BK7 substrate of the output coupler, so the OPO is resonant on the signal frequency only. Note that no saturation of average output power was seen at the highest pump power, which implied that larger OPO signal output power can be expected with higher pump power. The OPO pulse repetition rate and the pulse energy versus the launched pump power are shown in Fig. 3.20(b). The pulse repetition rate increased monotonically with the pump power up to 3.3 kHz at a pump power of 14.2 W. The pulse energy was nearly $140 \mu\text{J}$ for all the pump power range. The signal output pulse energy obtained with a Q-switched PCF laser was 3-6 times higher than the results obtained with solid-state Nd-doped crystal lasers at the same level of diodepumped power [112–114]. In other words, the Yb-doped gain medium has a superior energystoring ability than conventional Nd-doped laser crystals, such as Nd:YAG and Nd:YVO₄.

Figure 3.21 shows general oscilloscope traces for the fundamental and OPO signal output pulses. The top half of Fig. 3.21 depicts the temporal trace of the fundamental wavelength and the bottom half shows the pulse profile of the OPO signal wavelength. The pulse width of the OPO signal can be seen to be as short as 1.0 ns due to the efficient cavity-dumping effect. As a result, the maximum peak power of the signal wave can be up to 140 kW. The optical to optical conversion efficiency of OPO output power to laser diode launched pump power was about 3.3%, and the pulse energy conversion efficiency of OPO wavelength to 1030 nm wavelength was about 22.3%. The large pre- and post- pedestals in Fig. 3.21 arise from the SML effect. Note that the pulse shapes at 1030 nm were quite different for the cavity with and without the intracavity OPO. The number of the mode-locked pulses at 1030 nm shown in Fig. 3.21

was considerably less than that obtained with pure passive Q-switching shown in Fig. 3.18(a) because the effective output coupling in the intracavity OPO was a nonlinear cavity-dumping process. Since water absorption in eye tissue and the intraocular fluid prevents light in the spectral range of 1.4-1.8 μm from reaching the retina, there is a considerable interest in laser sources with wavelengths in this eye-safe regime [115-117]. A number of efficient eye-safe intracavity OPOs pumped by passively [112-114] Q-switched Nd-doped crystal lasers have been demonstrated to produce pulse energies of tens of μJ with pulse peak powers of 1-50 kW. Here the PCF laser was recently employed to realize an intracavity OPO with pulse energies greater than 100 μJ with peak powers greater than 100 kW. Although the conversion efficiency for the average power is inferior to that obtained with Nd-doped crystal lasers, this situation might be improved with a shorter cavity to match the OPO cavity. However, the challenge is to manufacture a shorter PCF with sufficient absorption efficiency.

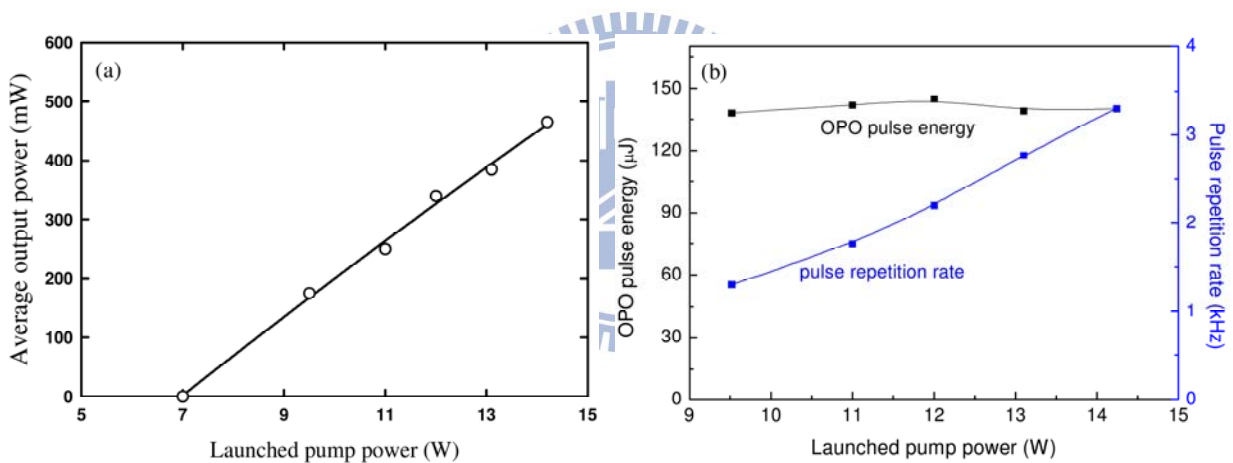


Fig 3. 20 (a) Average output power at 1515 nm with respect to launched pump power. (b) OPO pulse repetition rate and pulse energy versus launched pump power.

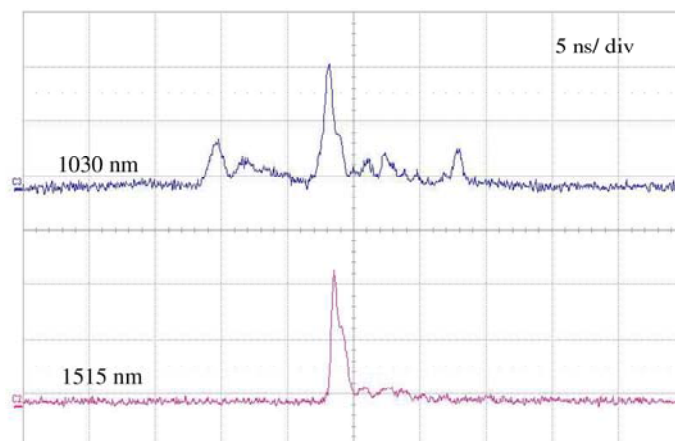


Fig 3. 21 General oscilloscope traces for the fundamental (top) and OPO signal (bottom) output pulses.

3.3.5 Conclusion

In conclusion, we have, for the first time to my knowledge, demonstrated a high-pulse-energy passively Q-switched Yb-doped PCF laser by utilizing Cr⁴⁺:YAG crystal as saturable absorber. Stable pulses with an average output power of 3.4 W and a repetition rate of 5.6 kHz were obtained at a launched pump power of 14.2 W. The maximum pulse energy reached 630 μJ which was superior to the results obtained in conventional Yb-doped fiber lasers. Furthermore, the passively Q-switched PCF laser has been employed to pump an intracavity OPO to generate a pulse energy of 140 μJ at a pulse repetition rate of 3.3 kHz with a 14.2 W diode pump power. Owing to the efficient cavity-dumping effect, the pulse duration of the signal wave was approximately 1.0 ns, leading to a peak power up to 140 kW. This high-peak-power intracavity OPO could be a potential light source for many technical applications.



Reference

1. Y. Jeong, J. K. Sahu, D. N. Payne, and J. Nilsson, "Ytterbium-doped large-core fiber laser with 1.36 kW continuous-wave output power," *Opt. Express* 12(25), 6088-6092 (2004).
2. A. Liem, J. Limpert, H. Zellmer, A. Tünnermann, V. Reichel, K. Mörl, S. Jetschke, S. Unger, H.-R. Müller, J. Kirchhof, T. Sandrock, and A. Harschak, "1.3 kW Yb-doped fiber laser with excellent beam quality," in *Proc. Conference on Lasers and Electro-Optics 2004*, San Francisco, USA, May 16-21, 2004, postdeadline paper CPDD2.
3. J. Limpert, F. Roser, S. Klingebiel, T. Schreiber, C. Wirth, T. Peschel, R. Eberhardt, and A. Tünnermann, "The Rising Power of Fiber Lasers and Amplifiers," *IEEE J. Sel. Top. Quantum Electron.* 13(3), 537-545 (2007).
4. S. D. Jackson, and A. Lauto, "Diode-pumped fiber lasers: a new clinical tool?" *Lasers Surg. Med.* 30(3), 184-190 (2002).
5. L. Quintino, A. Costa, R. Miranda, D. Yapp, V. Kumar, and C. J. Kong, "Welding with high power fiber lasers – A preliminary study," *Mater. Des.* 28(4), 1231-1237 (2007).
6. Z. J. Chen, A. B. Grudinin, J. Porta, and J. D. Minelly, "Enhanced Q switching in double-clad fiber lasers," *Opt. Lett.* 23(6), 454-456 (1998).
7. L. Pan, I. Utkin, and R. Fedosejevs, "Passively Q-switched ytterbium-doped double-clad fiber laser with a Cr⁴⁺:YAG saturable absorber," *IEEE Photon. Technol. Lett.* 19(24), 1979-1981 (2007).
8. J. Y. Huang, H. C. Liang, K. W. Su, and Y. F. Chen, "High power passively Q-switched ytterbium fiber laser with Cr⁴⁺:YAG as a saturable absorber," *Opt. Express* 15(2), 473-479 (2007).
9. J. Y. Huang, W. Z. Zhuang, W. C. Huang, K. W. Su, C. Hu, K. F. Huang, and Y. F. Chen, "Comparative studies for Cr⁴⁺:YAG crystal and AlGaInAs semiconductor used as a saturable absorber in Q-switched Yb-doped fiber lasers," *Opt. Express* 17(23), 20800-20805 (2009).
10. T. Hakulinen, and O. G. Okhotnikov, "8 ns fiber laser Q switched by the resonant saturable absorber mirror," *Opt. Lett.* 32(18), 2677-2679 (2007).
11. W. Z. Zhuang, W. C. Huang, Y. P. Huang, K. W. Su, and Y. F. Chen, "Passively Q-switched photonic crystal fiber laser and intracavity optical parametric oscillator,"

- Opt. Express 18(9), 8969-8975 (2010).
12. W. T. Tsang, and N. A. Olsson, "New current injection 1.5- μm wavelength Ga_xAl_yIn_{1-x-y}As/InP doubleheterostructure laser grown by molecular beam epitaxy," Appl. Phys. Lett. 42(11), 922-924 (1983).
 13. K. Alavi, H. Temkin, W. R. Wagner, and A. Y. Cho, "Optically pumped 1.55- μm double heterostructure Ga_xAl_yIn_{1-x-y}As/AluIn_{1-u}As lasers grown by molecular beam epitaxy," Appl. Phys. Lett. 42(3), 254-256 (1983).
 14. D. A. Bender, J. G. Cederberg, and G. A. Hebner, "Parametric Results of the AlGaInAs Quantum-Well Saturable Absorber for Use as a Passive Q-Switch," in Conference on Lasers and Electro-Optics, (Optical Society of America, San Jose, California, 2010), paper CThL3.
 15. J. A. Alvarez-Chavez, H. L. Offerhaus, J. Nilsson, P. W. Turner, W. A. Clarkson, and D. J. Richardson, "High-energy, high-power ytterbium-doped Q-switched fiber laser," Opt. Lett. 25(1), 37-39 (2000).
 16. A. Piper, A. Malinowski, K. Furusawa, and D. J. Richardson, "High-power, high-brightness, mJ Qswitched ytterbium-doped fibre laser," Electron. Lett. 40(15), 928-929 (2004).
 17. O. Schmidt, J. Rothhardt, F. Röser, S. Linke, T. Schreiber, K. Rademaker, J. Limpert, S. Ermeneux, P. Yvernault, F. Salin, and A. Tünnermann, "Millijoule pulse energy Q-switched short-length fiber laser," Opt. Lett. 32(11), 1551-1553 (2007).
 18. J. Limpert, A. Liem, H. Zellmer, A. Tünnermann, S. Knoke, and H. Voelckel, "High-average-power millijoule fiber amplifier system," Lasers and Electro-Optics, 2002. CLEO'02. Technical Digest, Long Beach, CA, paper CThX3, 591-592 (2002).
 19. C. D. Brooks, and F. Di Teodoro, "1-mJ energy, 1-MW peak-power, 10-W average-power, spectrally narrow, diffraction-limited pulses from a photonic-crystal fiber amplifier," Opt. Express 13(22), 8999-9002 (2005).
 20. F. D. Teodoro, M. K. Hemmat, J. Morais, and E. C. Cheung, "High peak power operation of a 100 μm -core, Yb-doped rod-type photonic crystal fiber amplifier," Fiber Lasers VII: Technology, Systems and Applications, Proc. of SPIE vol. 7580, 758006 (2010).
 21. M. Salhi, A. Hideur, T. Chartier, M. Brunel, G. Martel, C. Ozkul, and F. Sanchez, "Evidence of Brillouin scattering in an ytterbium-doped double-clad fiber laser,"

- Opt. Lett. 27(15), 1294-1296 (2002).
22. Y. X. Fan, F. Y. Lu, S. L. Hu, K. C. Lu, H. J. Wang, G. Y. Zhang, and X. Y. Dong, "Narrow-linewidth widely tunable hybrid Q-switched double-clad fiber laser," Opt. Lett. 28(7), 537-539 (2003).
 23. A. A. Fotiadi, P. Mégret, and M. Blondel, "Dynamics of a self-Q-switched fiber laser with a Rayleigh-stimulated Brillouin scattering ring mirror," Opt. Lett. 29(10), 1078-1080 (2004).
 24. Z. J. Chen, A. B. Grudinin, J. Porta, and J. D. Minelly, "Enhanced Q switching in double-clad fiber lasers," Opt. Lett. 23(6), 454-456 (1998).
 25. Y.-X. Fan, F.-Y. Lu, S.-L. Hu, K.-C. Lu, H.-J. Wang, X. Y. Dong, J. L. He, and H. T. Wang, "Tunable high-peak-power, high-energy hybrid Q-switched double-clad fiber laser," Opt. Lett. 29(7), 724-726 (2004).
 26. M. Laroche, H. Gilles, S. Girard, N. Passilly, and K. Ait-Ameur, "Nanosecond pulse generation in a passively Q-switched Yb-doped fiber laser by Cr⁴⁺:YAG saturable absorber," IEEE Photon. Technol. Lett. 18(6), 764-766 (2006).
 27. L. Pan, I. Utkin, R. J. Lan, Y. Godwal, and R. Fedosejevs, "High-peak-power subnanosecond passively Q-switched ytterbium-doped fiber laser," Opt. Lett. 35(7), 895-897 (2010).
 28. Y. F. Chen, S. W. Tsai, and S. C. Wang, "High-power diode-pumped Q-switched and mode-locked Nd:YVO₄ laser with a Cr⁴⁺:YAG saturable absorber," Opt. Lett. 25(19), 1442-1444 (2000).
 29. Y. F. Chen, and S. W. Tsai, "Simultaneous Q-switching and mode-locking in a diode-pumped Nd:YVO₄-Cr⁴⁺:YAG laser," IEEE J. Quantum Electron. 37(4), 580-586 (2001).
 30. S. Zhang, E. Wu, H. Pan, and H. Zeng, "Q-switched mode-locking with Cr⁴⁺:YAG in a diode pumped Nd:GdVO₄ laser," Appl. Phys. B 78(3-4), 335-338 (2004).
 31. J. Yang, J. Liu, and J. He, "A compact Q-switched and mode-locked diode-pumped Nd:GdVO₄ laser with Cr⁴⁺:YAG," Laser Phys. 15(8), 1137-1141 (2005).
 32. J. A. Fleck, Jr., "Ultrashort-pulse generation by Q-switched lasers," Phys. Rev. B 1(1), 84-100 (1970).
 33. P. G. Kryukov, and V. S. Letokhov, "Fluctuation mechanism of ultrashort pulse generation by laser with saturable absorber," IEEE J. Quantum Electron. 8(10), 766-782 (1972).
 34. S.G. Grubb, in: Proc. of the Optical Amplifiers and Their Applications Topical

- Meeting, Monterey, CA, USA, July 11 – 13, 1996, pp. 42 – 44.
35. B.K. Nayar, J.J. Lewandowski, F.J. Wilson, J.A. Chavez, A.B. Grudinin, J.D. Minelly, G. Kennedy, and A. Raven, in: Proc. of the IEEE Lasers and Electro-Optics Society Annual Meeting, Orlando, FL, USA, December 1 – 4, 1998 (LEOS' 98), vol. 2, pp. 397 – 398.
 36. Shaif-ul-Alam, P.W. Turner, A.B. Grudinin, and J. Nilsson, in: Tech. Digest of the Conference on Lasers and Electro-Optics, Baltimore, MD, USA, May 6 – 11, 2001 (CLEO 2001), pp. 218 – 219.
 37. J.E. Nettleton, B.W. Schilling, D.N. Barr, and J.S. Lei, Appl. Opt. 39, 2428 – 2432 (2000).
 38. A. Tünnermann, T. Schreiber, F. Röser, A. Liem, S. Höfer, H. Zellmer, S. Nolte, and J. Limpert, J. Phys. B 38, S681-S694 (2005).
 39. A.S. Kurkov, Ya.E. Sadovnikova, A.V. Marakulin, and E.M. Sholokhov, Laser Phys. Lett. 7, 795 – 797 (2010).
 40. M. Němec, W. Zendzian, H. Jelínková, J.K. Jabczynski, J. Šulc, L. Gorajek, and J. Kwiatkowski, Laser Phys. 20, 661 – 664 (2010).
 41. B. Peng, H. Zhang, M. Gong, and P. Yan, Laser Phys. 19, 2019 – 2022 (2009).
 42. Y. Jeong, J.K. Sahu, M. Laroche, W.A. Clarkson, K. Furusawa, D.J. Richardson, and J. Nilsson, in: Proc. of the Conference on Lasers and Electro-Optics Europe, Munich, Germany, June 22 – 27, 2003 (CLEO/Europe 2003), pp. 626 – 626.
 43. J. Limpert, S. Höfer, A. Liem, H. Zellmer, A. Tünnermann, S. Knoke, and H. Voelckel, Appl. Phys. B 75, 477 – 479 (2002).
 44. Y. Jeong, J.K. Sahu, R.B. Williams, D.J. Richardson, K. Furusawa, and J. Nilsson, Electron. Lett. 39, 977 – 978 (2003).
 45. Y. Jeong, J. Sahu, D. Payne, and J. Nilsson, Opt. Express 12, 6088 – 6092 (2004).
 46. A. Liem, J. Limpert, H. Zellmer, A. Tünnermann, V. Reichel, K. Mörl, S. Jetschke, S. Unger, H.-R. Müller, J. Kirchhof, T. Sandrock, and A. Harschak, in: Proc. of the Conference on Lasers and Electro-Optics, San Francisco, CA, USA, May 16 – 21, 2004 (CLEO 2004), paper CPDD2.
 47. A.A. Fotiadi, A. Kurkov, and I. Razdobreev, in: Tech. Digest of the European Conference on Lasers and Electro-Optics and European Quantum Electronics

- Conference, Munich, Germany, June 12-17, 2005 (CLEO/Europe-EQEC 2005), paper CJ2-3.
48. G.A. Ball and W.W. Morey, *Opt. Lett.* 17, 420-422 (1992).
 49. H. Zhang, D.Y. Tang, L.M. Zhao, Q.L. Bao, K.P. Loh, B. Lin, and S.C. Tjin, *Laser Phys. Lett.* 7, 591-596 (2010).
 50. S.K. Liaw, S. Wang, C.S. Shin, Y.L. Yu, N.K. Chen, K.C. Hsu, A. Manshina and Y. Tver'yanovich, *Laser Phys.* 20, 1744-1746 (2010).
 51. N.K. Chen, Z.Z. Feng, and S.K. Liaw, *Laser Phys. Lett.* 7, 363-366 (2010).
 52. Q.H. Mao and J.W.Y. Lit, *Appl. Phys. Lett.* 82, 1335-1337 (2003).
 53. H. Ahmad, M.Z. Zulkifli, A.A. Latif, and S.W. Harun, *Laser Phys. Lett.* 7, 164-167 (2010).
 54. D.-F. Liu and C.-H. Wang, *Laser Phys. Lett.* 7, 153-157 (2010).
 55. A.A. Latif, H. Ahmad, N.A. Awang, M.Z. Zulkifli, C.H. Pua, Z.A. Ghani, and S.W. Harun, *Laser Phys.* 21, 712-717 (2011).
 56. M.R.A. Moghaddam, S.W. Harun, M.R. Tamjis, and H. Ahmad, *Laser Phys. Lett.* 6, 586-589 (2009).
 57. M.E. Klein, C.K. Laue, D.-H. Lee, K.-J. Boller, and R. Wallenstein, *Opt. Lett.* 25, 490-492 (2000).
 58. S.E. Bisson, K.M. Armstrong, T.J. Kulp, and M. Hartings, *Appl. Opt.* 40, 6049-6055 (2001).
 59. J. Liu, Q. Liu, L. Huang, and M. Gong, *Laser Phys. Lett.* 7, 853-856 (2010).
 60. H.Y. Zhu, Y.M. Duan, G. Zhang, C.H. Huang, Y. Wei, W.D. Chen, H.Y. Wang, and G. Qiu, *Laser Phys. Lett.* 7, 703-706 (2010).
 61. J.W. Liu, C.Q. Gao, L. Wang, L. Zou, and J.Z. Li, *Laser Phys.* 20, 1886-1889 (2010).
 62. J.Y. Huang, S.C. Huang, H.L. Chang, K.W. Su, Y.F. Chen, and K.F. Huang, *Opt. Express* 16, 3002-3007 (2008).
 63. W.Z. Zhuang, W.C. Huang, P.Y. Chiang, K.W. Su, K.F. Huang, and Y.F. Chen, *Opt. Express* 18, 27910-27915 (2010).
 64. W.Z. Zhuang, W.C. Huang, Y.P. Huang, K.W. Su, and Y.F. Chen, *Opt. Express* 18, 8969-8975 (2010).
 65. M.M.J.W. van Herpen, S.E. Bisson, and F.J.M. Harren, *Opt. Lett.* 28, 2497 – 2499 (2003).
 66. X.-L. Dong, W.-Y. Yang, B.-G. Sun, J.-F. Yang, B.-T. Zhang, H.-T. Huang, and

- S.-D. Liu, *Laser Phys.* 20, 1787- 1790 (2010).
67. Z.-Y. Li, H.-T. Huang, J.-L. He, B.-T. Zhang, and J.-L. Xu, *Laser Phys.* 20, 1302-1306 (2010).
68. M. Salhi, A. Hideur, T. Chartier, M. Brunel, G. Martel, C. Ozkul, and F. Sanchez, *Opt. Lett.* 27, 1294-1296 (2002).
69. Y.-X. Fan, F.-Y. Lu, S.-L. Hu, K.-C. Lu, H.-J. Wang, G.-Y. Zhang, and X.-Y. Dong, *Opt. Lett.* 28, 537-539 (2003).
70. A.A. Fotiadi, P. Mégret, and M. Blondel, *Opt. Lett.* 29, 1078 – 1080 (2004).
71. Z.J. Chen, A.B. Grudinin, J. Porta, and J.D. Minelly, *Opt. Lett.* 23, 454 – 456 (1998).
72. Y.-X. Fan, F.-Y. Lu, S.-L. Hu, K.-C. Lu, H.-J. Wang, X.-Y. Dong, J.-L. He, and H.-T. Wang, *Opt. Lett.* 29, 724-726(2004).
73. M. Laroche, H. Gilles, S. Girard, N. Passilly, and K. Ait-Ameur, *IEEE Photon. Technol. Lett.* 18, 764-766 (2006).
74. L. Pan, I. Utkin, R.J. Lan, Y. Godwal, and R. Fedosejevs, *Opt. Lett.* 35, 895-897 (2010).
75. G.J. Edwards and M. Lawrence, *Opt. Quantum Electron.* 16, 373-375 (1984).
76. D.H. Jundt, *Opt. Lett.* 22, 1553-1555 (1997).
77. Y.F. Kong, W.L. Zhang, X.J. Chen, J.J. Xu, and G.Y. Zhang, *J. Phys. Condens. Matter* 11, 2139-2144 (1999).
78. A. Tünnermann, T. Schreiber, F. Röser, A. Liem, S. Höfer, H. Zellmer, S. Nolte, and J. Limpert, “The renaissance and bright future of fibre lasers,” *J. Phys. At. Mol. Opt. Phys.* 38(9), S681-S693 (2005).
79. Y. Jeong, J. K. Sahu, M. Laroche, W. A. Clarkson, K. Furusawa, D. J. Richardson, and J. Nilsson, “120-W Qswitched cladding-pumped Yb-doped fibre laser,” in *Proc. Conference on Lasers and Electro-Optics Europe, 2003. CLEO/Europe, Munich ICM, Germany, June 22-27, 2003*, 626-626 (2003).
80. J. Limpert, S. Höfer, A. Liem, H. Zellmer, A. Tünnermann, S. Knoke, and H. Voelckel, “100-W average-power, high-energy nanosecond fiber amplifier,” *Appl. Phys. B* 75(4-5), 477-479 (2002).
81. Y. Jeong, J. K. Sahu, R. B. Williams, D. J. Richardson, K. Furusawa, and J. Nilsson, “Ytterbium-doped largecore fibre laser with 272 W output power,” *Electron. Lett.* 39(13), 977-978 (2003).
82. Y. Jeong, J. K. Sahu, D. N. Payne, and J. Nilsson, “Ytterbium-doped large-core

- fiber laser with 1.36 kW continuous-wave output power,” *Opt. Express* 12(25), 6088-6092 (2004).
83. A. Liem, J. Limpert, H. Zellmer, A. Tünnermann, V. Reichel, K. Mörl, S. Jetschke, S. Unger, H.-R. Müller, J. Kirchhof, T. Sandrock, and A. Harschak, “1.3 kW Yb-doped fiber laser with excellent beam quality,” in *Proc. Conference on Lasers and Electro-Optics 2004*, San Francisco, USA, May 16-21, 2004, postdeadline paper CPDD2.
84. A. Fotiadi, A. Kurkov, and I. Razdobreev, “All-fiber passively Q-switched ytterbium laser,” *CLEO/Europe-EQEC 2005*, Technical Digest, CJ 2-3, Munich, Germany (2005).
85. Z. J. Chen, A. B. Grudinin, J. Porta, and J. D. Minelly, “Enhanced Q switching in double-clad fiber lasers,” *Opt. Lett.* 23(6), 454-456 (1998).
86. O. Schmidt, J. Rothhardt, F. Röser, S. Linke, T. Schreiber, K. Rademaker, J. Limpert, S. Ermeneux, P. Yvernault, F. Salin, and A. Tünnermann, “Millijoule pulse energy Q-switched short-length fiber laser,” *Opt. Lett.* 32(11), 1551-1553 (2007).
87. R. Ashinoff, and R. G. Geronemus, “Rapid response of traumatic and medical tattoos to treatment with the Q-switched ruby laser,” *Plast. Reconstr. Surg.* 91(5), 841-845 (1993).
88. C. C. Ranaud, H. L. Offerhaus, J. A. Alvarez-Chavez, C. J. Nilsson, W. A. Clarkson, P. W. Turner, D. J. Richardson, and A. B. Grudinin, “Characteristics of Q-switched cladding-pumped ytterbium-doped fiber lasers with different high-energy fiber designs,” *IEEE J. Quantum Electron.* 37(2), 199-206 (2001).
89. J. A. Alvarez-Chavez, H. L. Offerhaus, J. Nilsson, P. W. Turner, W. A. Clarkson, and D. J. Richardson, “Highenergy, high-power ytterbium-doped Q-switched fiber laser,” *Opt. Lett.* 25(1), 37-39 (2000).
90. J. Limpert, N. Deguil-Robin, I. Manek-Hönninger, F. Salin, F. Röser, A. Liem, T. Schreiber, S. Nolte, H. Zellmer, A. Tünnermann, J. Broeng, A. Petersson, and C. Jakobsen, “High-power rod-type photonic crystal fiber laser,” *Opt. Express* 13(4), 1055-1058 (2005).
91. J. J. Zayhowski, and C. Dill III, “Diode-pumped passively Q-switched picosecond microchip lasers,” *Opt. Lett.* 19(18), 1427-1429 (1994).
92. X. Zhang, S. Zhao, Q. Wang, Q. Zhang, L. Sun, and S. Zhang, “Optimization of Cr⁴⁺-doped saturable-absorber Q-switched lasers,” *IEEE J. Quantum Electron.*

- 33(12), 2286-2294 (1997).
93. A. Agnesi, and S. Dell'acqua, "High-peak-power diode-pumped passively Q-switched Nd:YVO₄ laser," *Appl. Phys. B* 76(4), 351-354 (2003).
 94. Y. Kalisky, "Cr⁴⁺-doped crystals: their use as lasers and passive Q-switches," *Prog. Quantum Electron.* 28(5), 249-303 (2004).
 95. A. Sennaroglu, U. Demirbas, S. Ozharar, and F. Yaman, "Accurate determination of saturation parameters for Cr⁴⁺-doped solid-state saturable absorbers," *J. Opt. Soc. Am. B* 23(2), 241-249 (2006).
 96. M. Laroche, H. Gilles, S. Girard, N. Passilly, and K. Aït-Ameur, "Nanosecond pulse generation in a passively Q-switched Yb-doped fiber laser by Cr⁴⁺:YAG saturable absorber," *IEEE Photon. Technol. Lett.* 18(6), 764-766 (2006).
 97. L. Pan, I. Utkin, and R. Fedosejevs, "Passively Q-switched ytterbium-doped double-clad fiber laser with a Cr⁴⁺:YAG saturable absorber," *IEEE Photon. Technol. Lett.* 19(24), 1979-1981 (2007).
 98. J. Y. Huang, W. Z. Zhuang, W. C. Huang, K. W. Su, C. Hu, K. F. Huang, and Y. F. Chen, "Comparative studies for Cr⁴⁺:YAG crystal and AlGaInAs semiconductor used as a saturable absorber in Q-switched Yb-doped fiber lasers," *Opt. Express* 17(23), 20800-20805 (2009).
 99. Y. X. Fan, F. Y. Lu, S. L. Hu, K. C. Lu, H. J. Wang, X. Y. Dong, J. L. He, and H. T. Wang, "Tunable high-peak-power, high-energy hybrid Q-switched double-clad fiber laser," *Opt. Lett.* 29(7), 724-726 (2004).
 100. P. Myslinski, J. Chrostowski, J. Koningstein, and J. Simpson, "Self-mode locking in a Q-switched erbium-doped fiber laser," *Appl. Opt.* 32(3), 286-290 (1993).
 101. M. H. Crowell, "Characteristics of mode-coupled lasers," *IEEE J. Quantum Electron.* 1(1), 12-20 (1965).
 102. H. Statz, and C. L. Tang, "Phase locking of modes in lasers," *J. Appl. Phys.* 36(12), 3923-3927 (1965).
 103. M. A. Duguay, S. L. Shapiro, and P. M. Rentzepis, "Spontaneous appearance of picosecond pulses in ruby and Nd: glass lasers," *Phys. Rev. Lett.* 19(18), 1014-1016 (1967).
 104. O. L. Gaddy, and E. M. Schaefer, "Self locking of modes in the argon ion laser," *Appl. Phys. Lett.* 9(8), 281-282 (1966).
 105. A. A. Grütter, H. P. Weber, and R. Dändliker, "Imperfectly mode-locked laser emission and its effects on nonlinear optics," *Phys. Rev.* 185(2), 629-643 (1969).

106. R. Dändliker, A. A. Grütter, and H. P. Weber, "Statistical amplitude and phase variations in mode-locked lasers," *IEEE J. Quantum Electron.* 6(11), 687-693 (1970).
107. H. Stutz, "On the condition for self-locking of modes in lasers," *J. Appl. Phys.* 38(12), 4648-4655 (1967).
108. H. Stutz, and M. Bass, "Locking in multimode solid-state lasers," *J. Appl. Phys.* 40(1), 377-383 (1969).
109. P. Glas, and M. Naumann, "Self pulsing versus self locking in a cw pumped neodymium doped double clad fiber laser," *Opt. Commun.* 161(4-6), 345-358 (1999).
110. H. C. Liang, R. C. Chen, Y. J. Huang, K. W. Su, and Y. F. Chen, "Compact efficient multi-GHz Kerr-lens mode-locked diode-pumped Nd:YVO₄ laser," *Opt. Express* 16(25), 21149-21154 (2008).
111. J. Y. Huang, W. C. Huang, W. Z. Zhuang, K. W. Su, Y. F. Chen, and K. F. Huang, "High-pulse-energy, passively Q-switched Yb-doped fiber laser with AlGaInAs quantum wells as a saturable absorber," *Opt. Lett.* 34(15), 2360-2362 (2009).
112. J. Miao, J. Peng, B. Wang, and H. Tan, "Compact KTA-based intracavity optical parametric oscillator driven by a passively Q-switched Nd:GdVO₄ laser," *Appl. Opt.* 47(23), 4287-4291 (2008).
113. H. T. Huang, J. L. He, X. L. Dong, C. H. Zuo, B. T. Zhang, G. Qiu, and Z. K. Liu, "High-repetition-rate eye-safe intracavity KTA OPO driven by a diode-end-pumped Q-switched Nd:YVO₄ laser," *Appl. Phys. B* 90(1), 43-45 (2008).
114. Z. Liu, Q. Wang, X. Zhang, Z. Liu, J. Chang, H. Wang, S. Fan, W. Sun, G. Jin, X. Tao, S. Zhang, and H. Zhang, "Efficient acousto-optically Q-switched intracavity Nd:YAG/KTiOAsO₄ optical parametric oscillator," *Appl. Phys. B* 92(1), 37-41 (2008).
115. E. Gregor, D. E. Nieuwsma, and R. D. Stultz, "20 Hz eyesafe laser rangefinder for air defense," *Proc. SPIE* 1207, 124-134 (1990).
116. L. R. Marshall, A. D. Hays, and J. Kasinski, "Highly efficient optical parametric oscillators," *Proc. SPIE* 1419, 141-152 (1991).
117. J. E. Nettleton, B. W. Schilling, D. N. Barr, and J. S. Lei, "Monoblock laser for a low-cost, eyesafe, microlaser range finder," *Appl. Opt.* 39(15), 2428-2432 (2000).

Chapter 4

Passively Q-switched fiber laser based on a MOFA configuration



4.1 Passively Q-switched double-cladding fiber amplifier

4.1.1 Introduction

High-peak-power, linearly-polarized lasers with pulse repetition rates up to several tens of kilohertz have a wide variety of applications in range finding, nonlinear wavelength conversion, and material processing [1-3]. The thermally induced distortion is the main hindrance for power scale-up in solid-state crystal lasers [4]. The master-oscillator fiber amplifier (MOFA or fiber MOPA) that collects the advantages of good beam quality, high efficiency, compactness, and superior heat dissipations has been identified as a promising light source [5-9]. To achieve the high-peak-power pulses with single-stage amplification, diode-pumped actively Q-switched (AQS) [10, 11] or passively Q-switched (PQS) [12-14] Nd-doped lasers are often used as the seed lasers of the Yb-doped MOFAs.

Compared to the active Q-switching, the PQS laser with a saturable absorber offers the advantages of compactness, robustness, and low cost. Since Cr^{4+} :YAG crystals possess the advantages of high absorption cross section near the infrared region, high damage threshold, and low temperature-sensitive properties [15-21], they have been proved to be reliable saturable absorbers for Nd^{3+} -doped lasers. Nevertheless, the Cr^{4+} :YAG crystal is usually not convenient for the Nd-doped vanadate crystal lasers due to the mismatch between the stimulated emission cross section of the gain medium and the absorption cross section of the absorber. Several methods, including the three-element resonator with the intra-cavity focusing [15, 20,22] or the employment of a c-cut crystal as the gain medium [23-25], have been proposed to overcome this mismatch. The three-element resonators, however, not only increase the complexity of the cavities but also lead to relatively long pulse durations owing to the long cavity lengths. On the other hand, the employment of a c-cut crystal inevitably raises the pumping threshold and loses the characteristic of linear polarization. Therefore, it is highly useful for the seed laser of MOFA to develop high-peak-power PQS lasers with a-cut vanadate crystals in a simple compact cavity.

In this work, we systematically consider the second threshold criterion and the thermal lensing effect to develop compact and high-peak-power Nd:YVO₄/Cr⁴⁺:YAG PQS lasers with nearly hemispherical cavities. I further exploit several Cr⁴⁺:YAG crystals with different initial transmissions (T_0) to realize the designed PQS laser.

Experimental results reveal that at a pump power of 5.4 W the output pulse energy increases from 22 to 36 μJ and the pulse repetition rate decreases from 50 to 25 kHz for the initial transmission of the Cr^{4+} :YAG crystal decreasing from 70% to 40%. Injecting the seed laser obtained with $T_0 = 70\%$ into a polarization maintained Yb-doped fiber, the pulse energy and peak power at a pump power of 16 W are enhanced up to 178 μJ and 37 kW, respectively. Excellent amplification confirms the PQS performance. Employing the seed laser obtained with $T_0 = 40\%$, we find that the surface damage of the fiber limits the maximum pulse energy and peak power to be 192 μJ and 120 kW, respectively. The polarization extinction ratio is approximately 100:1 for both MOFAs in the whole pump power. To the best of my knowledge, this is the first time to realize high-peak-power, single-stage, linearly-polarized MOFAs with the compact Nd:YVO₄/Cr⁴⁺:YAG PQS lasers as seed oscillators.

4.1.2 Analysis and optimization of the PQS laser

To achieve good passive Q-switching, absorption saturation in the absorber must occur before gain saturation in the laser crystal [22]. From the analysis of the coupled rate equation, the good passively Q-switching criterion which is also called second threshold condition is given by:

$$\frac{\ln(1/T_0^2)}{\ln(1/T_0^2) + \ln(1/R) + L} \frac{\sigma_{gsa}}{\sigma} \frac{A}{A_s} > \frac{\gamma}{1-\beta}, \quad (1)$$

where R is the reflectivity of the output coupler, σ is the stimulated emission cross-section of the gain medium, σ_{gsa} is the ground-state absorption cross-section of the saturable absorber with the initial transmission T_0 , L is the nonsaturable intracavity round-trip dissipative optical loss, A/A_s is the ratio of the effective area in the gain medium to that in the saturable absorber, γ is the inversion reduction factor with a value between 0 and 2 [26], and β is the ratio of the excited-state absorption cross-section to that of the ground-state absorption in the saturable absorber. The challenge of obtaining a compact and stable Nd:YVO₄/Cr⁴⁺:YAG PQS laser results from which the emission cross-section of Nd:YVO₄ crystals ($\sim 2.5 \times 10^{-18} \text{ cm}^2$) [15] is comparable with the ground-state absorption cross-section of Cr⁴⁺:YAG crystals ($\sim (2.0 \pm 0.5) \times 10^{-18} \text{ cm}^2$) [27]. It was found that unstable pulse trains with satellite pulses would occur when the good Q-switching criterion is not achieved [28,29]. To fulfill the good passive

Q-switching criterion in Nd:YVO₄/Cr⁴⁺:YAG PQS lasers, the ratio A/A_s generally needs to be greater than 10 [29].

Even though the three-element resonator can be used to achieve the requirement of the ratio $A/A_s \geq 10$, the long cavity usually leads to a wide pulse duration. Here we utilize the nearly hemispherical resonator to develop compact high-peak-power Nd:YVO₄/Cr⁴⁺:YAG PQS lasers to be seed oscillators. In terms of the g-parameters, the beam radii ω_1 and ω_2 on the rear and front mirrors are given by [30]:

$$g_i = 1 - \frac{L}{\rho_i} \quad , \quad (2)$$

$$\omega_i = \sqrt{\frac{\lambda L}{\pi}} \sqrt{\frac{g_j}{g_i(1-g_1g_2)}} \quad ; \quad i, j = 1, 2 \quad ; \quad i \neq j \quad , \quad (3)$$

where L is the cavity length, λ is the wavelength of laser mode, and ρ_1 and ρ_2 are the radii of curvature of the rear and front mirrors, respectively. For a simple plano-concave resonator, as depicted in Fig. 4.1(a), $g_1 = 1 - L/\rho_1$ and $g_2 = 1$. Given that the gain medium and the saturable absorber are as close as possible to the rear mirror and the flat output coupler, the ratio of the effective area in the gain medium to that in the saturable absorber A/A_s can be found to be

$$\frac{A}{A_s} = \frac{\omega_1^2}{\omega_2^2} = \frac{\rho_1}{\rho_1 - L} \quad . \quad (4)$$

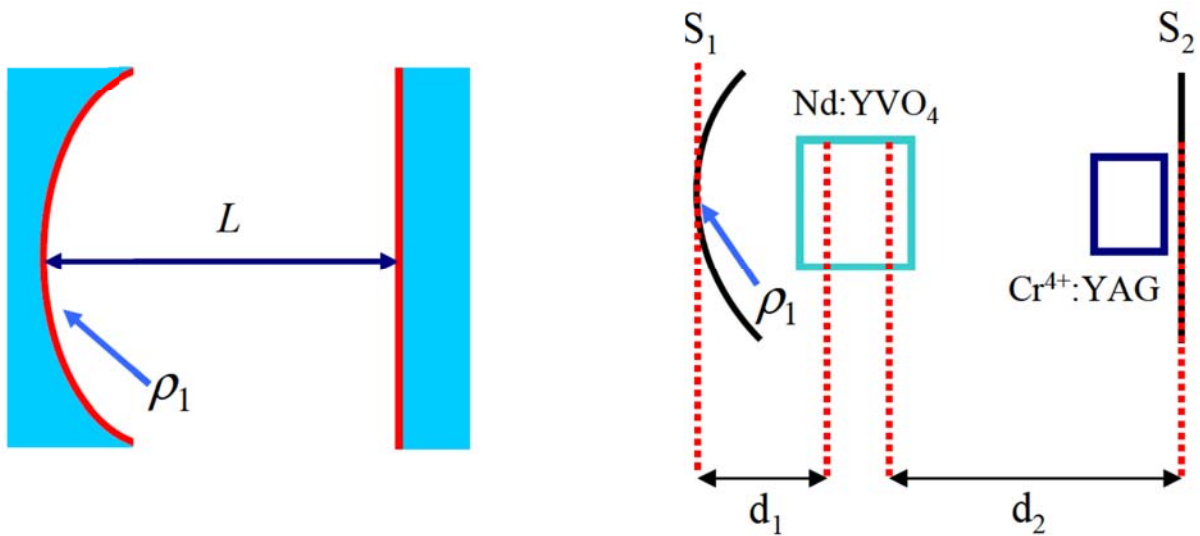


Fig 4. 1 Schematic diagram of the plano-concave cavity. (b) Equivalent cavity diagram of the Nd:YVO₄/Cr⁴⁺:YAG PQS laser.

Equation (4) reveals that the ratio A/A_s can be up to 10 under the circumstance of a nearly hemispherical cavity with $L = 0.9\rho_1$. A smaller ρ_1 consequently corresponds to a shorter cavity length that is beneficial for the generation of Q-switched pulses with narrower pulse duration. Nevertheless, the geometrical sizes of the gain medium, the saturable absorber, and the heat sinks limit the minimum cavity length. Therefore, $\rho_1 = 25$ mm is chosen for further optimizing the compact high-peak-power Nd:YVO₄/Cr⁴⁺:YAG PQS laser.

The next design parameter is the pump size that needs to be optimized to reach the good mode matching for the fundamental transverse mode. Since the thermal lensing effect in the gain medium always affects the cavity mode size, it is practically important to consider the thermal lensing effect for determining the optimum pump size. For an end-pumped crystal laser, the thermal lens is given by [31]:

$$\frac{1}{f_{th}} = \frac{\xi P_{in}}{\pi K_c} \int_0^l \frac{\alpha e^{-\alpha z}}{1 - e^{-\alpha l}} \frac{1}{\omega_p^2(z)} \left[\frac{1}{2} \frac{dn}{dT} + (n-1) \alpha_T \frac{\omega_p(z)}{l} \right] dz, \quad (5)$$

where

$$\omega_p = \omega_{po} \sqrt{1 + \left[\frac{\lambda_p M_p^2 (z - z_0)}{n \pi \omega_{po}^2} \right]^2}, \quad (6)$$

z_0 is the focal plane of the pump beam in the laser crystal, M_p^2 is the pump beam quality factor, ω_{po} is the pump beam radius, n is the refractive index of along the c-axis of the laser crystal, λ_p is the wavelength of the pump laser diode, ξ is the fractional thermal loading, K_c is the thermal conductivity, P_{in} is the incident pump power, α is the absorption coefficient of the gain medium, l is the crystal length, dn/dT is the thermal-optic coefficient of n , and α_T is the thermal expansion coefficient along the a-axis.

Figure 4.1(b) depicts the configuration of a nearly hemispherical resonator for a Nd:YVO₄/Cr⁴⁺:YAG PQS laser. Considering the thermal lens effect and taking S_1 as the reference plane, the ray transfer matrix from S_1 to S_2 of the cavity configuration can be presented as [32]:

$$M_D = \begin{pmatrix} g_1^* & L^* \\ \frac{g_1^* g_2^*}{L^*} & g_2^* \end{pmatrix}, \quad (7)$$

$$g_i^* = g_i - \frac{d_j}{f_{th}} \left(1 - \frac{d_i}{\rho_i} \right), \quad (8)$$

$$g_i = 1 - \frac{d_1 + d_2}{\rho_i} ; i, j = 1, 2 ; i \neq j , \quad (9)$$

$$L^* = d_1 + d_2 - \frac{d_1 d_2}{f_{th}} . \quad (10)$$

Here d_1 and d_2 are the optical path length between the cavity mirrors and the principal planes of the laser crystal, and f_{th} is the effective focal length of the thermal lens. With the following parameters: $\xi = 0.24$, $Kc = 5.23$ W/K m, $d_1 = 2$ mm, $d_2 = 0.9\rho_1 - d_1$, $\rho_2 = \infty$, $n = 2.165$, $l = 12$ mm, $dn/dT = 3.0 \times 10^{-6}$ K $^{-1}$, $\gamma = 80$, $\alpha = 0.6$ mm $^{-1}$, $\alpha T = 4.43 \times 10^{-6}$ K $^{-1}$, and $\lambda_p = 808$ nm, the effective focal length of the thermal lens effect and g^* -parameters of the resonator can be calculated as functions of the incident pump power. In terms of the g^* -parameters for the thermal lensing effect, the beam radii ω_1 and ω_2 on the rear and front mirrors can be expressed as [32]:

$$\omega_i = \sqrt{\frac{\lambda L^*}{\pi}} \sqrt{\frac{g_j^*}{g_i^*(1 - g_1^* g_2^*)}} ; i, j = 1, 2 ; i \neq j . \quad (11)$$

Figure 4.2 shows the mode_ to_ pump size ratio ω_1/ω_{pa} of different pumping spot radii as a function of the pump power with the radius of curvature of the rear mirror of 25 mm, where the averaged pump size along the gain medium is given by [33]:

$$\omega_{pa} = \int_0^l w_p(z) e^{-\alpha z} dz / \int_0^l e^{-\alpha z} dz . \quad (12)$$

According to the optimal mode matching condition [33], the ratio of ω_1/ω_{pa} should be in the range of 0.8 to 1.2 for $P_{in} < 10$ W. In our design, the maximum pump power is approximately 5.5 W. As can be seen from the Fig. 2, the optimum pump radius is in the region of 100 μ m.

With $\omega_{p0} = 100$ μ m and $\rho_1 = 25$ mm, we consider the thermal lensing effect to calculate the effective mode area ratio of A/A_s as a function of the pump power. Figure 4.3 shows the calculated result for the dependence of the effective mode area ratio of A/A_s on the pump power. It can be seen that the effective mode area ratio of A/A_s is generally greater than 10 for the pump power less than 5.5 W. To be brief, I choose a nearly hemispherical cavity with the radius of curvature of the rear mirror of 25 mm and the pumping spot radius of 100 μ m to simultaneously satisfy the optimal mode matching condition and the good Q-switching criterion.

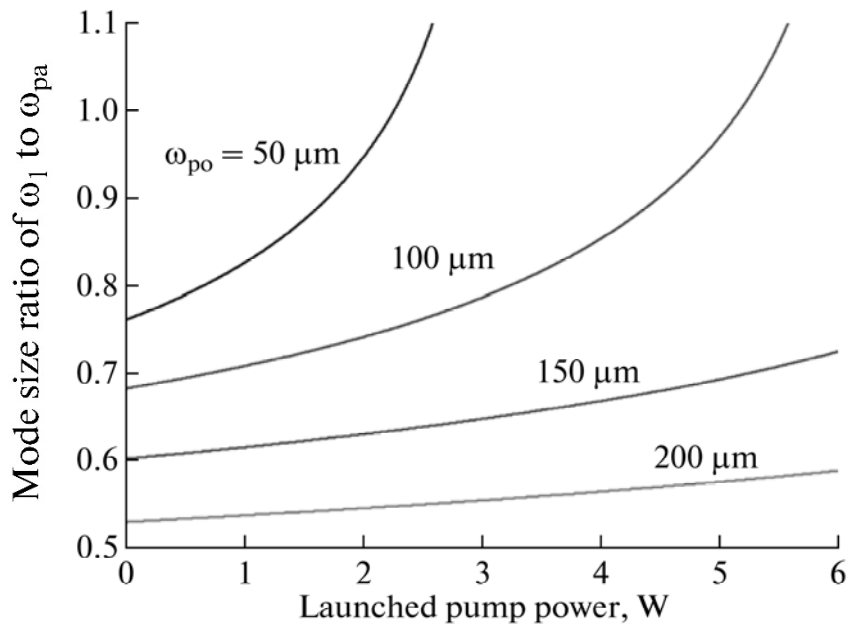


Fig 4. 2 Dependence of the mode-to-pump size ratio ω_1/ω_{pa} on the pump power for different pumping spot radii.

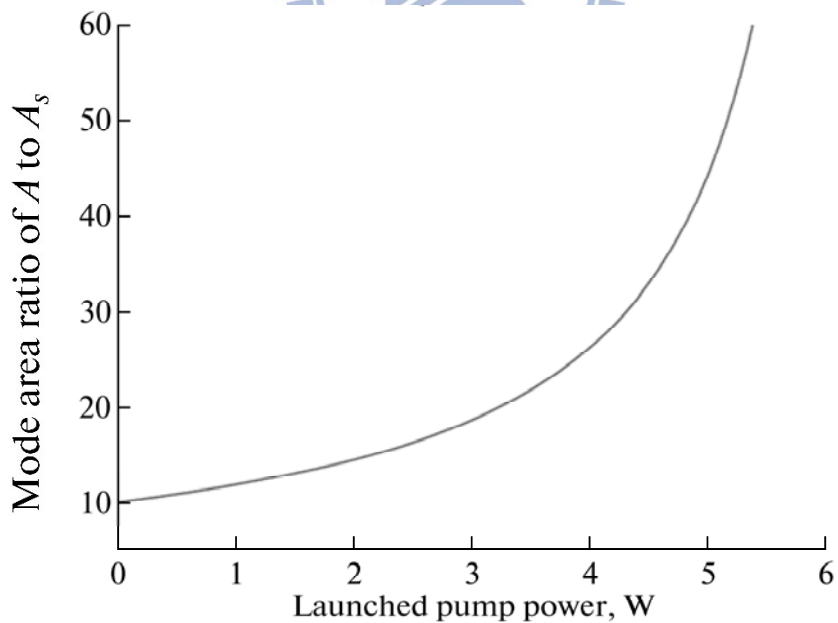


Fig 4. 3 Effective mode area ratio of A/A_s as a function of the pump power in the Nd:YVO₄/Cr⁴⁺:YAG PQS laser with $L = 0.9\rho_1$, $\rho_1 = 25 \text{ mm}$, $\omega_p = 100 \mu\text{m}$.

4.1.3 Experimental results for the PQS laser

We followed the theoretical analysis to construct a nearly hemispherical cavity for realizing the compact high-peak-power Nd:YVO₄/Cr⁴⁺:YAG PQS laser, as shown in Fig. 4.4 for the experimental setup. The rear mirror was a concave mirror with a radius-of-curvature of 25 mm with high-transmission coating at 808 nm ($T \sim 95\%$) and high-reflection at 1064 nm ($R > 99.8\%$). The output coupler was a flat mirror with partially reflection at 1064 nm ($R = 60\%$). The pumping source was a 7-W 808-nm fiber-coupled laser diode with a core diameter of 200 μm and a numerical aperture of 0.22. The focusing lens with 25 mm focal length and 80% coupling efficiency was used to re-image the pump beam into the laser crystal. The gain medium was an a-cut 12-mm-long Nd:YVO₄ crystal with 0.3 at % Nd³⁺ concentration. Several Cr⁴⁺:YAG absorbers with T₀ of 70, 60, 50%, and 40% were used to investigate the performance. The Cr⁴⁺:YAG crystals were all 2 mm in thickness. Both sides of the Nd:YVO₄ and the Cr:YAG crystals were coated for antireflection at 1064 nm. All the laser crystal were wrapped within indium foils and mounted in the water cooled heat sinks that keep at 19°C. The Nd:YVO₄ crystal and Cr⁴⁺:YAG crystals were placed as close as possible to the rear mirror and the output coupler respectively. The effective cavity length was set to be 22.5 mm based on the design rule of $L = 0.9\rho_1$. The pulse temporal behavior was recorded by Leroy digital oscilloscope (Wavepro 7100; 10G samples/s; 4 GHz bandwidth) with a fast InGaAs photodiode.

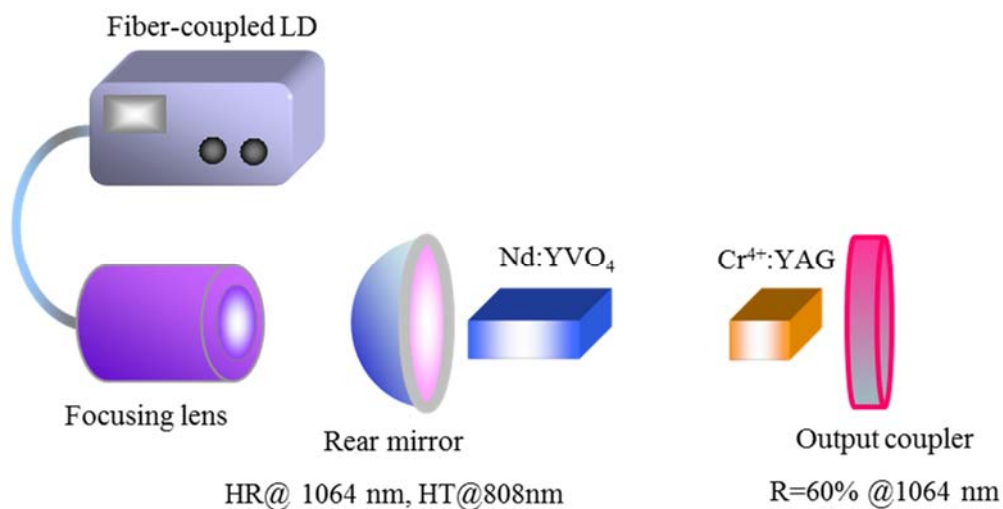


Fig 4. 4 Schematic diagram of a diode-pumped Nd:YVO₄ laser PQS with a Cr⁴⁺:YAG as a saturable absorber. HR:high reflection. HT:high transmission.

Figure 4.5(a) shows the output pulse energies and pulse repetition rates for Cr^{4+} :YAG saturable absorbers with different initial transmissions T_0 at the pump power of 5.4 W. It can be seen that for the initial transmission T_0 decreasing from 70 to 40% the output pulse energy increases from 22 to 36 μJ ; at the same time, the pulse repetition rate decreases from 50 to 25 kHz. Figure 4.5(b) depicts the pulse widths and peak powers for saturable absorbers with different initial transmissions T_0 at the pump power of 5.4 W. For the initial transmission T_0 decreasing from 70 to 40% the pulse width can be seen to decrease from 4.8 ns to 1.6 ns; consequently, the peak power was enhanced from 4.5 to 22.5 kW. Figures 4.6(a) and 4.6(b) show typical oscilloscope traces for a single pulse at the maximum output powers of the seeds with $T_0 = 70$ and 40%, respectively. Experimental results reveal that the characteristics of the output pulse in the present PQS laser display a simple pulse train without the satellite pulses phenomenon. It is worth mentioning that the satellite pulses phenomena such as two pulses oscillate simultaneously or one giant pulse followed by a weak pulse are often observed when the laser cavity does not properly comply with the second threshold criterion in Eq. (1). The spectral spectrum was measured by an optical spectrum analyzer with 0.1-nm resolution (Advantest Q8381A). The spectral linewidths for all the present PQS lasers were nearly the same to be 0.5 nm. In the next section, we will employ these high-peak-power PQS lasers to realize a single stage, linear-polarized fiber amplifier.

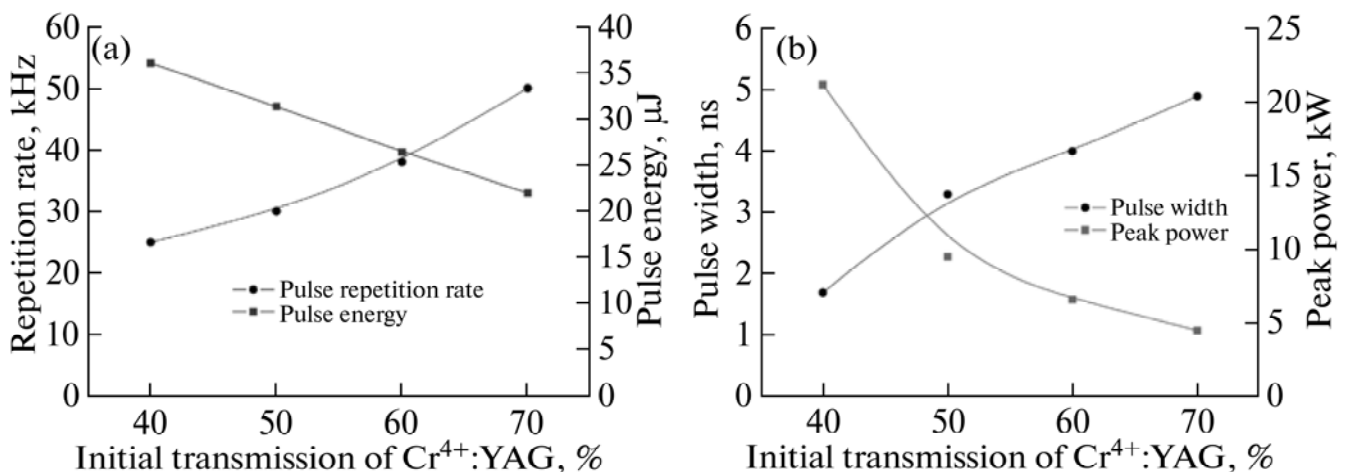


Fig 4. 5 (a) Dependence of the pulse repetition rate and the pulse energy on the initial transmission of Cr^{4+} :YAG at the pump power of 5.4 W. (b) Dependence of the pulse width and the peak power on the initial transmission of Cr^{4+} :YAG at the pump power of 5.4 W.

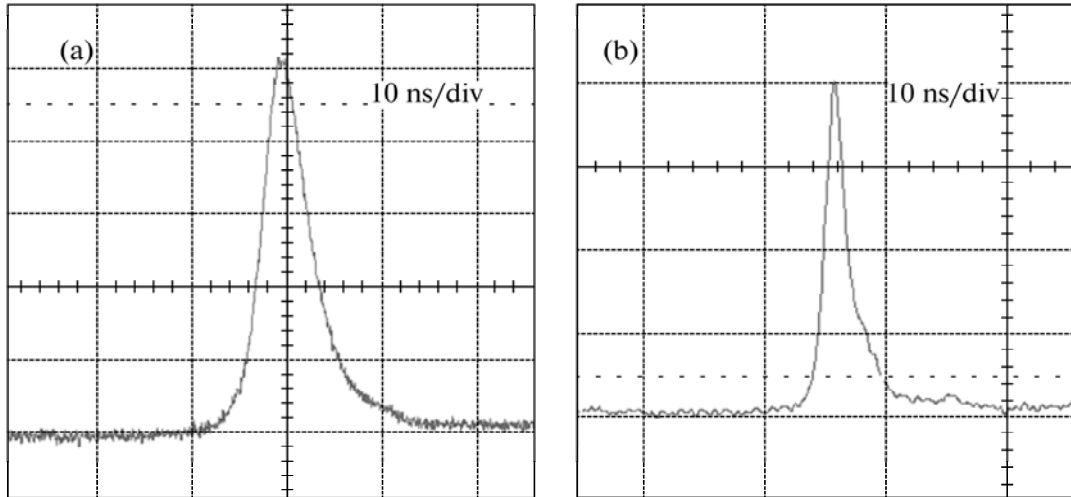


Fig 4. 6 Oscilloscope traces of a single pulse of (a) PQS laser with Cr⁴⁺:YAG of T₀ = 0%, (b) PQS laser with Cr⁴⁺:YAG of T₀ = 40%.

4.1.4 Experimental results for the mopa system

The experimental architecture for the MOFA system is shown in Fig. 4.7(a). The gain fiber was a 3-m-long Yb-doped Panda-style PM double clad fiber (Nufern) with a core diameter of 30 μm (N.A. = 0.06) and an inner clad diameter of 250 μm (N.A. = 0.46) with pump absorption of 6.6 dB/m at 975 nm. The Panda-style stress applying parts around the core generate a birefringence of 1.5×10^{-4} . A microscope image of the fiber cross-section is depicted in Fig. 4.7(b). Both ends of the fiber were polished at an angle of 8° to eliminate the end facet reflection. The pump source was a 20-W 976-nm fiber-coupled laser diode with a core diameter of 200 μm and a numerical aperture of 0.2. A focusing lens with 25-mm focal length was used to re-image the pump beam into the fiber through a dichroic mirror with high transmission (HT, T > 90%) at 976 nm and high reflectivity (HR, R > 99.8%) within 1030-1100 nm. The pump spot radius was approximately 100 μm , and the pump coupling efficiency was estimated to be nearly 80%. The seed laser was coupled through a focusing lens into the core of the fiber. A half-wave plate was used to control the polarization direction of the seed laser to match the fast-axis of the PM fiber.

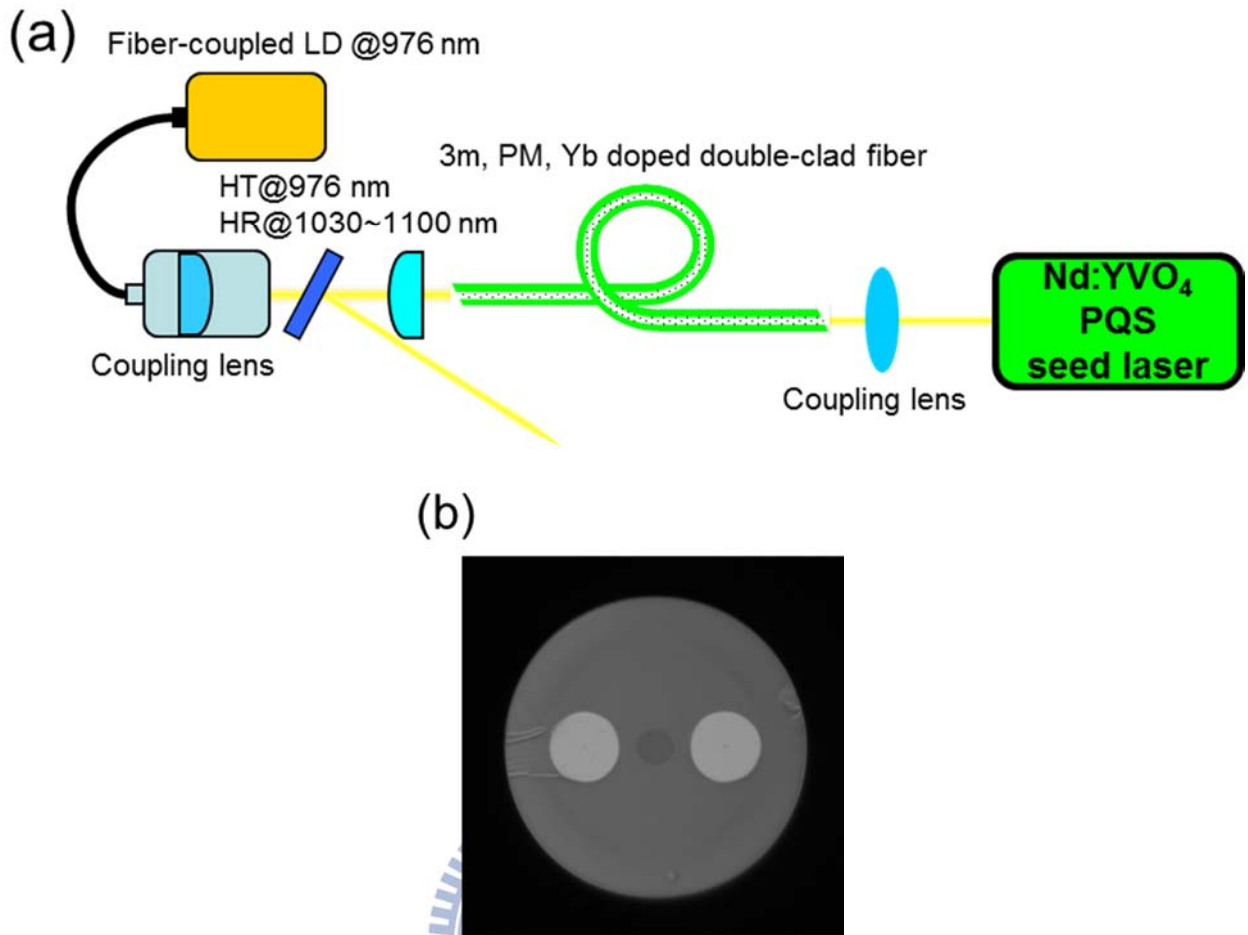


Fig 4. 7 (a) Scheme of the MOFA setup. HT: high transmission HR: high reflection. (b) Cross section of the PM Yb-doped fiber.

Figure 4.8(a) shows the average output power of the MOPA injected by the seed laser with $T_0 = 70\%$ as a function of launched pump power at a repetition rate of 50 kHz. Under the launched pump power of 16 W, the output power of the amplifier was 8.9 W, corresponding to the pulse energy of 178 μJ . The slope efficiency was approximately 54%. Figure 4.8(b) shows the typical oscilloscope trace for a single pulse at the maximum output power of amplifier. The pulse duration was 4.8 ns and the corresponding peak power was 37 kW. The oscilloscope trace of a train of output pulses of the amplifier is shown in Fig. 8c. The pulse-to-pulse amplitude fluctuation was generally less than 1.5% in root mean square (rms).

Figure 4.9(a) shows the average output power of the MOPA injected by the seed laser with $T_0 = 40\%$ as a function of launched pump power at a repetition rate of 25 kHz. It was found that the end facet damage of the fiber limited the maximum average output power to be approximately 4.8 W under the pump power of 10 W. As a result,

the maximum pulse energy was restricted to 192 μJ . Figure 4.10 depicts the microscope image of the damaged end view and the side view of the fiber. Figure 4.9(b) shows the typical oscilloscope trace for a single pulse at the maximum output powers of amplifier. The pulse duration was 1.6 ns and the corresponding peak power was 120 kW. The calculated optical intensity on the end facet of the fiber was 27.2 J/cm^2 which agrees with the surface damage threshold of fused silica at 1064 nm [34]. The oscilloscope trace of a train of output pulses of the amplifier is shown in Fig. 4.9(c). The pulse-to-pulse amplitude fluctuation was generally less than 4.0% in rms.

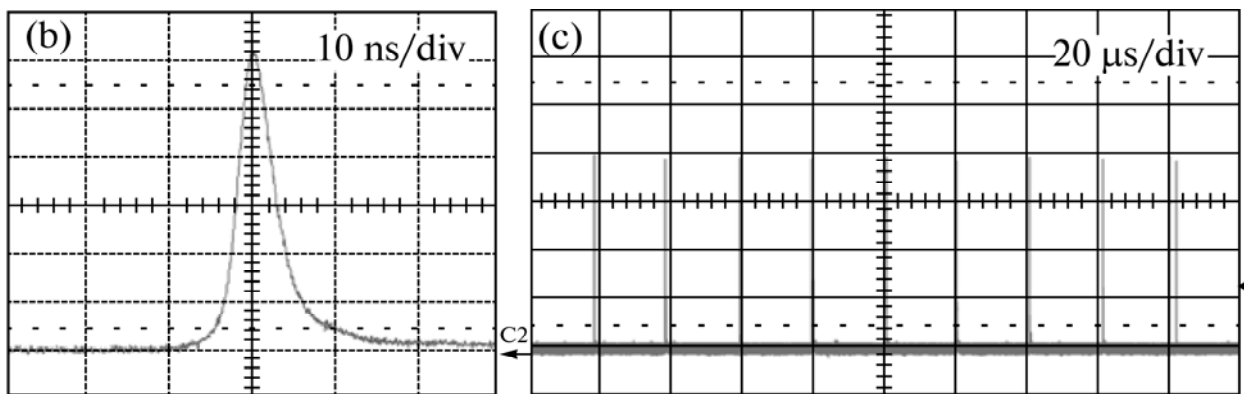
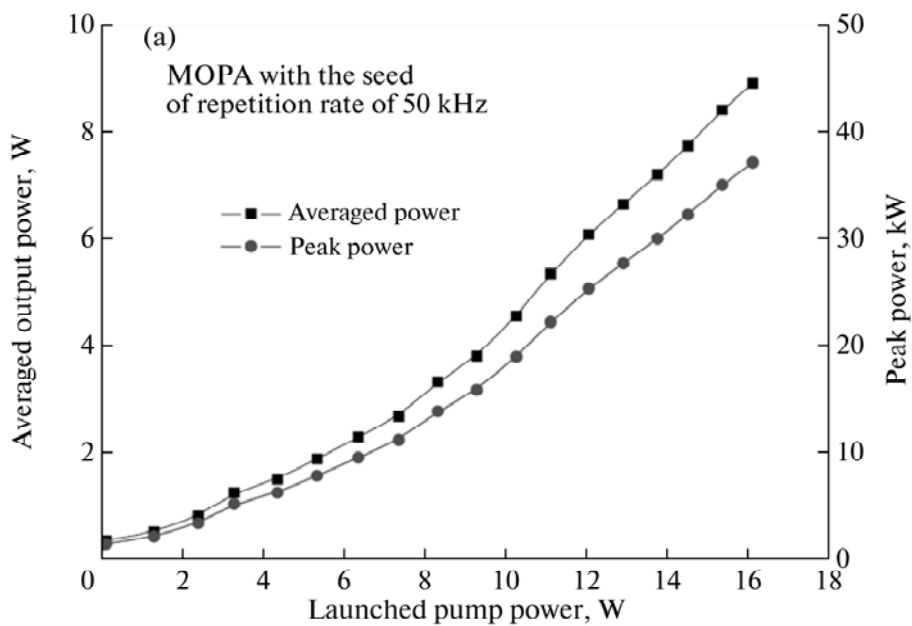


Fig 4. 8 (a) Average output power and peak power of MOFA with the seed of repetition rate of 50 kHz as a function of the launched pump power. (b) Oscilloscope traces of a single pulse of the output pulse of the amplifier. (c) Oscilloscope traces of a train of amplified pulses.

The timing jitters for both the amplifiers shown in Figs. 4.8 and 4.9 were generally less than 2% in rms. The M^2 factors were found to be smaller than 1.3 over the entire output power range. Furthermore, the polarization extinction ratios for both the amplifiers were measured to be about 100:1. Figures 11a and 11b show the optical spectra of the MOFAs at the maximum output powers injected by the seed lasers with $T_0 = 70$ and $T_0 = 40\%$, respectively. It can be seen that the peak levels of the amplified spontaneous emission (ASE) around 1040 nm shown in Figs. 4.11(a) and 4.11(b) were approximately 30 and 40 dB below the signal peak intensity, respectively. The power levels of the whole ASE intensities at the maximum output powers shown in Figs. 4.8(a) and 4.9(a) were measured to be less than 2% and 0.5%, respectively.

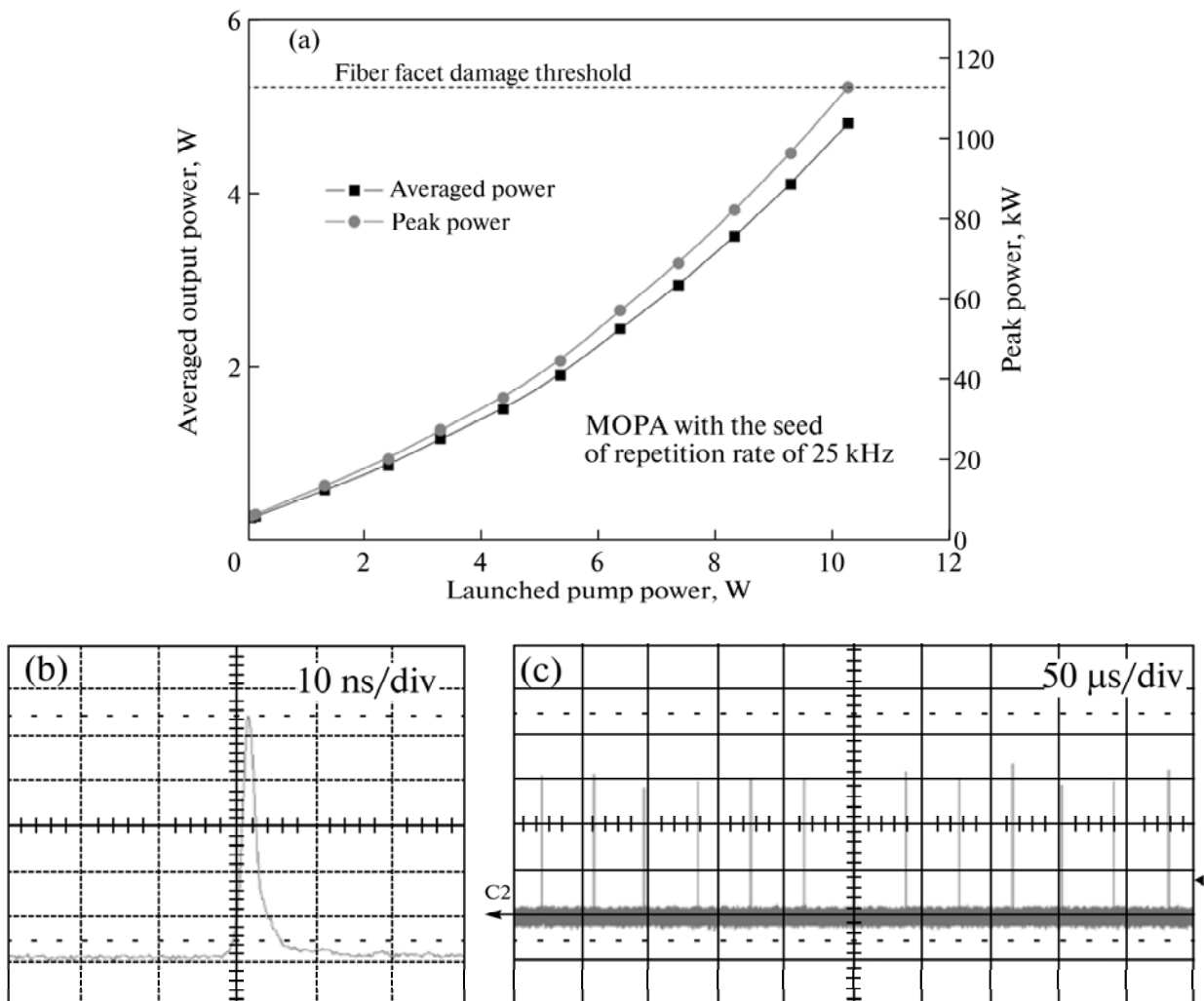


Fig 4. 9 (a) Average output power and peak power of MOFA with the seed of repetition rate of 25 kHz as a function of the launched pump power. (b) Oscilloscope traces of a single pulse of the output pulse of the amplifier. (c) Oscilloscope traces of a train of amplified pulses.

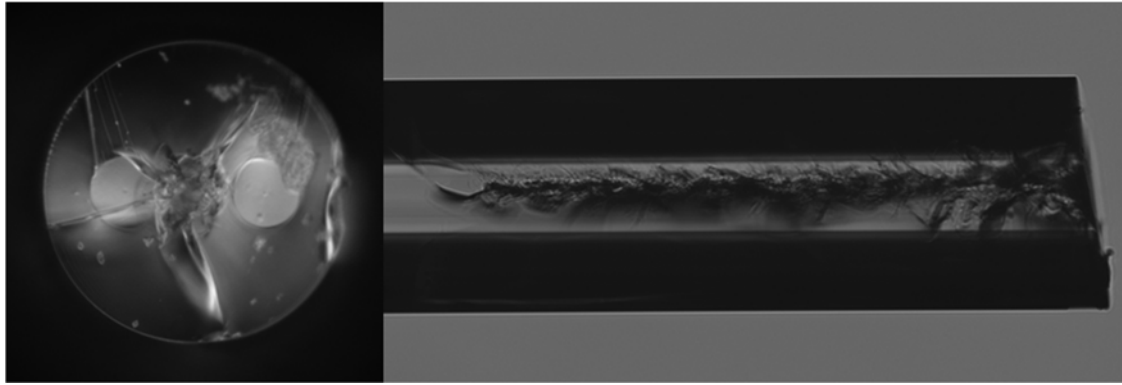


Fig 4. 10 End view and side view of the damaged fiber.

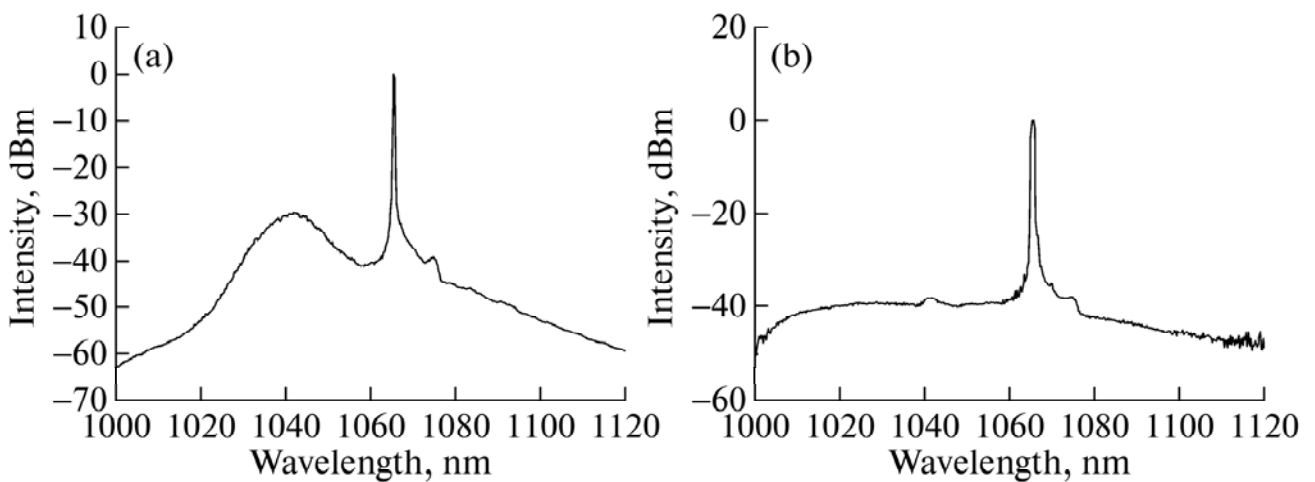


Fig 4. 11 Optical spectra of the MOFAs at the maximum output powers injected by the seed lasers with $T_0 =$ (a) 70 and (b) 40%.

4.1.5 Conclusion

In conclusion, we have developed compact Nd:YVO₄/Cr⁴⁺:YAG PQS lasers as seed oscillators for high-peak-power, single-stage, linear-polarized MOFAs. Compact and high-peak-power Nd:YVO₄/Cr⁴⁺:YAG PQS lasers were theoretically optimized by considering the second threshold criterion and the thermal lensing effect in a nearly hemi-spherical cavity. Several Cr⁴⁺:YAG crystals with different initial transmissions (T_0) have been used to confirm the performance of the designed PQS laser. It was experimentally found that at a pump power of 5.4 W the output pulse energy increases from 22 to 36 μ J and the pulse repetition rate decreases from 50 to 25 kHz for the initial transmission of the Cr⁴⁺:YAG crystal decreasing from 70 to 40%. Injecting the seed laser obtained with $T_0 = 70\%$ into a polarization maintained Yb-doped fiber, the pulse energy and peak power at a pump power of 16 W were found to be 178 μ J and 37 kW,

respectively. Employing the seed laser obtained with $T_0 = 40\%$, it was found that the surface damage of the fiber limited the maximum pulse energy and peak power to be 192 μJ and 120 kW, respectively. The polarization extinction ratio was approximately 100:1 for both MOPAs in the whole pump power. It is believed that the high peak-power and high polarization-extinction-ratio suggest further applications such as industrial material processing and nonlinear optics researches.



4.2 Passively Q-switched photonic crystal fiber amplifier and its applications

4.2.1 Introduction

High efficiency and short pulse duration pulsed light sources of ultraviolet (UV) radiation are attractive for a variety of applications in industry, scientific, and medical needs such as micro-precision processing, laser lithography, and optical data storage [35,36]. Shorter pulse duration is advantageous for laser processing that has lower material removal thresholds. In company with low material removal thresholds, laser machining with shorter pulses at low fluences also leads to cleaner and narrower scribes and reduced the potential damage to the electrical performance of the device [37,38]. Linearly polarized, good beam quality, and high peak power lasers with nanosecond-duration and multi-kilohertz repetition rate pulses are promising candidates for optical nonlinear wavelength conversions. Fiber lasers and amplifiers in the near-infrared (NIR) region, owing to the splendid heat dissipation and the wave-guiding property, have been extensively proved to be favorable light sources for the generation of UV radiation [39-43]. Fiber laser in actively Q-switched scheme [40] was employed for third harmonic generation (THG) and the wavelength conversion efficiency (from IR to THG) of 25% was attained. However, the pulse duration was relatively long (11 ns) due to the lengthy fiber oscillator configuration. The THG pumped by single-stage fiber amplifiers that seeded with passively Q-switched (PQS) Nd:YAG lasers were used to demonstrate UV radiation with shorter pulse width (approximately 1 ns). Nevertheless, the conversion efficiency was relatively lower with 12% [41] and 18% [42], respectively. With the higher conversion efficiency of 26%, the two-stage fiber amplifier [43] was used to produce 1 ns pulse with the average power of 1.5 W. However, the multi-stage architecture led to a complicated and power consuming system. Therefore, it is with much practical significance to design a compact, efficient THG with short pulse duration pumped by a single-stage fiber amplifier.

Large-mode-area (LMA) fibers were used to attain high peak powers and alleviate detrimental nonlinear effects such as stimulated Brillouin scattering (SBS), stimulated Raman scattering (SRS), and self-phase modulation which not only degrade the monochromaticity but also cause optical damages. Nevertheless, conventional LMA fibers suffer from mode-quality degradation with the increasing core size diameter. Recently, photonic crystal fiber (PCF) lasers and amplifiers [44-46] are proved to be

reliable light sources with high peak power and good beam quality thanks to the ultra-large mode area core, the high absorption efficiency, and the air holes assisted wave-guiding property. Consequently, a PCF amplifier is much advantageous for nonlinear wavelength conversions rather than the conventional LMA fiber amplifier. However, up to now, the extracavity THG pumped by a single-stage PCF amplifier has not been reported.

In this work, we use a single-stage rod-like PCF amplifier to demonstrate compact harmonic generations with high efficiency and short pulse width. We obtain pulses with average power of 3.3 W at the pulse repetition rate (PRR) of 14.9 kHz and pulse width of 2.2 ns in the IR wavelength by seeding an efficient PQS Nd:YVO₄/Cr⁴⁺:YAG laser into a LMA rod-like PCF amplifier. In addition, we utilize the extracavity nonlinear wavelength conversion architecture to attain the second harmonic generation (SHG) wave at 532 nm and the THG wave at 355 nm. Average powers for SHG and THG were 1.7 W and 1.1 W at the IR input power of 3.3 W which correspond to the conversion efficiency of 52% and 33%, respectively. The pulse width for the UV radiation was 2.1 ns with the pulse amplitude fluctuation of 7.4% in standard deviation.

4.2.2 Single-stage rod-like fiber amplifier

The scheme of the extracavity THG pumped by a single-stage rod-like PCF amplifier is depicted in Fig. 4.12 The experimental setup could be separated into two major parts, one is a PQS Nd:YVO₄/Cr⁴⁺:YAG laser seeded PCF amplifier and the other one is a single-pass harmonic generation. We have demonstrated that the Nd:YVO₄/Cr⁴⁺:YAG PQS laser was a compact and efficient laser source with high peak power and can be applied to THG generation [47] and seed laser [48]. The nearly hemispherical cavity based Nd:YVO₄/Cr⁴⁺:YAG PQS laser was used to simultaneously satisfy the optimal mode matching condition and the good Q-switching criterion. The seed laser is a home-made, nearly hemispherical cavity Nd:YVO₄/Cr⁴⁺:YAG PQS laser that emitted pulses with pulse energy of 38 μJ and pulse width of 2.2 ns at the PRR of 14.9 kHz. The seed laser was coupled through a focusing lens into the core of the fiber. A half-wave plate was used to control the polarization direction of the seed laser to match the fast-axis of the polarization maintaining (PM) fiber. The 36-cm in length, PM Yb-doped rod-type PCF has a signal core diameter of 70 μm and a low numerical

aperture (N.A.) of 0.02 to sustain the excellent beam quality. The pump cladding of the PCF has a diameter of 200 μm and an air-cladding to maintain a high N.A. of 0.6. The PCF was surrounded with a 1.7-mm thick outer cladding and was sealed with end-caps for protection. The boron doped stress-applying parts near the core were adopted to induce birefringence that produces diverse spectral losses to form a linearly polarization state for the fundamental mode. The pump source was a 15-W 976-nm fiber-coupled laser diode with a core diameter of 200 μm and a numerical aperture of 0.2. Focusing lens with 25-mm focal length was used to re-image the pump beam into the fiber through the dichroic mirror with high transmission (HT, $T > 90\%$) at 976 nm and high reflectivity (HR, $R > 99.8\%$) within 1030~1100 nm. The pump spot radius was approximately 100 μm , and the pump coupling efficiency was estimated to be around 80%. The laser spectrum was measured by an optical spectrum analyzer with 0.1 nm resolution (Advantest Q8381A). The pulse temporal behavior was recorded by Leroy digital oscilloscope (Wavepro 7100; 10G samples/sec; 1 GHz bandwidth) with a fast InGaAs photodiode.

The average output power and pulse energy versus the launched pump power of the fiber amplifier were shown in Fig. 4.13. Under a launched pump power of 10.5 W, 3.3 W of output power was acquired which corresponds to the pulse energy of 221 μJ . The inset of Fig. 4.13 shows the output spectrum of the PCF amplifier with the output power of 3.3 W. The signal peak wavelength was at 1064.6 nm and its full width at half maximum (FWHM) is around 0.6 nm. The M^2 factor was measured to be less than 1.3 over the complete output power range owing to the low-N.A. feature of the fiber. The output of the amplifier was linear polarized and the polarization extinction ratio was measured to be higher than 100:1 for all the pump power range that evidences the function of the PM structure in the fiber.

The oscilloscope trace of a train of output pulses of the amplifier is shown in Fig. 4.14(a). The pulse-to-pulse amplitude fluctuation was generally less than 8% in root mean square (rms). Figure 4.14(b) shows the typical oscilloscope trace for a single pulse at the maximum output power of the amplifier. The pulse duration was 2.2 ns and the corresponding peak power was 100 kW.

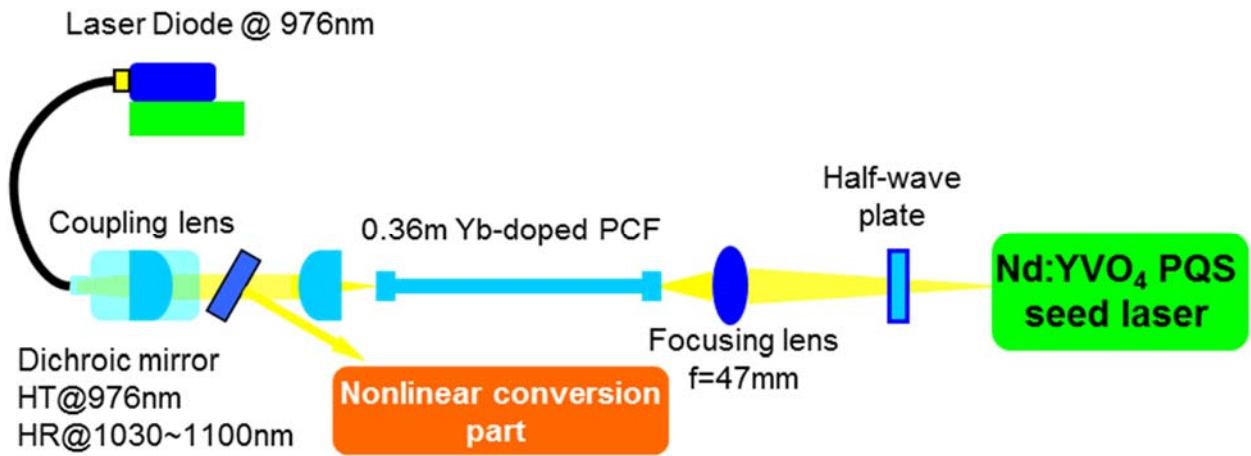


Fig 4. 12 Schematic sketch of the extracavity harmonic generations pumped by a single-stage rod-like photonic crystal fiber amplifier. HR: high reflection; HT: high transmission.

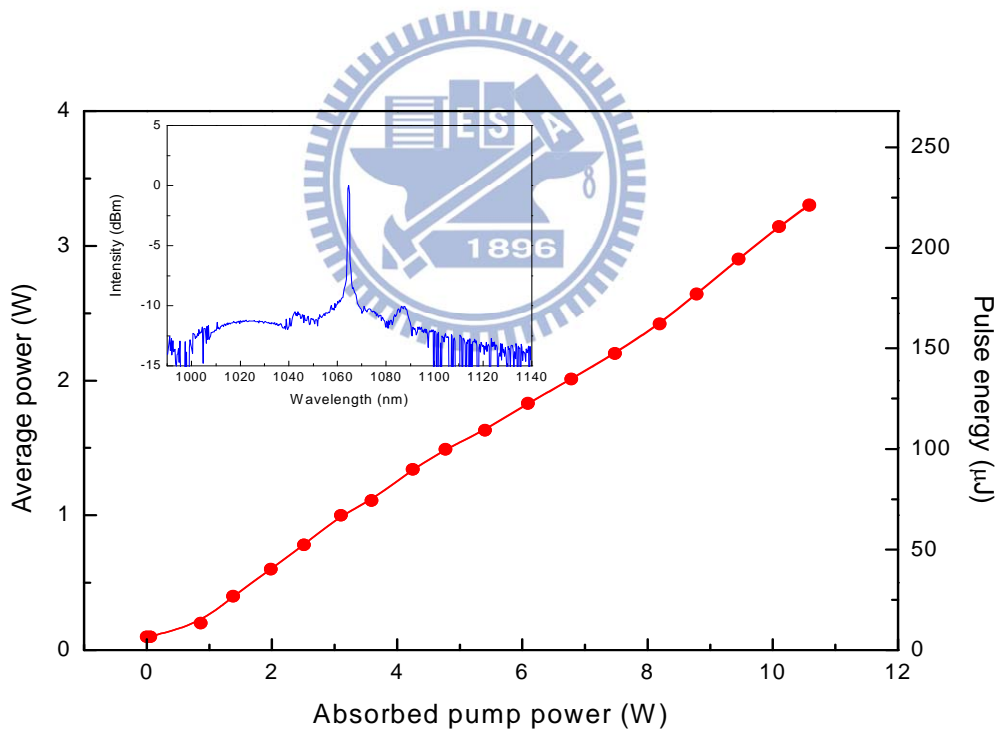


Fig 4. 13 Relevance of the average output power and the pulse energy with the launched pump power of the PCF amplifier. Inset: the output lasing spectrum of the PCF amplifier obtained with 10.5 W of pump power.

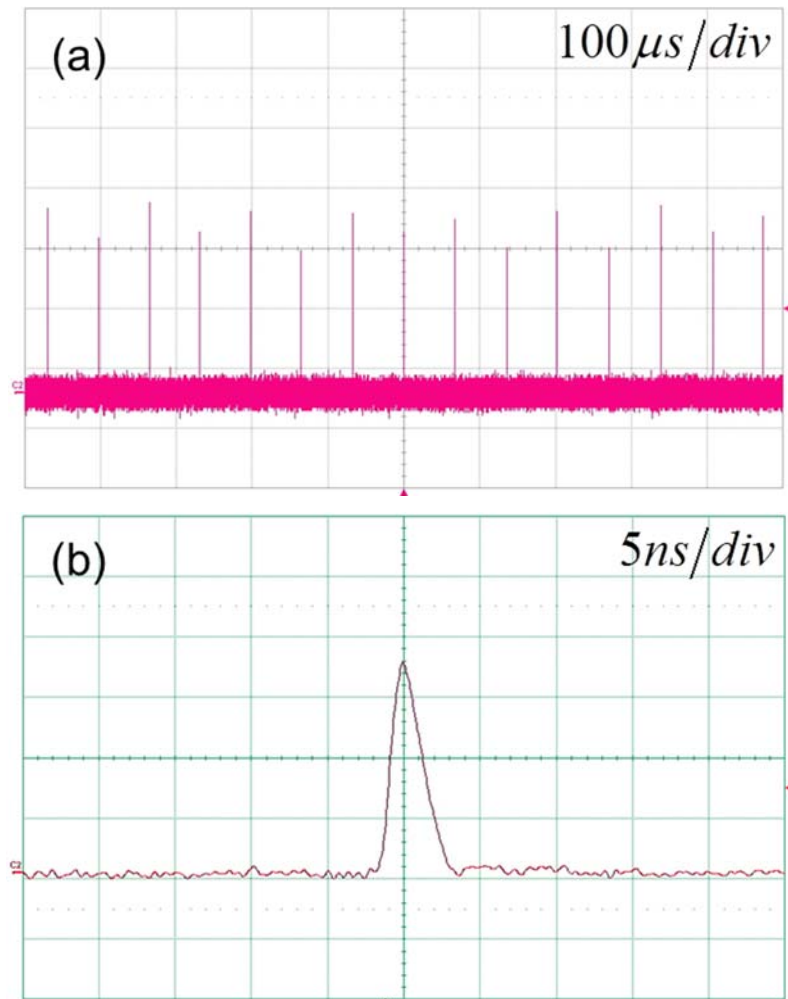


Fig 4. 14 Oscilloscope traces of a train of amplified pulses. (b) Oscilloscope trace of a single pulse of the output pulse of the amplifier.

4.2.3 Second and third harmonic generation

The scheme of the extracavity harmonic generations was depicted in Fig. 4.15. The IR source from the amplifier was focused by a lens with a focal length of 75 mm which was with anti-reflection (AR) coating at 1064 nm. The SHG was demonstrated by delivering the focused IR beam into a 3x3x15 mm³-in-dimension, type I phase-matched lithium triborate (LBO) crystal which was cut at $\theta=90^\circ$ and $\phi=10.4^\circ$ and operated at 46.6 °C. Both end facets of the LBO crystal were coated with AR coating at 1064 nm and 532 nm. The residual IR laser and the generated 532 nm beam were then focused by a lens which had the focal length of 19 mm and was coated with AR coating at 1064 nm and 532 nm. The type II, 3x3x10 mm³-in-dimension LBO

crystal cut at $\theta=44^\circ$ and $\phi=90^\circ$ was used for sum-frequency-mixing operated at 48 °C. The entrance together with the exit end facets of the LBO crystal were coated with AR coating at 1064 nm and 532 nm. The temperature of the SHG and THG nonlinear crystals were temperature-controlled by thermoelectric coolers with the precision of 0.1°C.

Figure 4.16 shows the average power obtained with the SHG (532nm) and the THG (355nm), respectively. Under a pump power of 3.3 W of the IR wavelength, an average output power of SHG was 1.7 W corresponding to the pulse energy of 114 μJ and the wavelength conversion efficiency (from IR to SHG) of 52%. The average output power of the THG increased monotonically with pump power of the IR wavelength. At a launched pump power of 3.3 W, the sum-frequency-mixing was found to generate an output power of 1.1 W and pulse energy of 74 μJ , corresponding to a slope efficiency of 39% and wavelength conversion efficiency of 33% (from IR to THG). The spatial intensity distribution of the far field of 355 nm output was shown in the inset of Fig. 4.16

Oscilloscope traces of a train of output pulses of the SHG (top) and the THG (bottom) is shown in Fig. 4.17(a). The pulse-to-pulse amplitude fluctuations for SHG and THG were approximately less than 6% and 8% in rms, respectively. Figure 4.17(b) depicts the oscilloscope trace for a single pulse at the maximum output power of THG. The pulse duration was measured to be about 2.1 ns which correspond to the peak power of 35 kW.

In order to obtain compact, efficient, and shorter pulse duration of the UV light source, single-stage fiber amplifiers were the preferable light sources for extracavity THG rather than fiber lasers. Besides, for higher wavelength conversion efficiency, the selection of the extracavity THG nonlinear crystal is also of great importance. The choice of the THG crystal is the compromise between finding a high nonlinear coefficient and a wide acceptance angle combined with a small walk-off angle [49]. The extracavity THGs by using a type I phase-matched LBO as the THG crystal were demonstrated with single-stage fiber amplifiers [41, 42]. The relatively large walk-off angle of the type I phase-matched LBO for THG (18.3 mrad to type I and 9.3 mrad to type II) [50] will deteriorate the beam overlap between the IR and the green beams that is seriously detrimental to conversion efficiency. Besides, in ref. 41, polarization instability caused by using a non-PM fiber as the amplifier also led to the lower wavelength conversion efficiency of only 12%. Furthermore, two type I phase-matched

LBO were utilized for SHG and THG with a PM fiber amplifier as the fundamental light source [42]. The conversion efficiency was limited to be 18% because the polarization state between the residual IR beam and the green light in the THG crystal was not re-optimized. Here I realize the efficient extracavity UV light generation by employing the type II LBO as the THG crystal owing to its smaller walk-off angle and relatively large acceptance angle [50] (5.0 mrad cm for type II and 1.7 mrad cm for type I). Combining the efficient THG module and the single-stage PM PCF amplifier, we obtained, to the best of our knowledge, the highest wavelength conversion efficiency of 33% and the short pulse duration of approximately 2 ns in the same time.

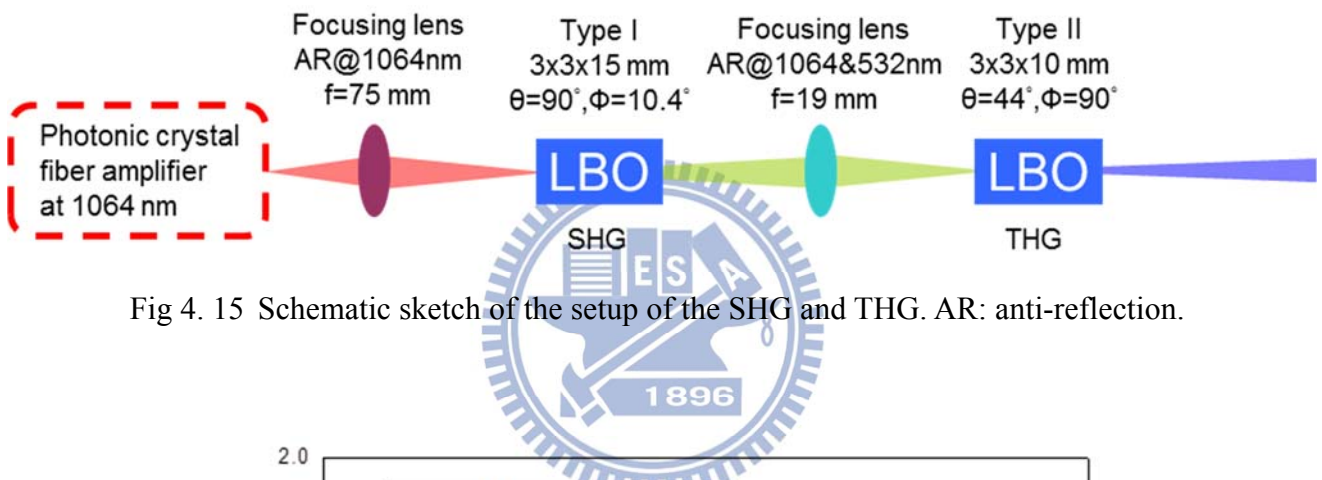


Fig 4. 15 Schematic sketch of the setup of the SHG and THG. AR: anti-reflection.

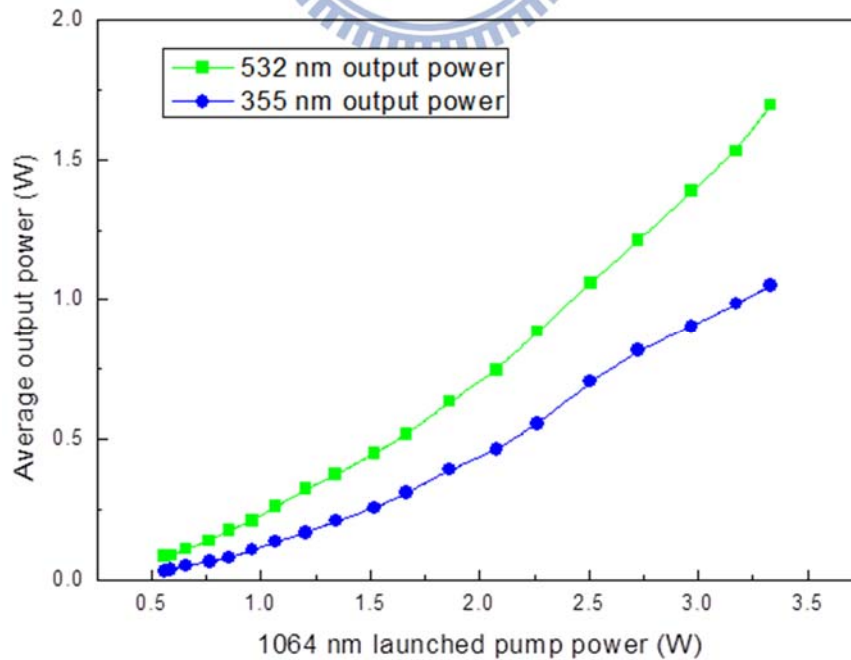


Fig 4. 16 Dependences of the average output power at 532 nm and 355 nm on the incident pump power at 1064 nm. Inset: the spatial intensity distribution of far field of the THG output.

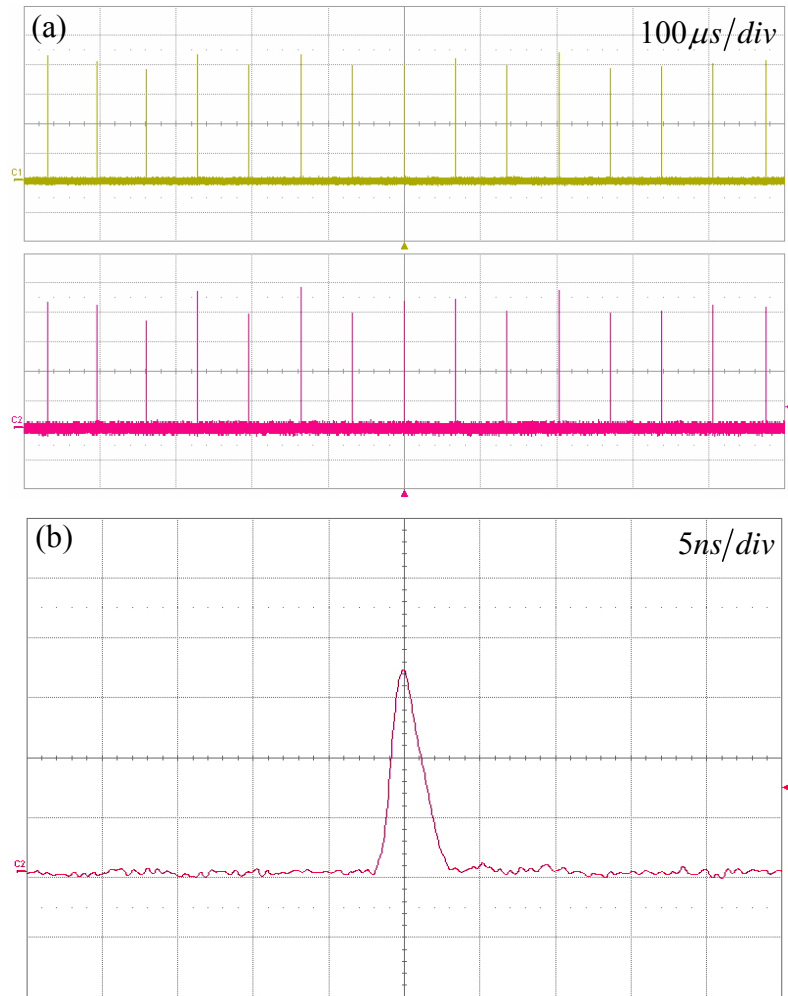


Fig 4. 17 (a) Oscilloscope traces of a train of output pulses of 532 nm (top) and 355 nm (bottom). (b) Oscilloscope trace of a single pulse of the output pulse of the THG.

4.2.4 Conclusions

In conclusion, we have used a Nd:YVO₄/Cr⁴⁺:YAG PQS laser to seed a single-stage rod-like PCF amplifier to acquire a single polarization, high beam quality, and efficient IR pulsed light source with the pulse energy of 221 μJ and pulse width of 2.2 ns at the PRR of 14.9 kHz. We further utilize the developed PCF amplifier to demonstrate the extracavity SHG and THG. Under an incident pump power of 3.3 W at the IR wavelength, the average output powers of the SHG and the THG were measured to be up to 1.7 W and 1.1 W which amount to the wavelength conversion efficiencies of 52% and 33%, respectively. This is the highest conversion efficiency in the generation of UV light by means of the fiber amplifier pumped THG. It is believed that the high efficiency UV light source suggest further applications such as industrial material processing and scientific researches.

Reference

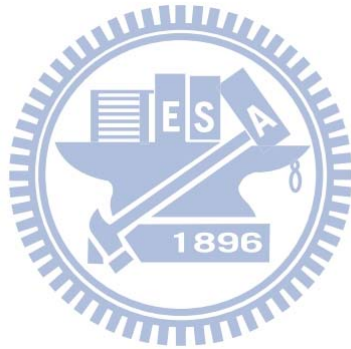
1. E. Molva, "Microchip lasers and their applications in optical microsystems," *Opt. Mater.* **11**, 289-299 (1999).
2. Q. Liu, and X. P. Yan, "High power all-solid-state fourth harmonic generation of 266 nm at the pulse repetition rate of 100 kHz," *Laser Phys. Lett.* **6**, 203-206 (2009).
3. S. V. Garnov, V. I. Konov, T. Kononenko, V. P. Pashinin, and M. N. Sinyavsky, "Microsecond laser material processing at 1.06 μm ," *Laser Phys.* **14**, 910-915 (2004).
4. L. Sun, L. Zhang, H. J. Yu, L. Guo, J. L. Ma, J. Zhang, W. Hou, X. C. Lin, and J. M. Li, "880 nm LD pumped passive mode-locked TEM₀₀ Nd:YVO₄ laser based on SESAM," *Laser Phys. Lett.* **7**, 711 (2010).
5. X. S. Cheng, B. A. Hamida, A. W. Naji, H. Ahmad, and S. W. Harun, "67 cm long bismuth-based erbium doped fiber amplifier with wideband operation," *Laser Phys. Lett.* **8**, 814-817 (2011).
6. A. S. Kurkov, V. A. Kamynin, E. M. Sholokhov, and A. V. Marakulin, "Mid-IR supercontinuum generation in Ho-doped fiber amplifier," *Laser Phys. Lett.* **8**, 754-757 (2011).
7. X. Wushouer, P. Yan, H. Yu, Q. Liu, X. Fu, X. Yan, and M. Gong, "High peak power picosecond hybrid fiber and solid-state amplifier system," *Laser Phys. Lett.* **7**, 644-649 (2010).
8. H. J. Liu, and X. F. Li, "High power tunable picosecond green laser pulse generation by frequency doubling of an Yb-doped fiber power amplifier seeded by a gain switch laser diode," *Laser Phys.* **21**, 2118-2121 (2011).
9. Z. Y. Dong, S. Z. Zou, H. J. Yu, Z. H. Han, Y. G. Liu, L. Sun, W. Hou, X. C. Lin, and J. M. Li, "High peak power green light generation using ytterbium fiber amplifier and lithium triborate crystal," *Laser Phys.* **21**, 1804-1807 (2011).
10. Z. Y. Dong, S. Z. Zou, Z. H. Han, H. J. Yu, L. Sun, W. Hou, X. C. Lin, and J. M. Li, "High power, high energy nanosecond pulsed fiber amplifier with a 20 μm core fiber," *Laser Phys.* **21**, 536-539 (2011).
11. C. Ye, P. Yan, L. Huang, Q. Liu, and M. Gong, "Stimulated Brillouin scattering phenomena in a nanosecond linearly polarized Yb-doped double-clad fiber amplifier," *Laser Phys. Lett.* **4**, 376-381 (2007).

12. A. V. Kir'yanov, S. M. Klimentov, I. V. Mel'nikov, and A. V. Shestakov, "Specialty Yb fiber amplifier for microchip Nd laser: Towards ~1-mJ/1-ns output at kHz-range repetition rate," *Opt. Commun.* **282**, 4759-4764 (2009).
13. P. E. Schrader, R. L. Farrow, D. A. V. Kliner, J.-P. Fève and N. Landru, "High-Power fiber amplifier with widely tunable repetition rate, fixed pulse duration, and multiple output wavelengths," *Opt. Express* **14**, 11528-11538 (2006).
14. C. D. Brooks and F. Di Teodoro, "Multimegawatt peak-power, single-transverse-mode operation of a 100 μ m core diameter, Yb-doped rodlike photonic crystal fiber amplifier," *Appl. Phys. Lett* **89**, 111119 (2006).
15. C. Li, J. Song, D. Shen, N. S. Kim, J. Lu, and K. Ueda, "Diode-pumped passively Q-switched Nd:GdVO₄ lasers operating at 1.06 μ m wavelength," *Appl. Phys. B* **70**, 471 (2000).
16. Z.-Y. Li, H.-T. Huang, J.-L. He, B.-T. Zhang, and J.-L. Xu, "High peak power eye safe intracavity optical parametric oscillator pumped by a diode pumped passively Q-switched Nd:GGG laser," *Laser Phys.* **20**, 1302-1306 (2010).
17. J.-L. Li, D. Lin, L.-X. Zhong, K. Ueda, A. Shirakawa, M. Musha, and W.-B. Chen, "Passively Q-switched Nd:YAG ceramic microchip laser with azimuthally polarized output," *Laser Phys. Lett.* **6**, 711-714 (2009).
18. R. J. Lan, M. D. Liao, H. H. Yu, Z. P. Wang, X. Y. Hou, X. G. Xu, H. J. Zhang, D. W. Hu, and J. Y. Wang, "3.3 ns Nd:LuVO₄ micro-type laser," *Laser Phys. Lett.* **6**, 268-271 (2009).
19. S. Y. Zhang, H. T. Huang, M. J. Wang, L. Xu, W. B. Chen, J. Q. Xu, J. L. He, and B. Zhao, "Diode-pumped continuous wave and passively Q-switched operation of Nd:Gd_{0.33}Lu_{0.33}Y_{0.33}VO₄ crystal," *Laser Phys. Lett.* **8**, 189-192 (2011).
20. Y. Bai, N. Wu, J. Zhang, J. Li, S. Li, J. Xu, and P. Deng, "Passively Q-switched Nd:YVO₄ laser with a Cr⁴⁺:YAG crystal saturable absorber," *Appl. Opt.* **36**, 2468-2472 (1997).
21. M. Liu, J. Liu, S. Liu, L. Li, F. Chen, and W. Wang, "Experimental study on passively Q-switched mode-locking diode-pumped Nd:KGW laser with Cr⁴⁺:YAG," *Laser Phys.* **19**, 923-926 (2009).
22. Y. F. Chen, S. W. Tsai, and S. C. Wang, "High-power diode-pumped Q-switched and mode-locked Nd:YVO₄ laser with a Cr⁴⁺:YAG saturable absorber," *Opt. Lett.* **25**, 1442-1444 (2000).
23. F. Q. Liu, J. L. He, J. L. Xu, B. T. Zhang, J. F. Yang, J. Q. Xu, C. Y. Gao, and H. J.

- Zhang, "Passively Q-switched mode-locking in a diode-pumped c-cut Nd:LuVO₄ laser with Cr⁴⁺:YAG," *Laser Phys. Lett.* **6**, 567-570 (2009).
24. H. Yu, H. Zhang, Z. Wang, J. Wang, Z. Shao, and M. Jiang, "CW and Q-switched laser output of LD-end-pumped 1.06 μ m c-cut Nd:LuVO₄ laser," *Opt. Express* **15**, 3206-3211 (2007).
 25. H. Yu, H. Zhang, Z. Wang, J. Wang, Y. Yu, M. Jiang, and X. Zhang, "Passively Q-switched laser performance of c-cut Nd:Gd_{0.63}Y_{0.37}VO₄ crystal," *Opt. Commun.* **281**, 5199-5201 (2008).
 26. H.-J. Qi, X.-D. Liu, X.-Y. Hou, Y.-F. Li, and Y.-M. Sun, "A c-cut Nd:GdVO₄ solid-state laser passively Q-switched with Co²⁺:LaMgAl₁₁O₁₉ lasing at 1.34 μ m," *Laser Phys. Lett.* **4**, 576-579 (2007).
 27. G. Xiao, J. H. Lim, S. Yang, E. Van Stryland, M. Bass, and L. Weichman, "Z-Scan Measurement of the Ground and Excited State Absorption Cross Sections of Cr⁴⁺ in Yttrium Aluminum Garnet," *IEEE J. Quantum Electron.* **35**, 1086 (1999).
 28. A. Agnesi and S. Dell'acqua, "High-peak-power diode-pumped passively Q-switched Nd:YVO₄ laser," *Appl. Phys. B* **76**, 351-354 (2003).
 29. Y.F. Chen, Y.C. Chen, S.W. Chen, and Y.P. Lan, "High-power efficient diode-pumped passively Q-switched Nd:YVO₄/KTP/Cr⁴⁺:YAG eye-safe laser," *Opt. Commun.* **234**, 337-342 (2004).
 30. N. Hodgson, and H. Weber, *Laser Resonators and Beam Propagation*, 2nd edn. (Springer, Berlin, 2005), Ch. 5.
 31. W. Koechner, *Solid-State Laser Engineering*, 6th edn. (Springer, Berlin, 2005), Ch.7.
 32. N. Hodgson, and H. Weber, *Laser Resonators and Beam Propagation*, 2nd edn. (Springer, Berlin, 2005), Ch. 8.
 33. Y. F. Chen, T. M. Huang, C. F. Kao, C. L. Wang, and S. C. Wang, "Optimization in scaling fiber-coupled laser-diode end-pumped lasers to higher power: influence of thermal effect," *IEEE J. Quantum Electron.* **33**, 1424-1429 (1997).
 34. J. H. Campbell, and F. Rainer, "Optical glasses for high-peak-power laser applications," *Proc. of SPIE* **1761**, 246-255 (1992).
 35. L. Canioni, M. Bellec, A. Royon, B. Bousquet, and T. Cardinal, "Three-dimensional optical data storage using third-harmonic generation in silver zinc phosphate glass," *Opt. Lett.* **33**(4), 360-362 (2008).
 36. N. Kramer, M. Niesten, and C. Schöenberger, "Resistless high resolution optical

- lithography on silicon,” *Appl. Phys. Lett.* 67(20), 2989-2991 (1995).
37. R. S. Patel, J. Bovatsek, and A. Tamhankar, “Why pulse duration matters in photovoltaics,” *Laser Technik Journal* 7(1), 21–24 (2010).
 38. A. Tamhankar, and R. S. Patel, “Optimization of UV laser scribing process for light emitting diode sapphire wafers,” *J. Laser Appl.* 23(3), 032001 (2011).
 39. J. Saby, B. Cocquelin, A. Meunier, S. Pierrot, P.-J. Devilder, P. Deslandes, and F. Salin, “High average and peak power pulsed fiber lasers at 1030 nm, 515 nm, and 343 nm”, *Proc. SPIE* 7580, (2010).
 40. M. Laurila, J. Saby, T. T. Alkeskjold, L. Scolari, B. Cocquelin, F. Salin, J. Broeng, and J. Lægsgaard, “Q-switching and efficient harmonic generation from a single-mode LMA photonic bandgap rod fiber laser,” *Opt. Express* 19(11), 10824–10833 (2011).
 41. D. A. V. Kliner, F. Di Teodoro, J. P. Koplow, S. W. Moore, and A. V. Smith, “Efficient second, third, fourth, and fifth harmonic generation of a Yb-doped fiber amplifier,” *Opt. Commun.* 210, 393–398 (2002).
 42. P. E. Schrader, R. L. Farrow, D. A. V. Kliner, J.-P. Fève, and N. Landru, “High-power fiber amplifier with widely tunable repetition rate, fixed pulse duration, and multiple output wavelengths,” *Opt. Express* 14(24), 11528-11538 (2006).
 43. C. D. Brooks and F. Di Teodoro, “High peak power operation and harmonic generation of a single-polarization, Yb-doped photonic crystal fiber amplifier,” *Opt. Commun.* 280, 424–430 (2007).
 44. H. L. Chang, W. Z. Zhuang, W. C. Huang, J. Y. Huang, K. F. Huang, and Y. F. Chen, “Widely tunable eye-safe laser by a passively Q-switched photonic crystal fiber laser and an external-cavity optical parametric oscillator,” *Laser Phys. Lett.* 8(9), 678-683 (2011).
 45. W. Z. Zhuang, W. C. Huang, P. Y. Chiang, K. W. Su, K. F. Huang, and Y. F. Chen, “Millijoule-level Yb-doped photonic crystal fiber laser passively Q-switched with AlGaInAs quantum wells,” *Opt. Express* 18(26), 27910–27915 (2010).
 46. F. Di Teodoro, M. K. Hemmat, J. Morais, and E. C. Cheung, “High peak power operation of a 100 μ m-core, Yb-doped rod-type photonic crystal fiber amplifier,” *Fiber Lasers VII: Technology, Systems and Applications*, *Proc. of SPIE* vol. 7580, 758006 (2010).
 47. Y. J. Huang, Y. P. Huang, P. Y. Chiang, H. C. Liang, K. W. Su, and Y. F. Chen,

- “High-power passively Q-switched Nd:YVO₄ UV laser at 355 nm,” *Appl. Phys. B* 106(4), 893-898 (2012).
48. W. Z. Zhuang, W. C. Huang, C. Y. Cho, Y. P. Huang, J. Y. Huang, and Y. F. Chen, “>100-kW linearly polarized pulse fiber amplifier seeded by a compact efficient passively Q-switched Nd:YVO₄ laser,” *Laser Phys.* (to be published).
49. C. X. Wang, G. Y. Wang, A. V. Hicks, D. R. Dudley, H. Y. Pang, and N. Hodgson, “High power Q-switched TEM₀₀ mode diode-pumped solid state lasers with >30 W output power at 355 nm,” *Proc. SPIE* 6100, 610019 (2006).
50. H. Kitano, T. Matsui, K. Sato, N. Ushiyama, M. Yoshimura, Y. Mori, and T. Sasaki, “Efficient 355-nm generation in CsB₃O₅ crystal,” *Opt. Lett.* 28(4), 263-265 (2003).



Chapter 5

Summary and Future works



5.1 Summary

5.1.1 Passively Q-switched double-cladding fiber lasers

In this section we demonstrate efficient, high repetition rate, and high peak power double-cladding fiber lasers passively Q-switched by AlGaInAs QWs and Cr⁴⁺:YAG crystal as the saturable absorbers respectively. The performances of these fiber lasers are showed in table.

SA	AlGaInAs	Cr ⁴⁺ :YAG
Pulse energy (mJ)	0.45	0.35
Pulse width (ns)	60	70
Peak power (kW)	7.5	5
Repetition rate (kHz)	30	38

Table 5. 1 Performances of the passively Q-switched fiber laser

5.1.2 Passively Q-switched photonic crystal fiber lasers

In this section we demonstrate efficient, high repetition rate, and high peak power fiber lasers passively Q-switched with AlGaInAs QWs and Cr⁴⁺:YAG crystal as the saturable absorbers respectively by using the photonic crystal fiber with large core diameter of 70 μm . The pulse energy was scaled up and the pulse width was also reduced due to the large core which means high gain and then short fiber length. The performances of these PCF lasers are showed in table 5.2.

In addition to Cr⁴⁺:YAG crystal, three types of AlGaInAs, 3 x 50 QWs, 3 x30 QWs, and 2 x30 QWs, are also used as the saturable absorbers. Compared with the conventional DCF lasers mentioned above in the same condition, the higher pulse energy and the shorter pulse width make the peak power 14.7 and 3.5 times higher with 3x50 AlGaInAs QWs and Cr⁴⁺:YAG crystal respectively.

Based on the PQS PCF laser, we also demonstrate the intracavity optical parametric oscillator (IOPO) and the extracavity optical parametric oscillator (EOPO) by using the Cr⁴⁺:YAG crystal and the AlGaInAs QWs as the saturable absorbers respectively. Owing to the high refractive-index-temperature coefficient of the PPLN used in the EOPO scheme, the wavelength can be tuned over a broad range. Table 5.3 are the performances of IOPO and EOPO.

SA	3x50 AlGaInAs	3x30 AlGaInAs	2x30 AlGaInAs	Cr ⁴⁺ :YAG
Pulse energy (mJ)	1.1	0.49	0.35	0.63
Pulse width (ns)	10	38	47.3	36
Peak power (kW)	110	12.8	7.4	17.5
Repetition rate (kHz)	6.5	16	23	5.6

Table 5. 2 Performances of the passively Q-switched PCF laser

Type	IOPO with KTP	EOPO with PPLN
Wavelength (nm)	1515	1513~1593
Pulse energy (mJ)	0.14	0.14
Pulse width (ns)	1	7.3
Peak power (kW)	140	19
Repetition rate (kHz)	3.3	6.5
Conversion efficiency (%)	22.3	35

Table 5. 3 Performances of the OPO

5.1.3 Passively Q-switched fiber laser based on a MOFA configuration

In this section we demonstrate efficient, high repetition rate, and high peak power fiber lasers based on the master oscillator fiber amplifier. By this configuration, it is very easy to get the short pulse width which is useful in some applications, because the low-power seed laser is easily modulated. The performances of MOFA-based fiber lasers seeded by Nd:YVO₄/Cr⁴⁺:YAG PQS lasers are showed in table 5.4. The PCF amplifier is also used for the harmonic generations. The results reveal it is efficient and simple to use the single stage PCF amplifier as the fundamental wavelength light source.

Type	DCF (1)	DCF (2)	PCF
Pulse energy (mJ)	0.178	0.192	0.221
Pulse width (ns)	4.8	1.6	2.2
Peak power (kW)	37.1	120	100
Repetition rate (kHz)	50	25	14.9

Table 5. 4 The performances of MOFA-based fiber lasers seeded by Nd:YVO₄/Cr⁴⁺:YAG PQS lasers

5.2 Future work

To achieve high-peak-power fiber laser, using the MOFA configuration with more pumping power, shortening the pulse width of seed laser, and operating at high gain wavelength regime are necessary. In the Yb-doped fiber, as shown in figure 1.6, the net gain in the regime of 1030 nm is higher than the others, so lasing at 1030 nm regime can attain the highest energy conversion efficiency in the same condition. Comparing with Nd:YVO₄ crystals, Yb:YAG crystals have longer fluorescence lifetime, lower quantum defects, broader absorption bandwidth, and shorter cavity length for good passive Q-switching with Cr⁴⁺:YAG[1,2]. Besides, Yb:YAG crystals can have lasing wavelength of 1030 nm, so they are more suitable for the seed lasers. By seeding this light source into the PCF with more pumping power, it can be expected that power scales up significantly.

Reference

1. W. Z. Zhuang, Yi-Fan Chen, K. W. Su, K. F. Huang, and Y. F. Chen, "Performance enhancement of sub-nanosecond diode-pumped passively Q-switched Yb:YAG microchip laser with diamond surface cooling," *Opt. Express* 20(20), 22602-22608 (2012).
2. W. Z. Zhuang, W. C. Huang, C. Y. Cho, Y. P. Huang, J. Y. Huang, and Y. F. Chen, ">100-kW Linearly Polarized Pulse Fiber Amplifier Seeded by a Compact Efficient Passively Q-switched Nd:YVO₄ Laser," *Laser Phys.* (to be published).

Curriculum Vitae

Personal Data

Name: Wen-Cheng Huang

Sex: Male

Birthday: Oct. 15, 1976

Nationality: Taiwan

E-mail: york.ep97g@nctu.edu.tw

Mobile Phone: 886-928-123002

Education

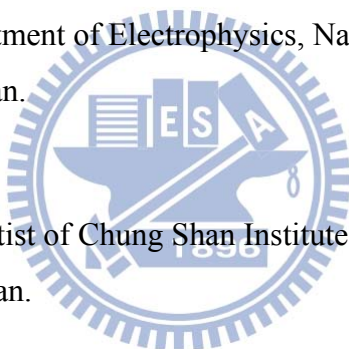
1995-2001 B.S. in Department of Physics, Soochow University, Taipei, Taiwan.

2001-2003 M.S. in Department of Optics and Photonics, Central University,
Taoyuan, Taiwan.

2008-2014 Ph.D. in Department of Electrophysics, National Chiao Tung University,
Hsinchu, Taiwan.

Work Experience

2003 - now Assistant Scientist of Chung Shan Institute of Science and Technology,
Taoyuan, Taiwan.



Research Interest

Yb-doped fiber lasers

Publication List

Journal papers:

1. J. Y. Huang, W. C. Huang, W. Z. Zhuang, K. W. Su, Y. F. Chen, and K. F. Huang, "High-pulse-energy, passively Q-switched Yb-doped fiber laser with AlGaInAs quantum wells as a saturable absorber," Opt. Lett. 34(15), 2360-2362 (2009).
2. J. Y. Huang, W. Z. Zhuang, W. C. Huang, K. W. Su, C. Hu, K. F. Huang, and Y. F. Chen, "Comparative studies for Cr⁴⁺:YAG crystal and AlGaInAs semiconductor used as a saturable absorber in Q-switched Yb-doped fiber lasers," Opt. Express 17(23), 20800-20805 (2009).
3. H. C. Liang, H. L. Chang, W. C. Huang, K. W. Su, Y. F. Chen, and Y. T. Chen, "Self-mode-locked Nd:GdVO₄ laser with multi-GHz oscillations: manifestation of third-order nonlinearity," Appl. Phys. B 97, 451 (2009).
4. W. Z. Zhuang, W. C. Huang, Y. P. Huang, K. W. Su, and Y. F. Chen, "Passively Q-switched photonic crystal fiber laser and intracavity optical parametric oscillator," Opt. Express 18(9), 8969-8975 (2010).
5. W. Z. Zhuang, W. C. Huang, P. Y. Chiang, K. W. Su, K. F. Huang, and Y. F. Chen, "Millijoule-level Yb-doped photonic crystal fiber laser passively Q-switched with AlGaInAs quantum wells," Opt. Express 18(26), 27910-27915 (2010).
6. H. C. Liang, Y. J. Huang, W. C. Huang, K. W. Su, and Y. F. Chen, "High-power, diode-end-pumped, multigigahertz self-mode-locked Nd:YVO₄ laser at 1342 nm," Opt. Lett. 35, 4 (2010).
7. J. Y. Huang, W. Z. Zhuang, W. C. Huang, K. W. Su, K. F. Huang, and Y. F. Chen, "Hybrid Q-switched Yb-doped fiber laser," Opt. Express 19(10), 9364-9370 (2011).
8. H. L. Chang, W. Z. Zhuang, W. C. Huang, J. Y. Huang, K. F. Huang, and Y. F. Chen, "Widely tunable eye-safe laser by a passively Q-switched photonic crystal fiber laser and an external-cavity optical parametric oscillator," Laser Phys. Lett. 8(9), 678-683 (2011).
9. W. Z. Zhuang, W. C. Huang, C. Y. Cho, Y. P. Huang, J. Y. Huang, and Y. F. Chen,

“>100-kW linearly polarized pulse fiber amplifier seeded by a compact efficient passively Q-switched Nd:YVO₄ laser,” Laser Phys. 22(11), 1721-1728 (2012).

